



ECAR-2322 As-Run Thermal Analysis Of The AGC-2 Experiment

August 2021

Changing the World's Energy Future

Grant L Hawkes



DISCLAIMER

This information was prepared as an account of work sponsored by an agency of the U.S. Government. Neither the U.S. Government nor any agency thereof, nor any of their employees, makes any warranty, expressed or implied, or assumes any legal liability or responsibility for the accuracy, completeness, or usefulness, of any information, apparatus, product, or process disclosed, or represents that its use would not infringe privately owned rights. References herein to any specific commercial product, process, or service by trade name, trade mark, manufacturer, or otherwise, does not necessarily constitute or imply its endorsement, recommendation, or favoring by the U.S. Government or any agency thereof. The views and opinions of authors expressed herein do not necessarily state or reflect those of the U.S. Government or any agency thereof.

ECAR-2322 As-Run Thermal Analysis Of The AGC-2 Experiment

Grant L Hawkes

August 2021

**Idaho National Laboratory
Idaho Falls, Idaho 83415**

<http://www.inl.gov>

**Prepared for the
U.S. Department of Energy
Under DOE Idaho Operations Office
Contract DE-AC07-05ID14517**

Engineering Calculations and Analysis

ECAR Title: As-Run Thermal Analysis of the AGC-2 ExperimentECAR No.: 2322

Performer:	P. E. Murray	C660	See eCR 621150	
	(Name)	(Organization)	(Signature)	(Date)
Checker ¹ :	G. L. Hawkes	C120	See eCR 621150	
	(Name)	(Organization)	(Signature)	(Date)
Independent Peer Reviewer ² :	Not Required			
	(Name)	(Organization)	(Signature)	(Date)
CUI Reviewer:	M. E. Davenport	C630	See eCR 621150	
	(Name)	(Organization)	(Signature)	(Date)
Manager ³ :	D. J. Schoonen	C660	See eCR 621150	
	(Name)	(Organization)	(Signature)	(Date)
Owner ⁴ :	M. E. Davenport	C630	See eCR 621150	
	(Name)	(Organization)	(Signature)	(Date)
Cognizant engineer ⁴ :	J. Palmer	C120	See eCR 621150	
	(Name)	(Organization)	(Signature)	(Date)
VHTR Technical Development ⁴ :	W. E. Windes	B120	See eCR 621150	
	(Name)	(Organization)	(Signature)	(Date)
Nuclear Safety ⁴ :	Not Required			
	(Name)	(Organization)	(Signature)	(Date)
ATR Experiment Engineering Manager ³ :	Not Required			
	(Name)	(Organization)	(Signature)	(Date)

Doc control Michele Robb Michele Robb 4/15/14

1. Confirmation of completeness, mathematical accuracy, and correctness of data and appropriateness of assumptions.
2. Concurrence of method or approach. See definition, LWP-10106.
3. Concurrence of procedure compliance. Concurrence with method/approach and conclusion.
4. Concurrence with the document's assumptions and input information. See definition of Acceptance, LWP-10200.

REVISION LOG

Rev.	Date	Affected Pages	Revision Description
0	04/07/14	ALL	Initial issue.

1. Quality Level (QL) No.	2	Professional Engineer's Stamp See LWP-10010 for requirements.
2. QL Determination No.	RTC-000486	
3. Engineering Job (EJ) No.	N/A	
4. eCR No.	N/A	
5. SSC ID	AGC-2 Experiment	
6. Building	TRA-670	
7. Site Area	ATR Complex	
8. Objective/Purpose: <p>The second Advanced Graphite Creep (AGC-2) experiment was designed to irradiate various types of graphite specimens at a temperature of 600°C. The specimens were irradiated in an instrumented leadout capsule experiment in the south flux trap of the ATR during cycles 149A, 149B, 150B, 151A, and 151B. Temperature was monitored using twelve thermocouples located at various elevations in the reactor core, and a helium-argon gas mixture was used for gas gap temperature control of the specimens.</p> <p>The purpose of this analysis is to calculate specimen temperature using measured data on reactor power and helium-argon gas flows, and as-run calculations of heating rates and displacement per atom (DPA) in graphite. The accuracy of the model is assessed by comparing measured and calculated thermocouple temperatures. Uncertainty in gas gaps may preclude an accurate temperature calculation. In these cases, adjustments are made to the thermal model in order to reconcile the measured and calculated thermocouple temperature and to ensure the accuracy of the calculated specimen temperature.</p>		
9. Conclusions/Recommendations: <p>A finite element, steady-state heat transfer analysis of the entire AGC-2 test train was performed using ABAQUS. The analysis was performed at three selected days during each cycle, using the measured south source power, measured gas flows, as-run heating rates, and as-run graphite DPA, to obtain best-estimate temperatures of the specimens and thermocouples. The accuracy of the model was confirmed by comparing measured and calculated thermocouple temperatures. The maximum difference between the measured and calculated temperature of each thermocouple in the test train is 35°C, while in all cases except one the difference is within ±30°C.</p> <p>The temperature of each creep specimen is desired to be maintained at 600°C ±50°C. However, the results of this analysis show that temperature of the specimen stacks is outside the desired range at the bottom of the test train where temperature is less than the desired temperature and at core mid-plane where temperature is greater than the desired temperature. In most cases, temperature of the specimen stacks at core mid-plane is approximately 100°C greater than the desired temperature. Moreover, specimen temperature varies significantly with elevation because of the difficulty in attaining temperature uniformity using a single temperature control gas zone.</p>		

CONTENTS

SCOPE OF ANALYSIS AND BRIEF DESCRIPTION.....	5
DESIGN OR TECHNICAL PARAMETER INPUTS AND SOURCES.....	5
EXPERIMENT DESCRIPTION AND OTHER BACKGROUND DATA.....	5
ASSUMPTIONS	8
SOFTWARE VALIDATION	8
ANALYSIS RESULTS.....	10
CONCLUSIONS AND RECOMMENDATIONS	36
DATA FILES	37
REFERENCES	38
DRAWINGS.....	39

APPENDICES

- Appendix A – Thermo-physical properties, hydrodynamics, heat transfer coefficients, and heating rates
- Appendix B – Results of ABAQUS validation

FIGURES

Figure 1. Effect of temperature and DPA on thermal conductivity of graphite.	6
Figure 2. Effect of DPA on diameter of graphite specimens.	7
Figure 3. Model geometry and finite element mesh (cross-sectional view of the experiment).	10
Figure 4. Model geometry and finite element mesh (cutaway view of the experiment).	11
Figure 5. Temperature (°C) of experiment cross-section at 18 inches above core mid-plane.....	12
Figure 6. Temperature (°C) of experiment cross-section at 13 inches above core mid-plane.....	13
Figure 7. Temperature (°C) of experiment cross-section at 6 inches above core mid-plane.....	14
Figure 8. Temperature (°C) of experiment cross-section at 2 inches above core mid-plane.....	15
Figure 9. Temperature (°C) of experiment cross-section at 6 inches below core mid-plane.	16
Figure 10. Temperature (°C) of experiment cross-section at 11.25 inches below core mid-plane.	17
Figure 11. Temperature (°C) of experiment cross-section at 18 inches below core mid-plane.....	18
Figure 12. Measured and calculated temperature (°C) of TC-01 during all irradiation cycles.	19
Figure 13. Measured and calculated temperature (°C) of TC-02 during all irradiation cycles.	20
Figure 14. Measured and calculated temperature (°C) of TC-03 during all irradiation cycles.	21
Figure 15. Measured and calculated temperature (°C) of TC-04 during all irradiation cycles.	22
Figure 16. Measured and calculated temperature (°C) of TC-05 during all irradiation cycles.	23
Figure 17. Measured and calculated temperature (°C) of TC-06 during all irradiation cycles.	24
Figure 18. Measured and calculated temperature (°C) of TC-07 during all irradiation cycles.	25
Figure 19. Measured and calculated temperature (°C) of TC-08 during all irradiation cycles.	26
Figure 20. Measured and calculated temperature (°C) of TC-09 during all irradiation cycles.	27
Figure 21. Measured and calculated temperature (°C) of TC-10 during all irradiation cycles.	28
Figure 22. Measured and calculated temperature (°C) of TC-11 during all irradiation cycles.	29
Figure 23. Measured and calculated temperature (°C) of TC-12 during all irradiation cycles.	30
Figure 24. Distribution of specimen temperature (°C) during a selected day in cycle 149A.	31
Figure 25. Distribution of specimen temperature (°C) during a selected day in cycle 149B.	32
Figure 26. Distribution of specimen temperature (°C) during a selected day in cycle 150B.	33
Figure 27. Distribution of specimen temperature (°C) during a selected day in cycle 151A.	34
Figure 28. Distribution of specimen temperature (°C) during a selected day in cycle 151B.	35

SCOPE OF ANALYSIS AND BRIEF DESCRIPTION

The second Advanced Graphite Creep (AGC-2) experiment was designed to irradiate various types of graphite specimens at a temperature of 600°C. The specimens were irradiated in an instrumented leadout capsule experiment in the south flux trap of the ATR during cycles 149A, 149B, 150B, 151A, and 151B. Temperature was monitored using thermocouples, and a helium-argon gas mixture was used for gas gap temperature control of the specimens. A pneumatic piston was used to apply a maximum compressive load of 3000 psi to approximately half the specimens, resulting in corresponding pairs of stressed and unstressed specimens. The dimensional changes of corresponding specimen pairs will be used to determine irradiation-induced creep by distinguishing the separate effects of shrinkage occurring in all specimens and creep occurring in the stressed specimens only.

The purpose of this analysis is to calculate specimen temperature using measured data on reactor power and helium-argon gas flows, and as-run calculations of heating rates and displacement per atom (DPA) in graphite. The AGC-2 experiment contains twelve thermocouples located at various elevations in the reactor core. The accuracy of the model is assessed by comparing measured and calculated thermocouple temperatures. Uncertainty in gas gaps may preclude an accurate temperature calculation. In these cases, adjustments are made to the thermal model in order to reconcile the measured and calculated thermocouple temperature and to ensure the accuracy of the calculated specimen temperature.

DESIGN OR TECHNICAL PARAMETER INPUTS AND SOURCES

The technical and functional requirements for the AGC-2 experiment are given in TFR-645. The quality level of the analysis is "2" (important to safety) per quality level determination RTC-000486.

EXPERIMENT DESCRIPTION AND OTHER BACKGROUND DATA

The AGC-2 experiment is the second in a series of irradiation experiments to obtain data on fine-grained isotropic graphite used in the next generation very high temperature reactor (VHTR). The test train consists of seven stacks of cylindrical graphite specimens 0.5 inches in diameter contained in a graphite holder. The center stack contains unstressed specimens, while the peripheral stacks contain stressed specimens above core mid-plane and unstressed specimens below core mid-plane. The holder is contained in a stainless steel capsule, with a stainless steel heat shield placed between them. The holder has a stepped outside diameter to provide an axially varying temperature control gas gap to compensate for the axial variation in heating. All specimens are desired to be irradiated at the same temperature, while corresponding stressed and unstressed specimens are desired to be irradiated to the same DPA. Other capsule internal components include tungsten spacers that provide heat generation at the top of the test train, zirconia spacers that provide heat generation and thermal insulation at the bottom of the test train, and a ceramic insulator at the top of the test train. Thermocouples and gas tubing are located in holes and grooves in the holder. Design details are from the drawings listed at the end of this document.

The thermal analysis was performed using a detailed finite element model of the experiment. Data on material properties are obtained from the handbooks and databases listed in the references. Results are given in Appendix A.1. The change in diameter of the capsule components due to thermal expansion and the change in diameter of graphite due to irradiation-induced shrinkage are calculated in Appendix A.2. The resulting heat transfer coefficients for the fluence-dependent "hot" gas gaps are computed using various helium-argon gas mixtures and various values of DPA. Results are given in Appendix A.3.

The thermal conductivity of graphite depends on temperature and neutron fluence. Experimental data for NBG-25, IG-110, and H-451 is shown in Fig. 1, along with the temperature and DPA-dependent profiles assumed in this analysis. The calculated profiles show the correct trends observed in irradiated graphite: increasing conductivity with increasing temperature due to annealing of defects, and decreasing conductivity with increasing fluence due to generation of defects. The calculated profiles are similar to those used in previous as-run analysis of graphite experiments (Hawkes, 2012), and are consistent with the data reported in Vreeling, Wouters, and van der Lann, 2008, Maruyama and Harayama, 1992, and Price, 1975.

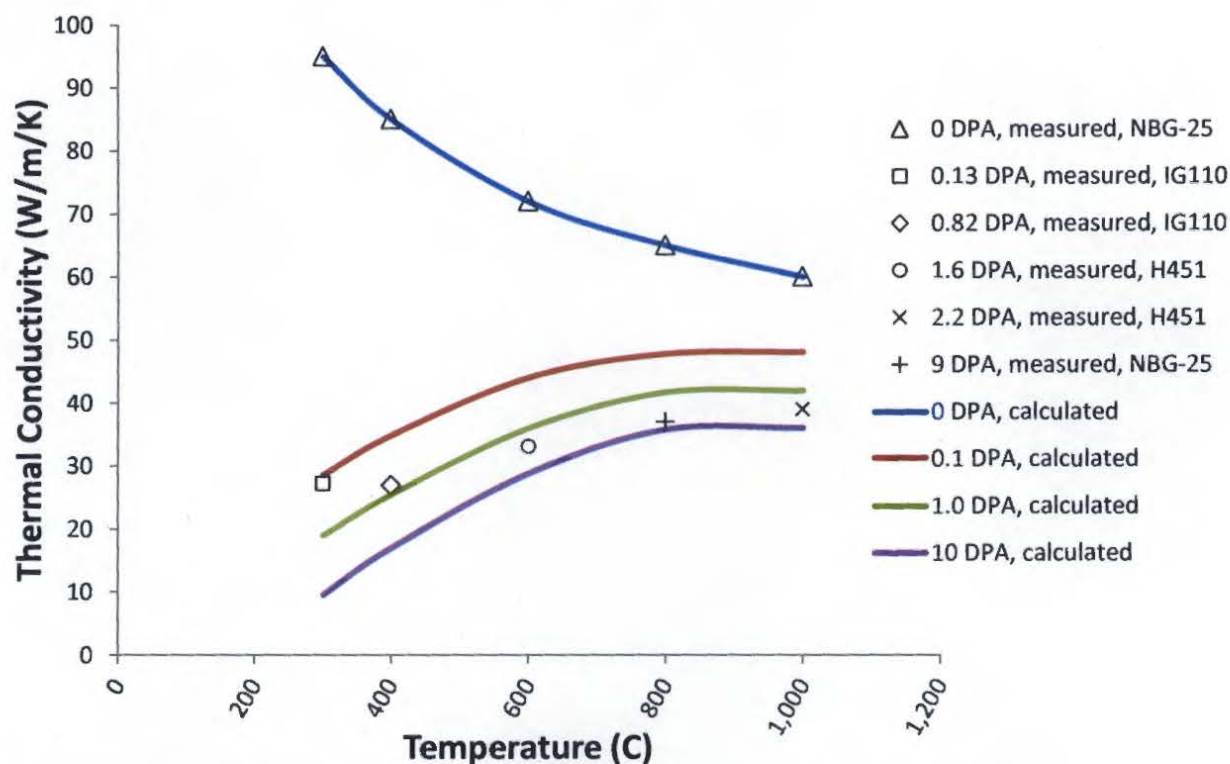


Figure 1. Effect of temperature and DPA on thermal conductivity of graphite.

The size of the temperature control gas gap between the graphite holder and stainless steel heat shield depends on temperature and neutron fluence. The temperature dependence results from thermal expansion, and the fluence dependence results from irradiation-induced shrinkage of graphite. Experimental data for the change in diameter of graphite due to irradiation-induced shrinkage is shown in Fig. 2, along with a linear regression of the data which provides a relation between diameter change and DPA. The data was obtained from measurements of the dimensional change of NBG-25 specimens irradiated in the AGC-1 experiment (Windes, 2012). The graphite in the AGC-2 experiment was irradiated to a peak fast neutron (energy > 0.1 MeV) fluence of approximately 6.5×10^{21} neutrons/cm² which corresponds to a peak DPA of approximately 4.6 (ECAR-2291). At this neutron fluence, the diameter reduction is expected to be approximately 0.9%. The size of the gas gap between the graphite holder and graphite specimens was assumed to be independent of neutron fluence since the irradiation-induced shrinkage of the specimens and holder is approximately equal.

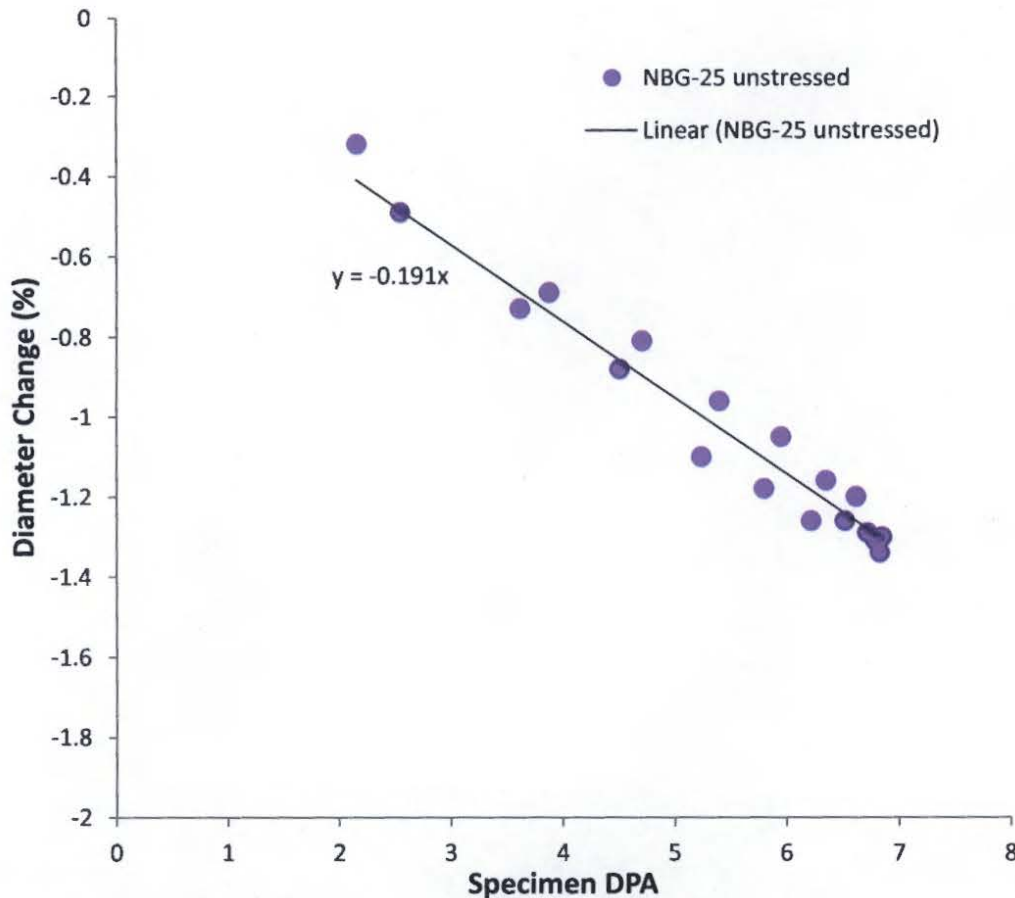


Figure 2. Effect of DPA on diameter of graphite specimens.

The flow of primary coolant in the annular gap between the capsule and chopped dummy in-pile tube is calculated for two-pump operation. Heat transfer coefficients for turbulent forced convection to the primary coolant were obtained from an experimental correlation using the film temperature method to account for fluid property variation. Details are given in Appendix A.4.

The heat loads in the south flux trap at 23.2 MW source power were obtained from the as-run reactor physics analysis (ECAR-2291). Heat loads for each component in the test train were obtained as a function of position with respect to core mid-plane. For the capsule, heat shield, graphite holder and specimens, thermocouples, and primary coolant, a cosine-shaped profile was used to represent the axial variation in heating (IN-1260). The axial profile was split into separate profiles above and below core mid-plane, producing an unsymmetrical profile that preserves total core heating. The unsymmetrical heating profile improves temperature calculations as compared to using a symmetrical profile. Heat loads at a different power are obtained by linear scaling using the nominal operating heat loads provided in ECAR-2291 as a baseline. Details are given in Appendix A.5.

Reactor power, temperature control gas flows, and thermocouple temperatures are obtained from the Reactor Data Acquisition System (RDAS) system. Spreadsheets contain data recorded at five minute intervals and are stored on the server "fsisc1" in folder \Projects. Reactor power, temperature control gas flows, and thermocouple temperatures at selected days during each cycle are computed by averaging the

data over the entire day. Peak DPA at those days was obtained from the as-run reactor physics analysis (ECAR-2291). Results are given in Appendix A.6.

ASSUMPTIONS

One significant uncertainty is the gap between heat shield and capsule which can vary from the case where the dimples on the inside surface of the heat shield contact the holder to the case where the dimples on the outside surface of the heat shield contact the capsule. In this analysis, the location of the heat shield is calculated assuming the dimples on the outside surface of the heat shield contact the inside surface of the capsule, leading to a 0.005 inch gap between heat shield and capsule. The resulting temperature control gas gaps are calculated using the assumed location of the heat shield and accounting for thermal expansion and shrinkage of the capsule and holder. The gas gap between heat shield and capsule is varied to account for uncertainty in the exact location of the heat shield and the increased thermal conductance due to contact between the capsule and dimples on the heat shield. The variable gas gap between heat shield and capsule was adjusted in order to bring into agreement the measured and calculated thermocouple temperatures.

For each component, the heating rate at a particular elevation in the core is computed by averaging the heating rates over azimuthal segments. Sensitivity studies show that azimuthal variations in heating rates in the test train do not have a significant effect on temperature because conduction heat transfer between components tends to equalize the temperature. Results obtained with azimuthal-averaged heating were compared to those obtained with variable heating, and the difference in temperature is approximately 1°C to 5°C. Therefore, it is unnecessary to include in the analysis the effect of test train rotation during the cycle 151A outage.

The length of the specimen stacks under axial compression will change during irradiation due to irradiation-induced creep. In this analysis, temperature is evaluated in the undeformed configuration. Therefore, this analysis provides specimen temperature as a function of elevation. For a given specimen, its temperature at a particular time during irradiation may be determined by estimating its location with respect to core mid-plane, including the effect of axial compression, and then using the results of this analysis to obtain the temperature at that location.

Another significant uncertainty is the gap between thermocouples and holder which has a nominal value of 0.0095 inch but can vary from zero to 0.019 inch around the circumference of the thermocouple. Sensitivity studies show that the assumed gas gap has a significant effect on thermocouple temperature due to thermocouple self-heating and heat transfer resistance in the gas gap. Therefore, a study was conducted to determine the difference between the measured thermocouple temperature and measured graphite temperature in the case of loose-fitting thermocouples like those used in AGC-2 (ECAR-2429). The results of this study indicate that a thermocouple should be modeled by assuming that it is located off-center with a minimum gas gap that is 5% of the nominal gap corresponding to the case where the thermocouple is centered. In this case, the thermocouples are assumed to be off-center with a gas gap that varies from 0.0005 inch to 0.00185 inch.

SOFTWARE VALIDATION

A finite element heat transfer analysis of the AGC-2 experiment was performed using ABAQUS version 6.12-2 on a 384-core DELL distributed memory system ("Quark" on the INL network). The operating system is OpenSUSE 11.4, and each processor core is a 2.67 GHz Intel X5650. ABAQUS is listed in the INL Enterprise Architecture (EA) repository of qualified scientific and engineering analysis software

(EA Identifier 238858). ABAQUS has been validated for thermal analysis of ATR experiments by solving several test problems and verifying the results against analytical solutions provided in heat transfer textbooks. A complete description of the validation test problems is given in ECAR-131. Scripts were developed to automate the execution, data collection, and relative error calculation for each test problem. The scripts were run on computer "Quark" and a report file containing the results of validation testing was automatically generated (Appendix B). The test results meet the acceptance criterion that the relative error is less than 3%. Calculations given in the appendices were performed using Mathcad version 15, and verification of the computer-generated results was done during checking.

ANALYSIS RESULTS

A finite element, steady-state heat transfer analysis of the AGC-2 test train, including the capsule and all internal components, was performed using ABAQUS. The 8-node linear brick element was used to model all solid components except the heat shield which was modeled using the 4-node linear shell element. The 8-node forced convection brick element was used to model the primary coolant with a prescribed mass flow rate. The model geometry and finite element mesh of the experiment cross-section at core mid-plane is shown in Fig. 3. A 3-D cutaway view of the experiment is shown in Fig. 4. In these figures, the capsule is blue, specimen holder is green, specimens are red, and thermocouples are orange. The heat shield is modeled as a thin shell and is not clearly visible in the figure. The primary coolant and chopped dummy in-pile tube are also not shown.

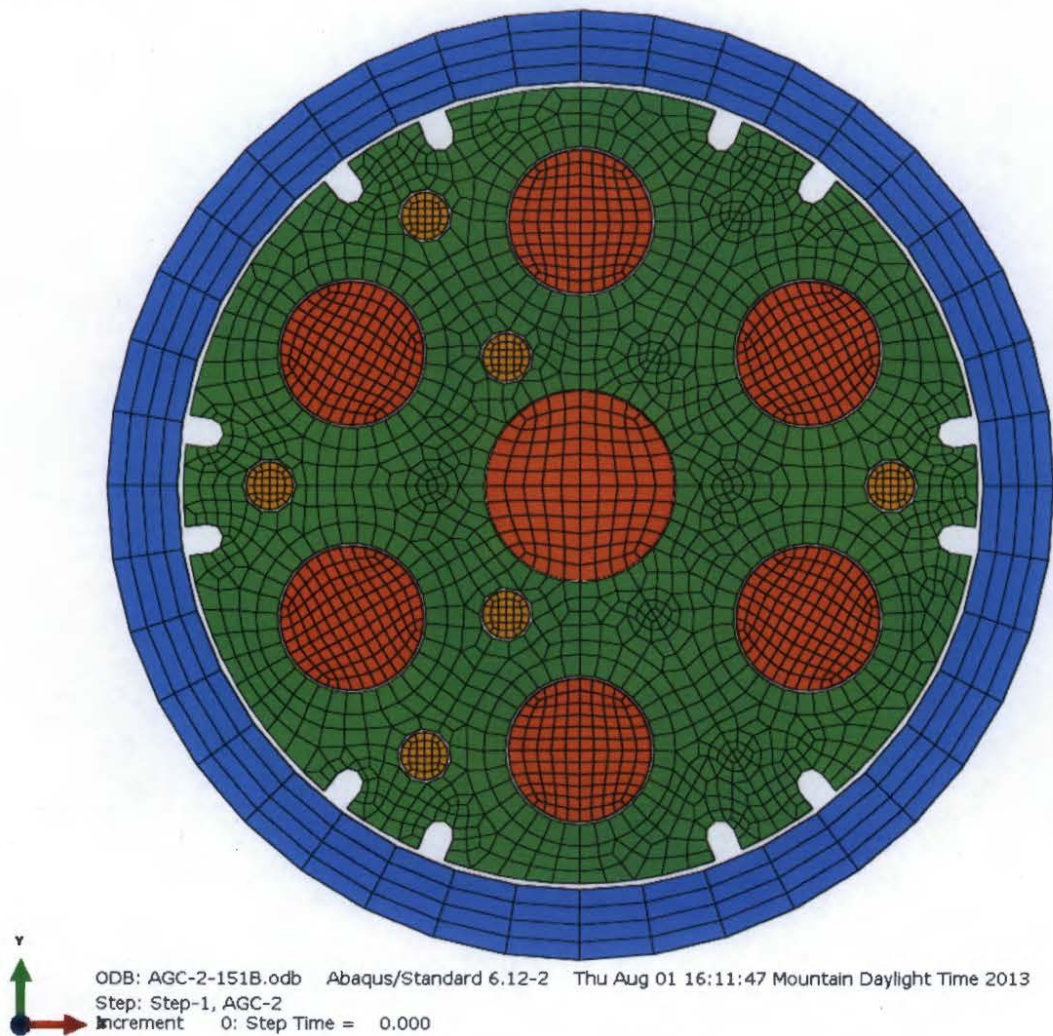


Figure 3. Model geometry and finite element mesh (cross-sectional view of the experiment).

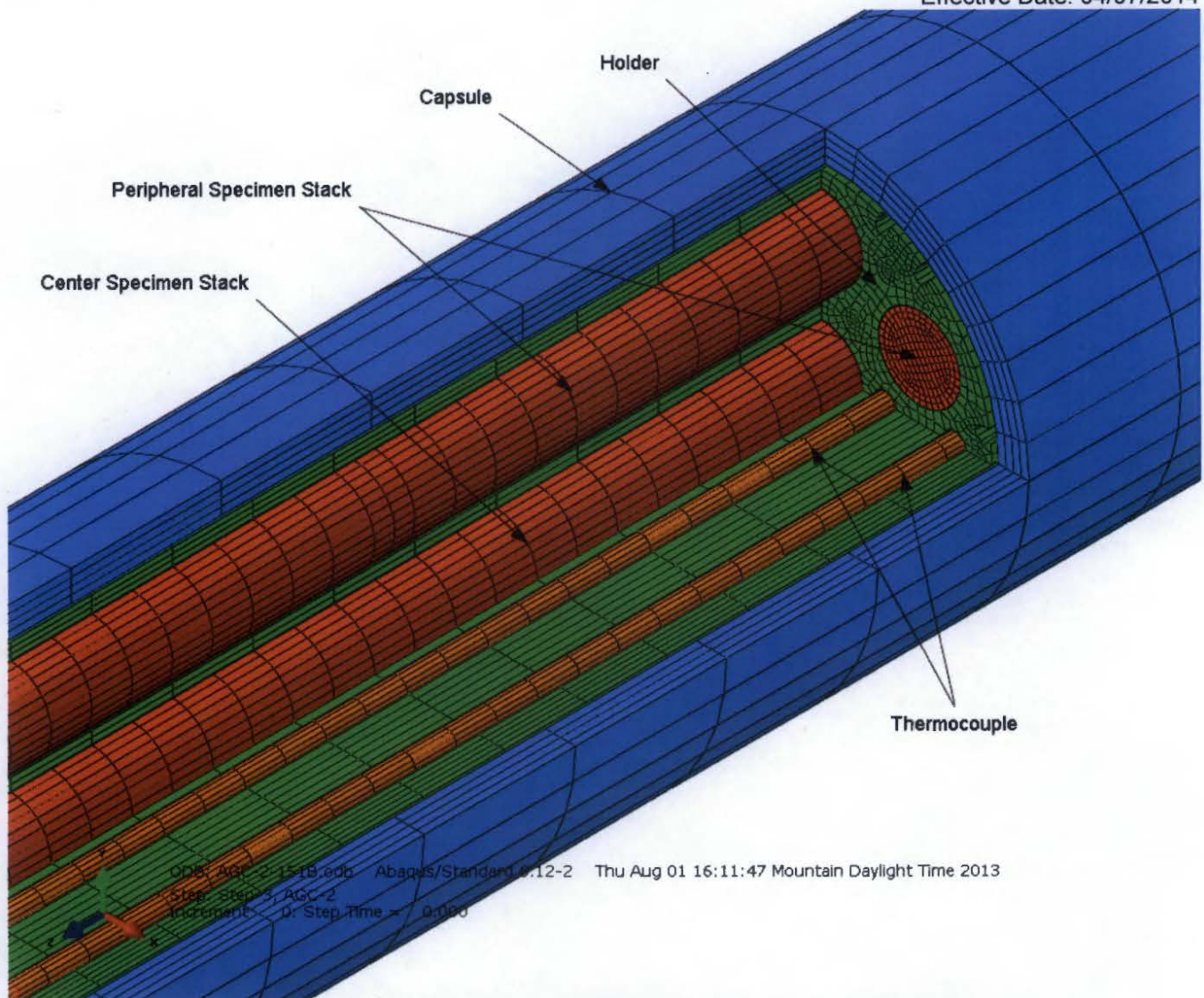


Figure 4. Model geometry and finite element mesh (cutaway view of the experiment).

A thermal analysis was performed at three selected days during each cycle, using the measured south source power, measured gas flows, as-run heating rates, and as-run graphite DPA, to obtain best-estimate temperatures of the specimens. Contour plots of the temperature of the experiment cross-sections located at the elevations of the thermocouple junctions, at a selected day in cycle 151B, are shown in Figs. 5 – 11. Temperature units are °C. Note that the highest temperature occurs in the center specimen stack which is significantly hotter than the peripheral stacks.

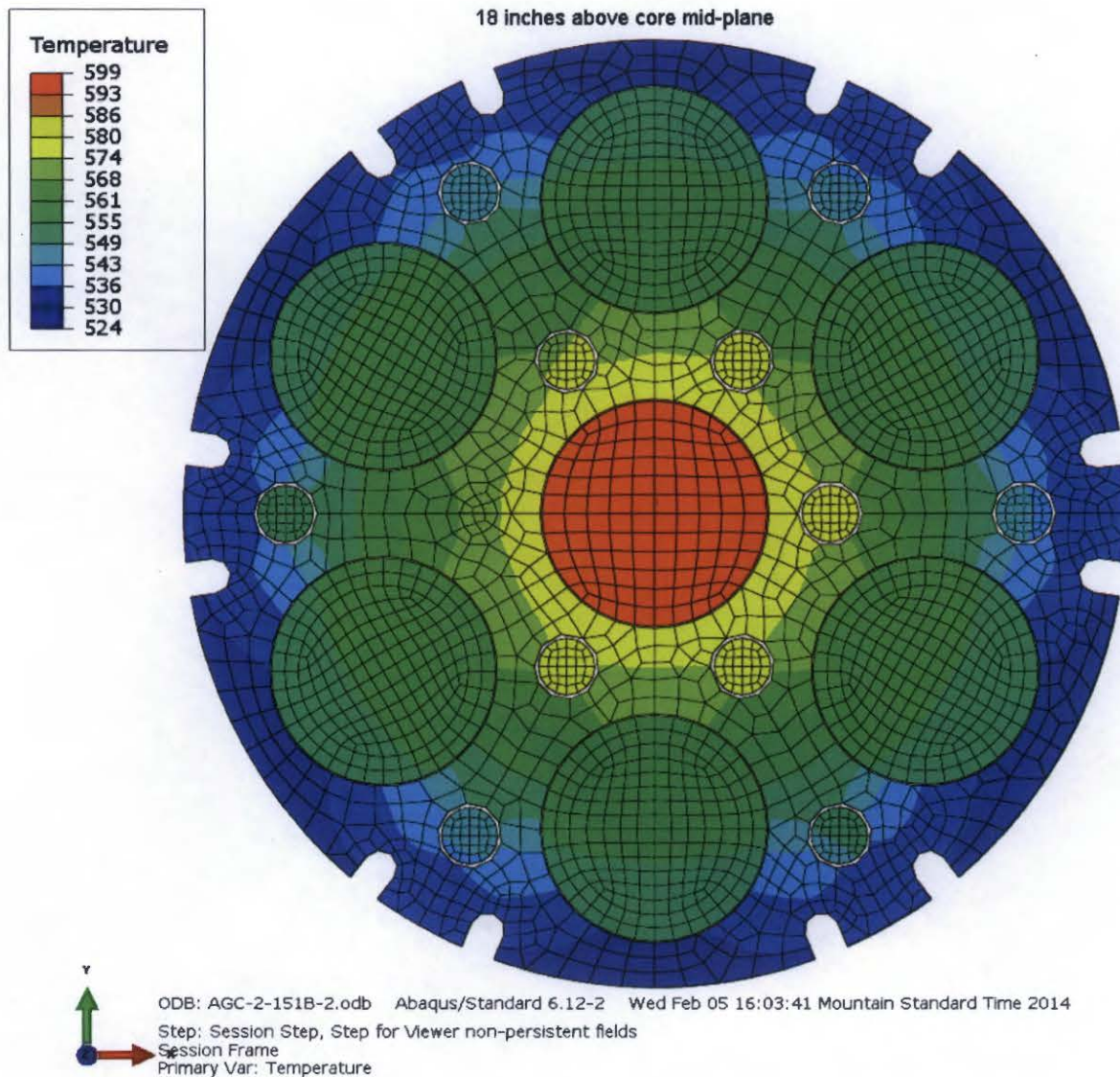


Figure 5. Temperature (°C) of experiment cross-section at 18 inches above core mid-plane.

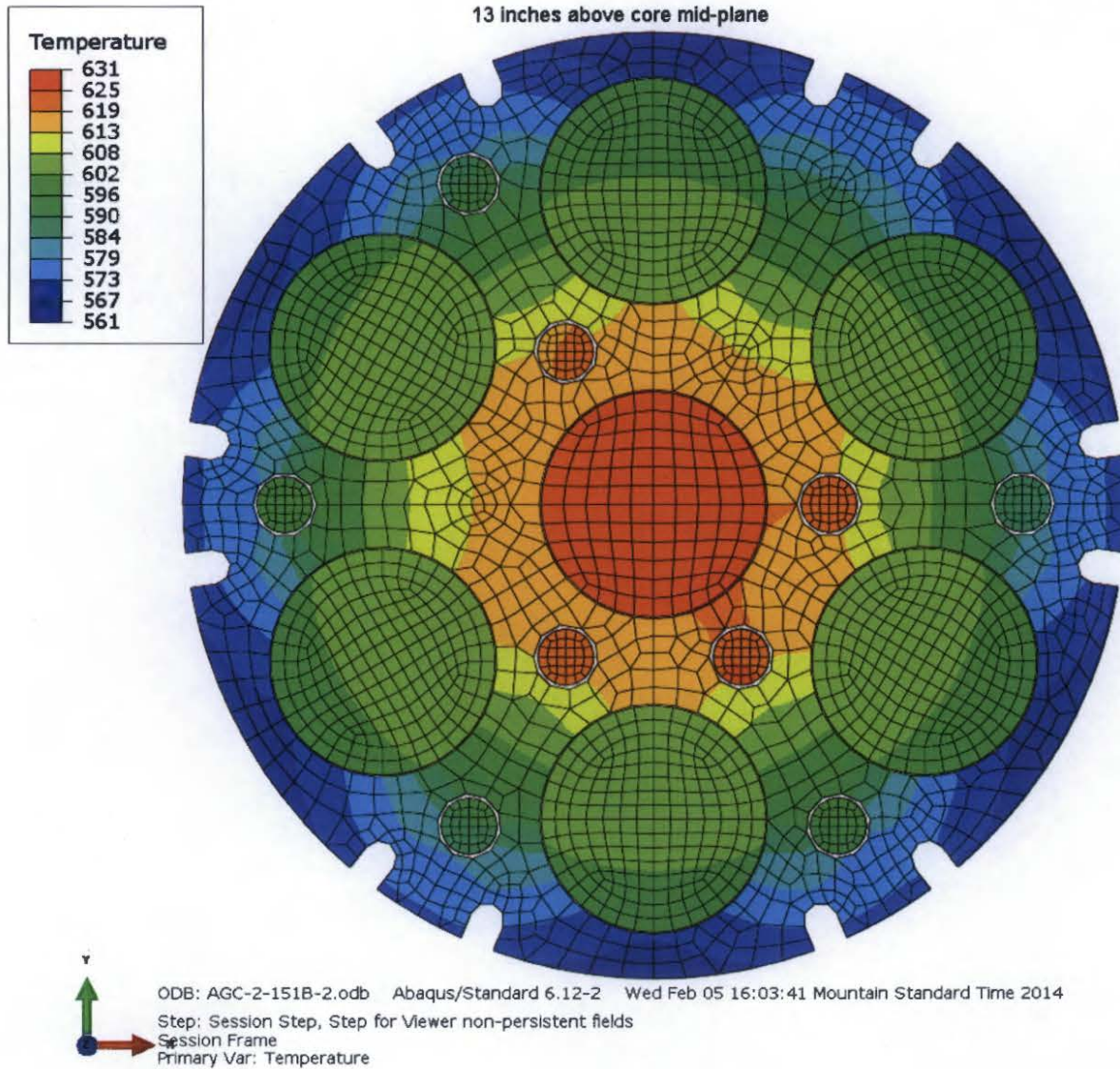


Figure 6. Temperature (°C) of experiment cross-section at 13 inches above core mid-plane.

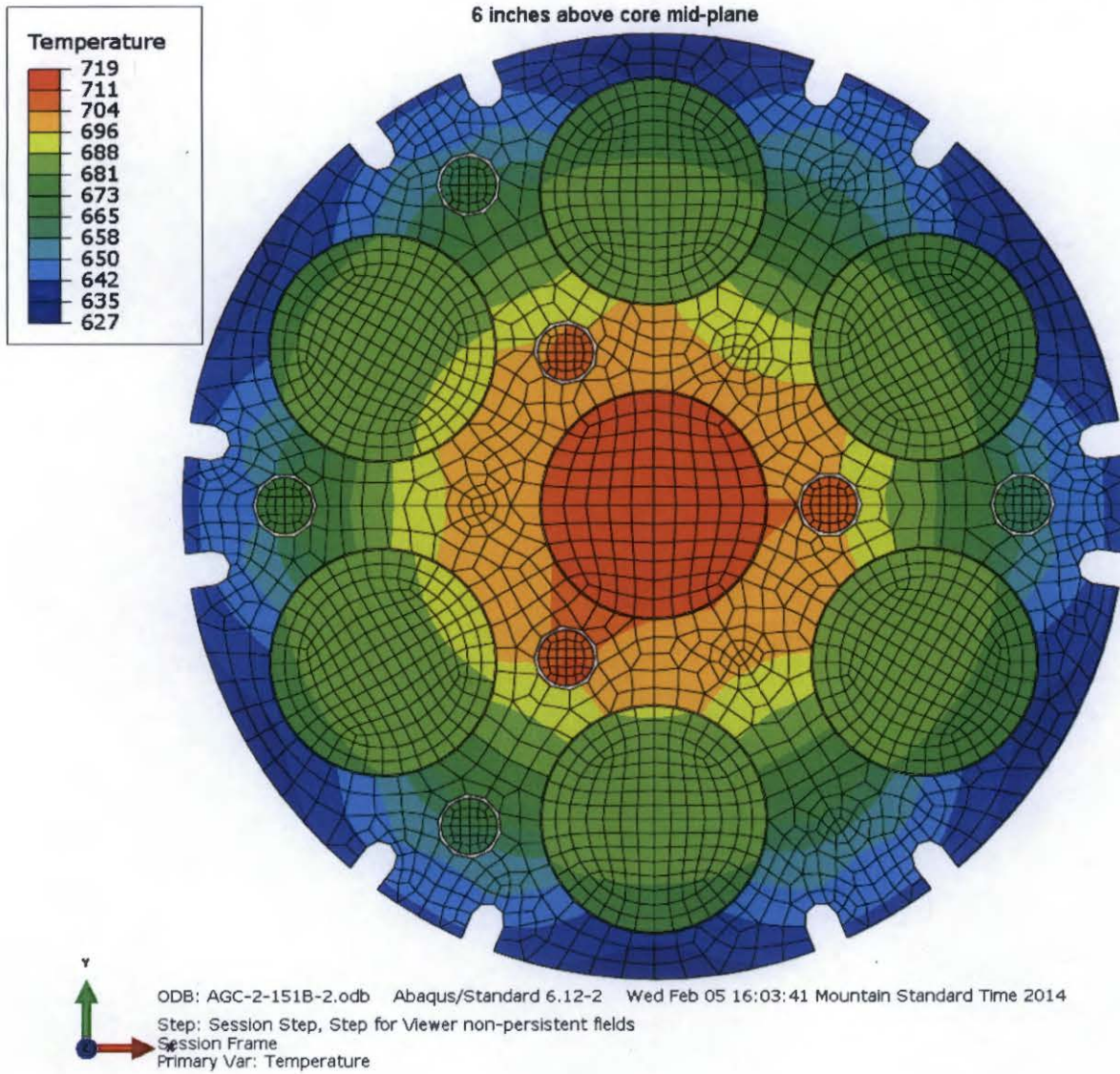


Figure 7. Temperature (°C) of experiment cross-section at 6 inches above core mid-plane.

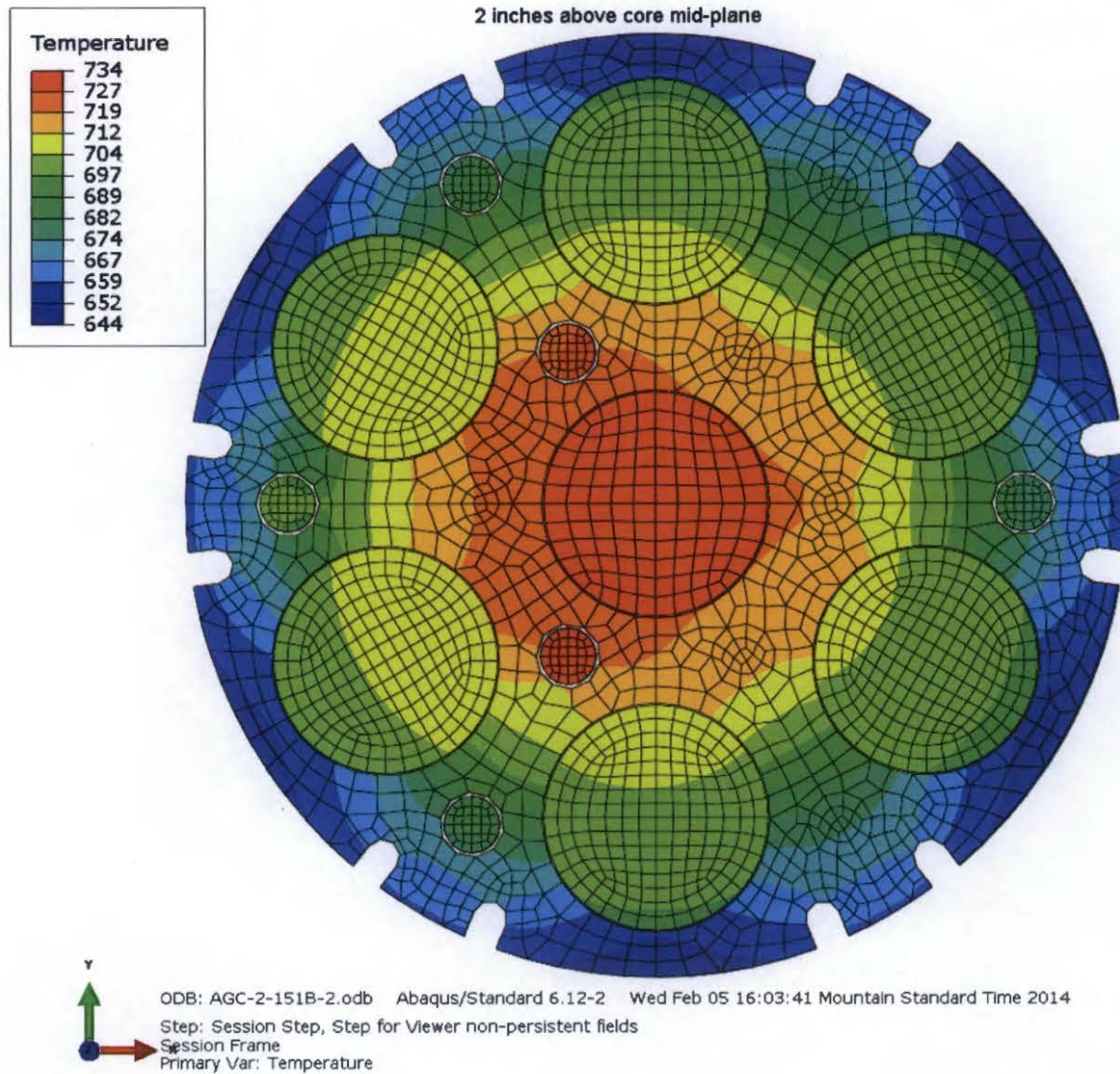


Figure 8. Temperature (°C) of experiment cross-section at 2 inches above core mid-plane.

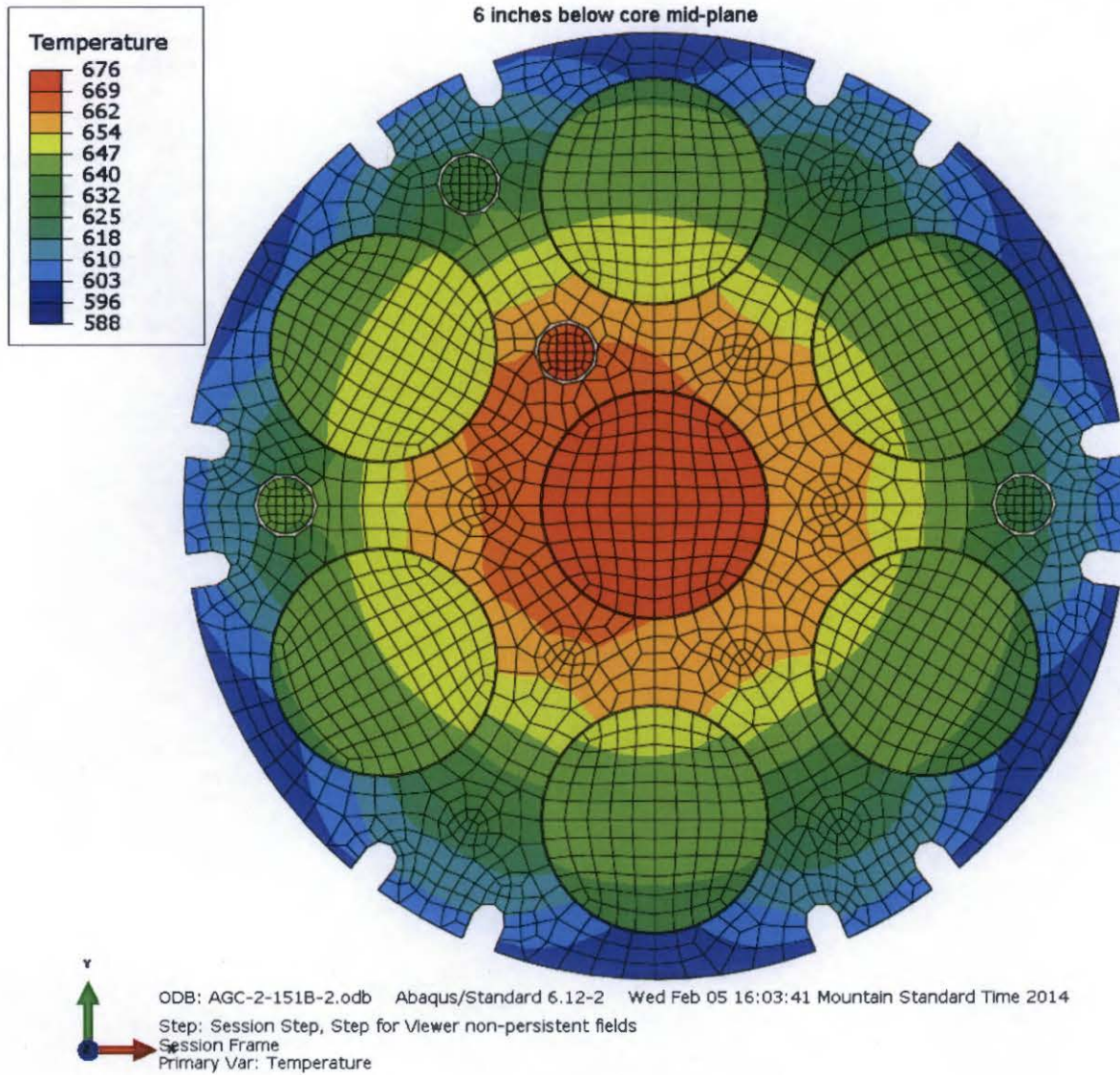


Figure 9. Temperature ($^{\circ}\text{C}$) of experiment cross-section at 6 inches below core mid-plane.

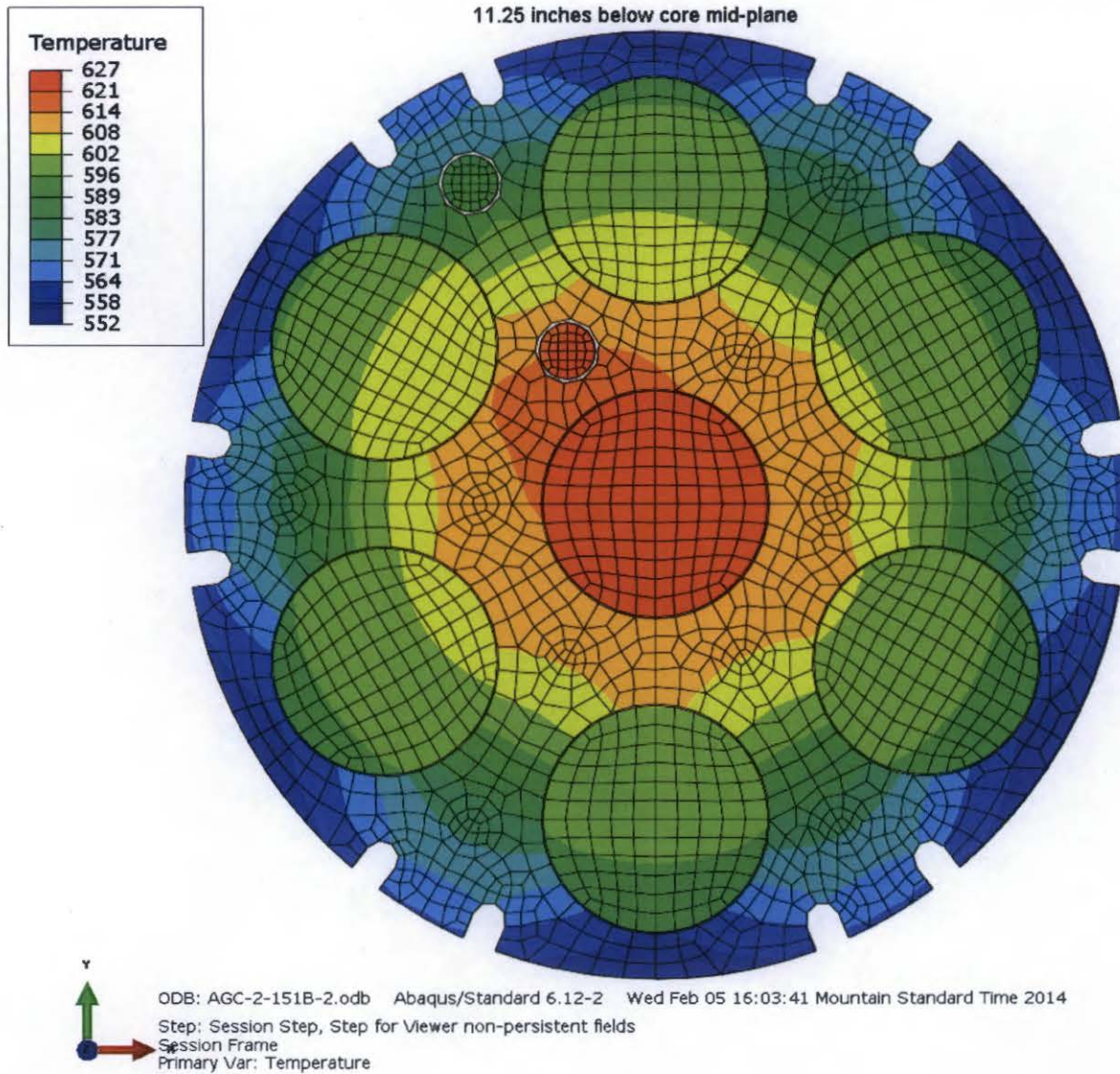


Figure 10. Temperature (°C) of experiment cross-section at 11.25 inches below core mid-plane.

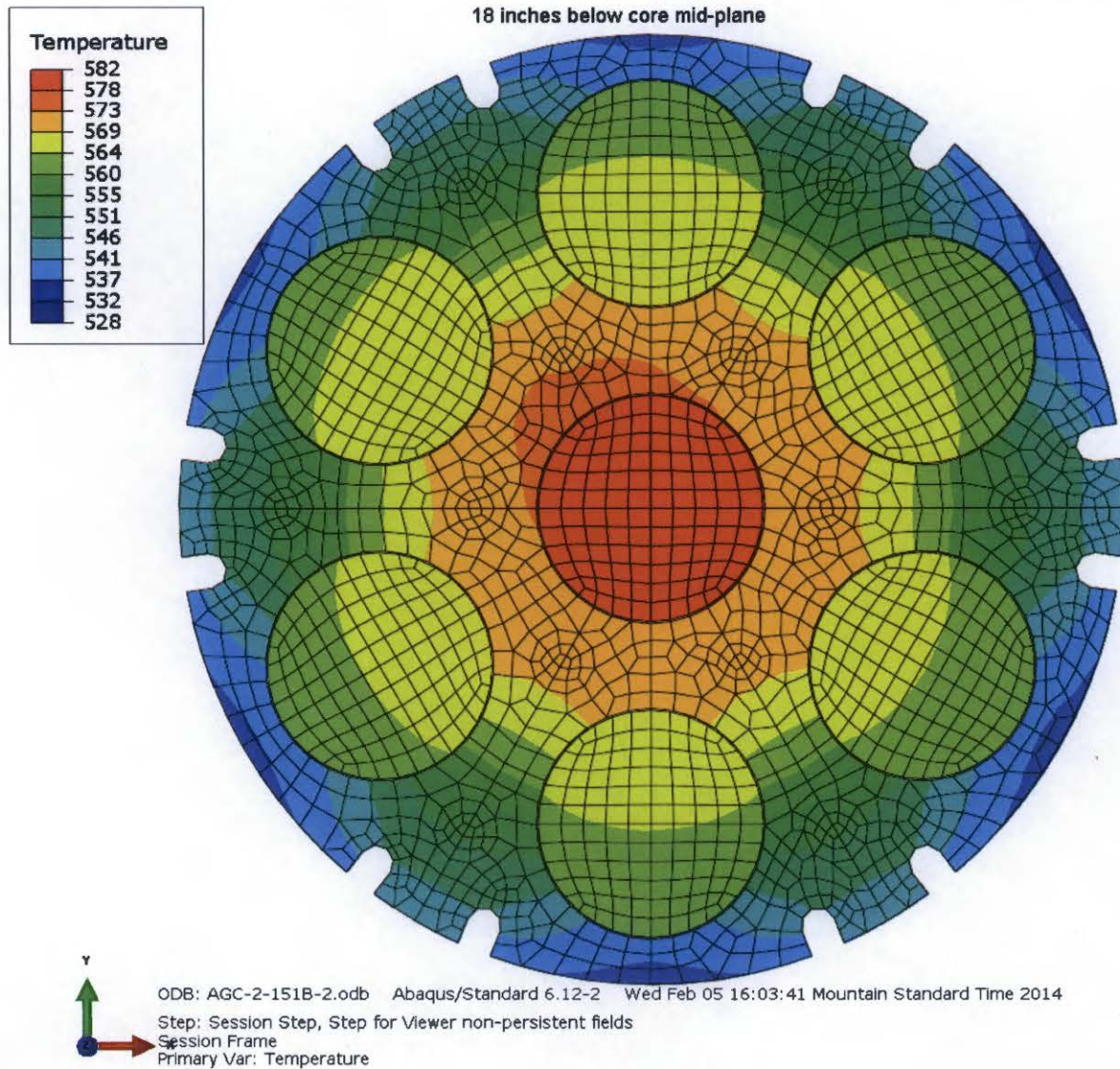


Figure 11. Temperature (°C) of experiment cross-section at 18 inches below core mid-plane.

Comparisons of the measured and calculated temperatures ($^{\circ}\text{C}$) of each thermocouple in the test train, during all irradiation cycles, are shown in Figs. 12 – 23. The maximum difference between the measured and calculated temperature is 35°C , while in all cases except one the difference is within $\pm 30^{\circ}\text{C}$.

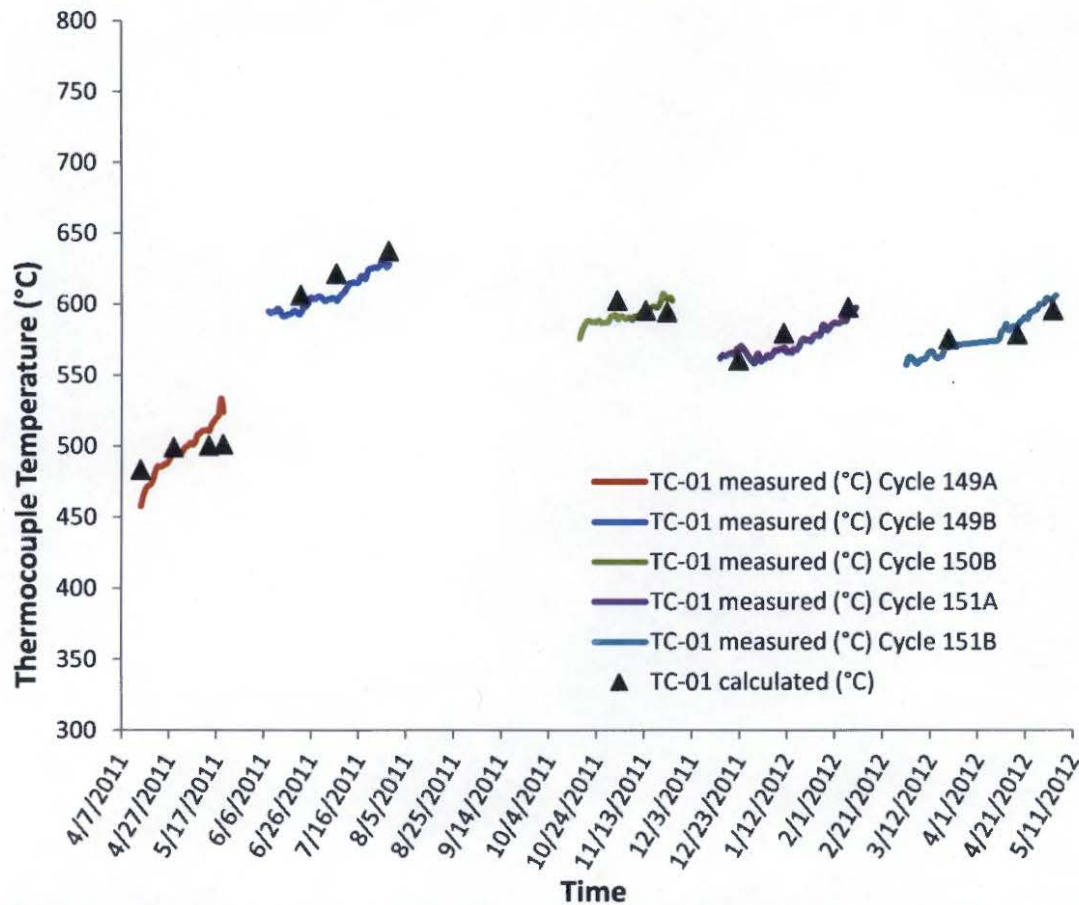


Figure 12. Measured and calculated temperature ($^{\circ}\text{C}$) of TC-01 (18 inches above core mid-plane) during all irradiation cycles.

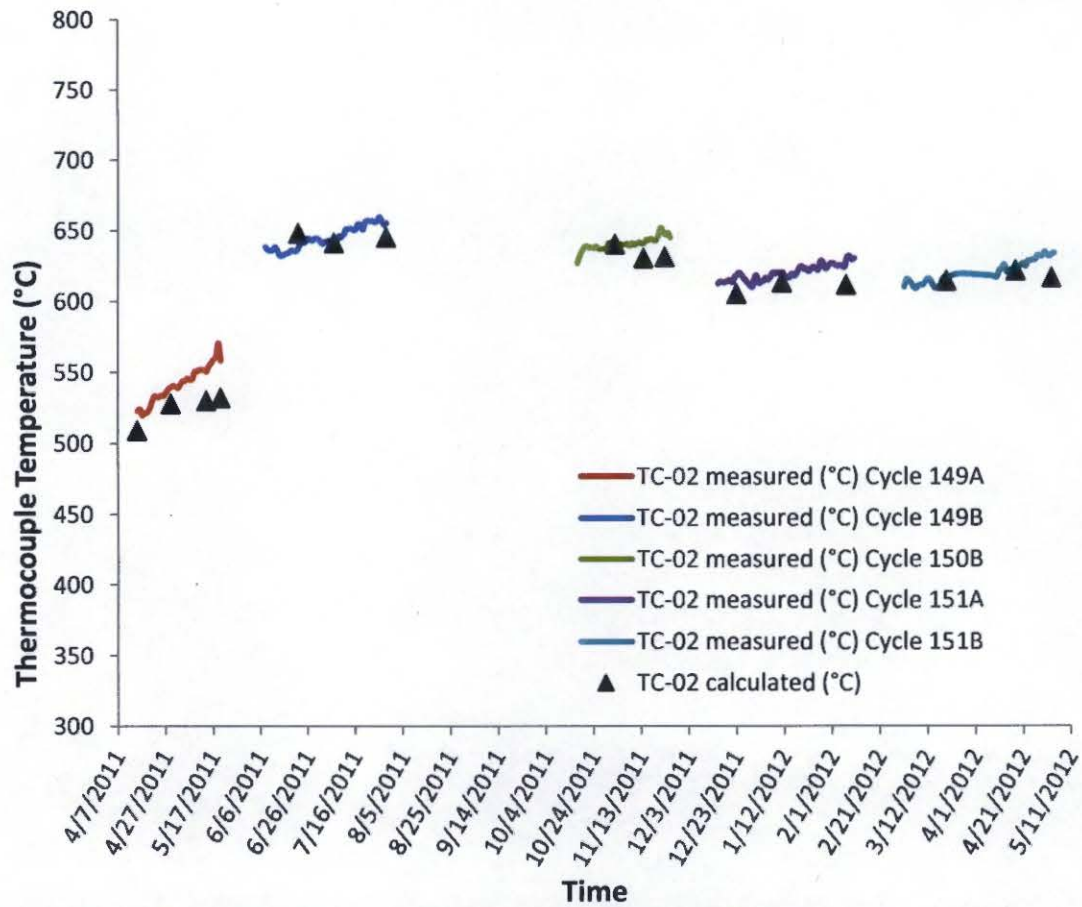


Figure 13. Measured and calculated temperature (°C) of TC-02 (13 inches above core mid-plane) during all irradiation cycles.

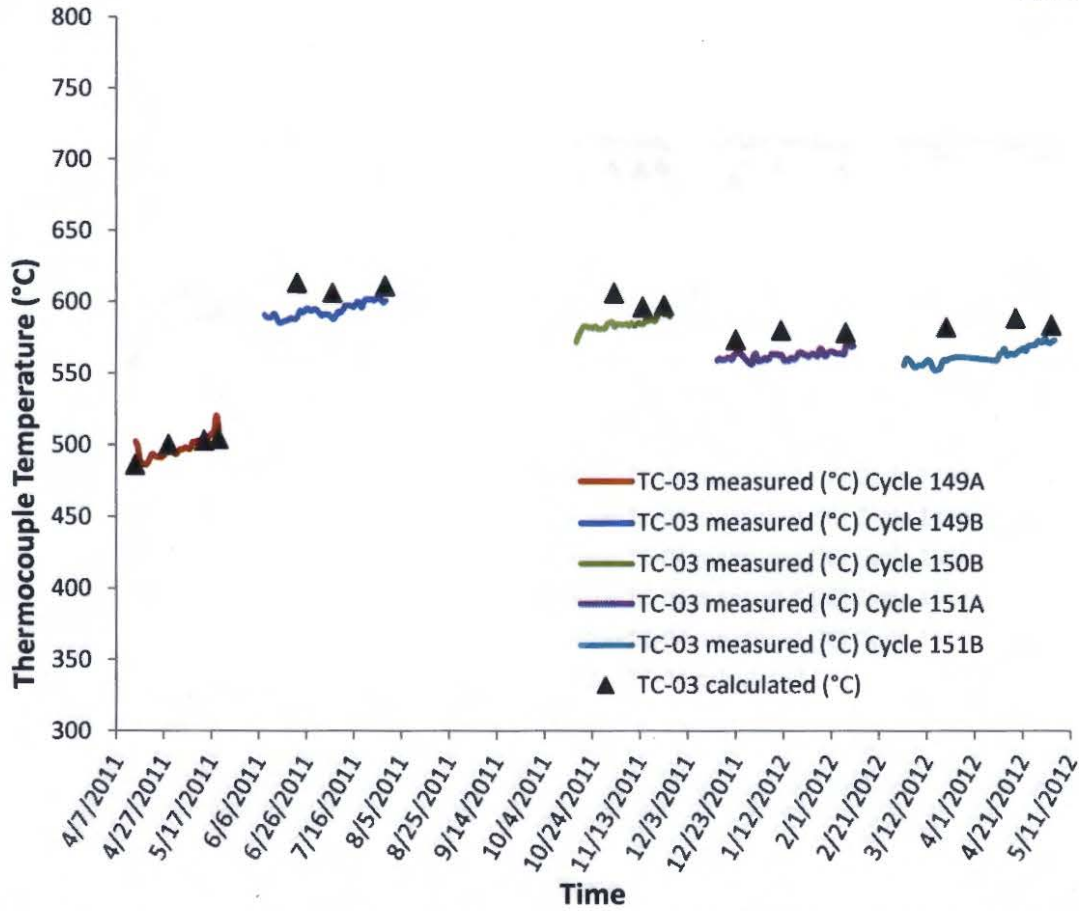


Figure 14. Measured and calculated temperature (°C) of TC-03 (13 inches above core mid-plane) during all irradiation cycles.

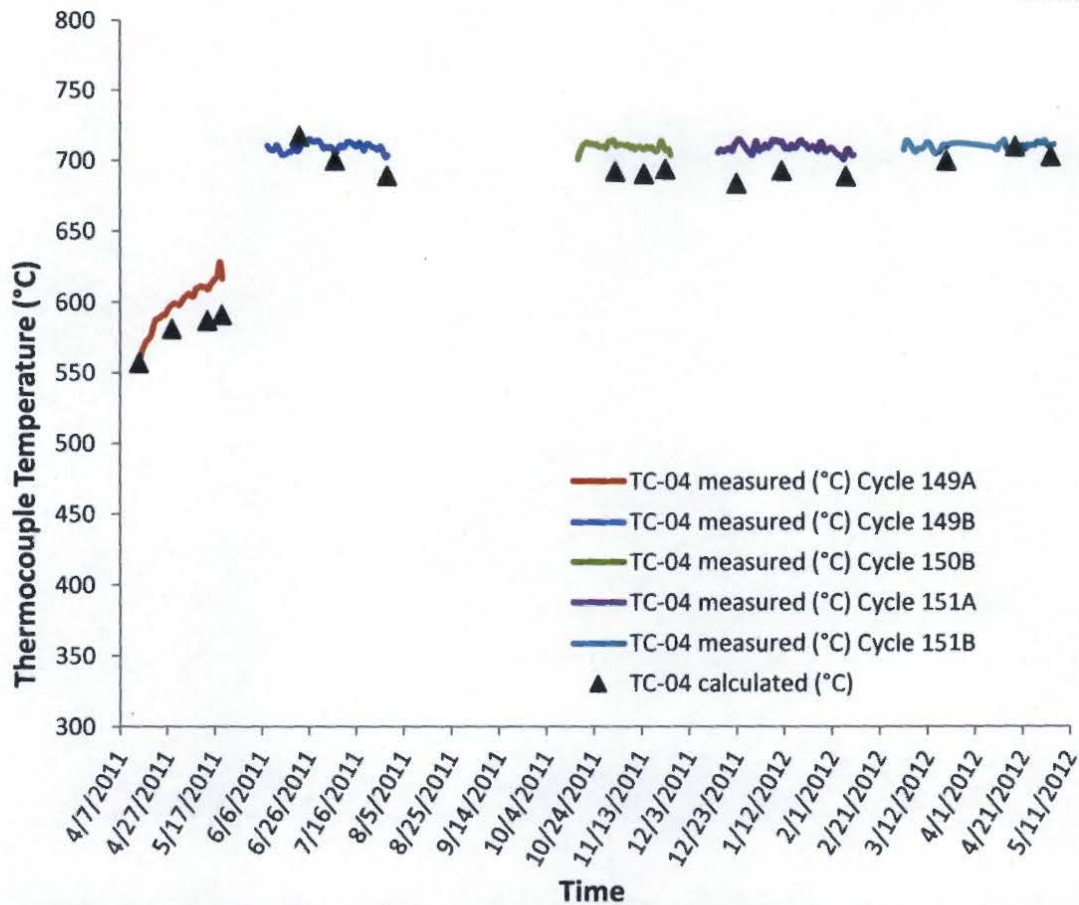


Figure 15. Measured and calculated temperature (°C) of TC-04 (6 inches above core mid-plane) during all irradiation cycles.

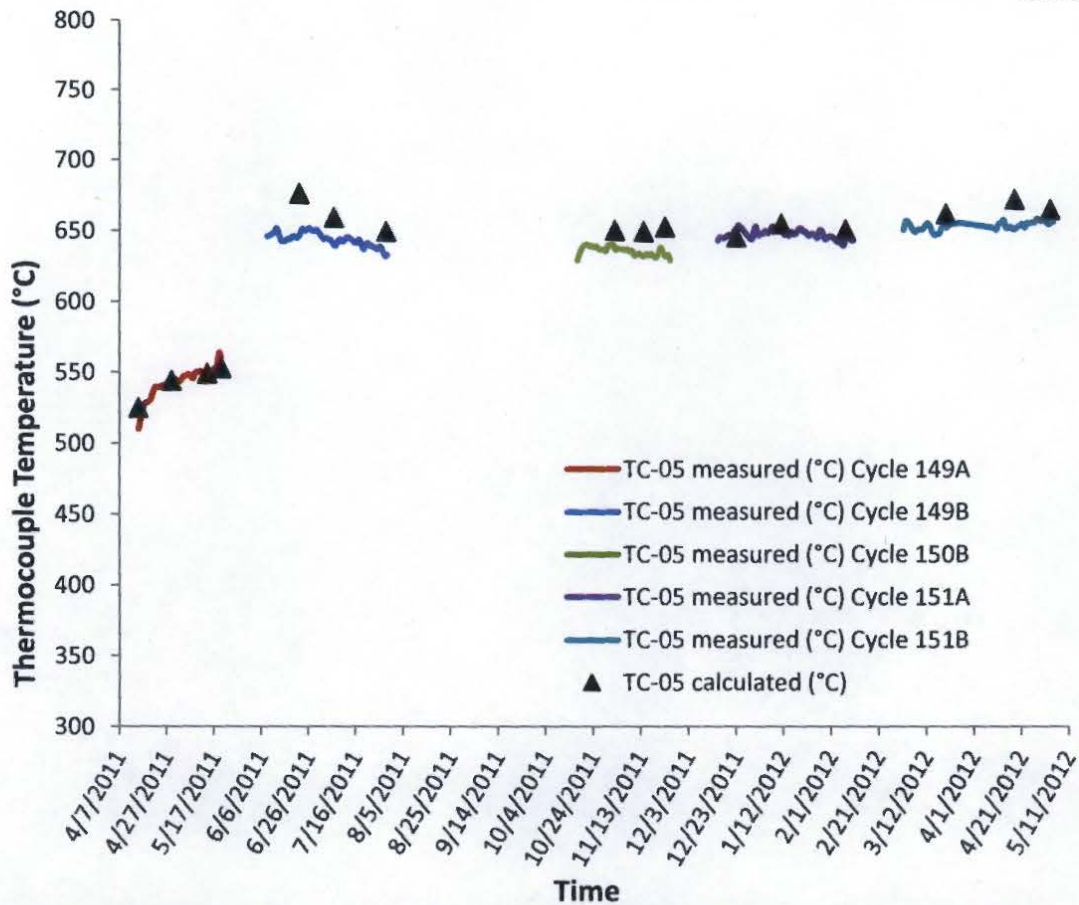


Figure 16. Measured and calculated temperature (°C) of TC-05 (6 inches above core mid-plane) during all irradiation cycles.

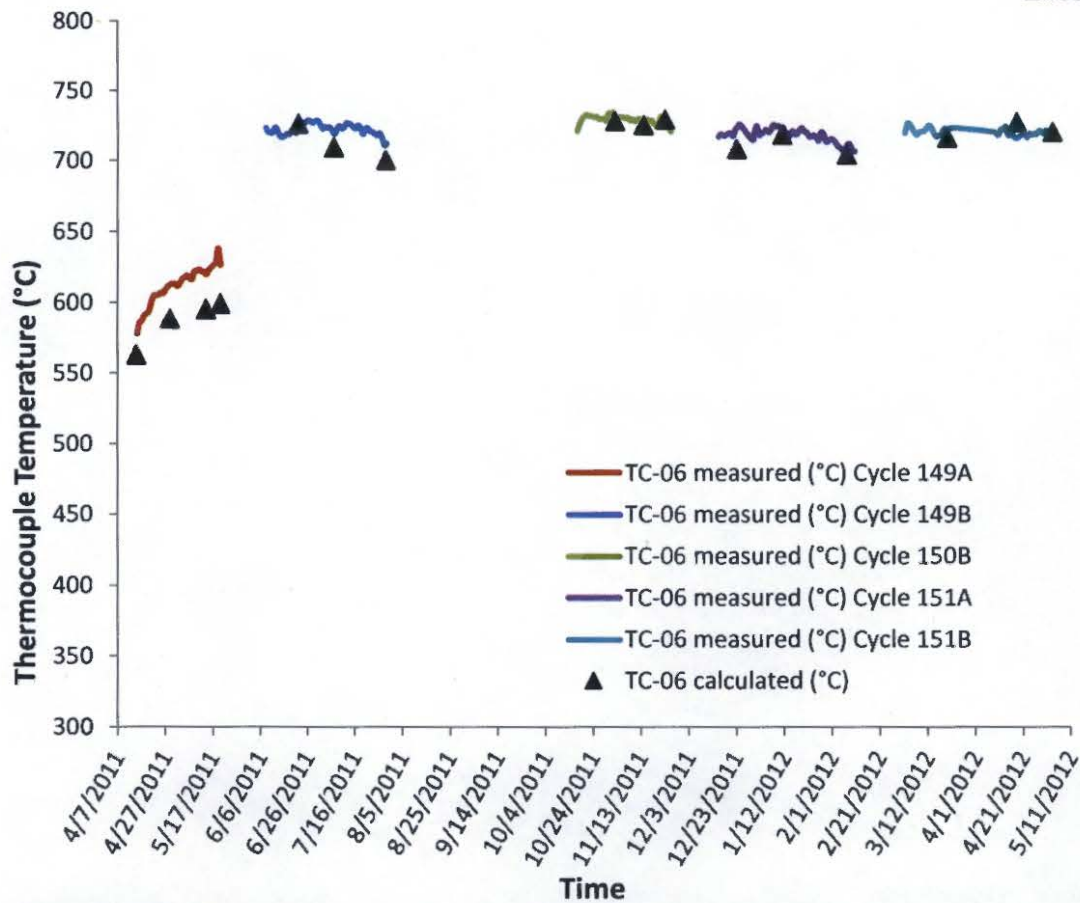


Figure 17. Measured and calculated temperature (°C) of TC-06 (2 inches above core mid-plane) during all irradiation cycles.

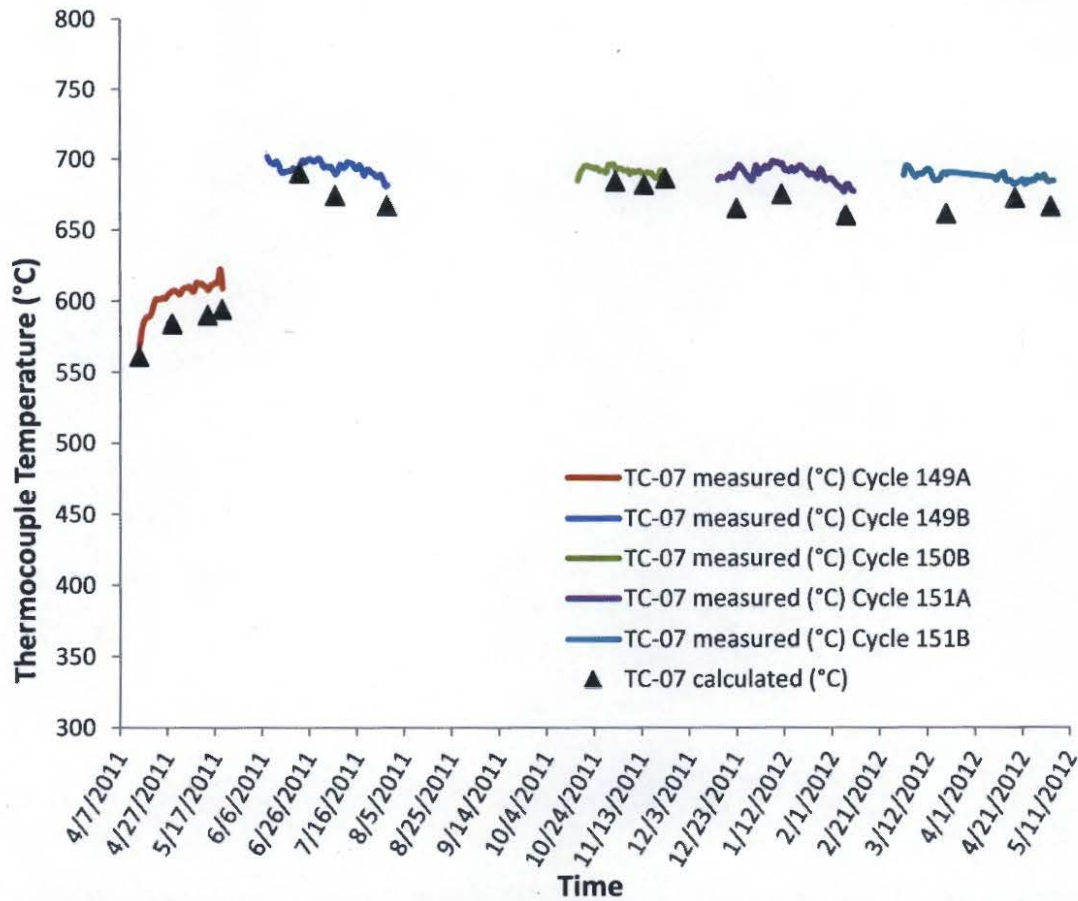


Figure 18. Measured and calculated temperature (°C) of TC-07 (6 inches below core mid-plane) during all irradiation cycles.

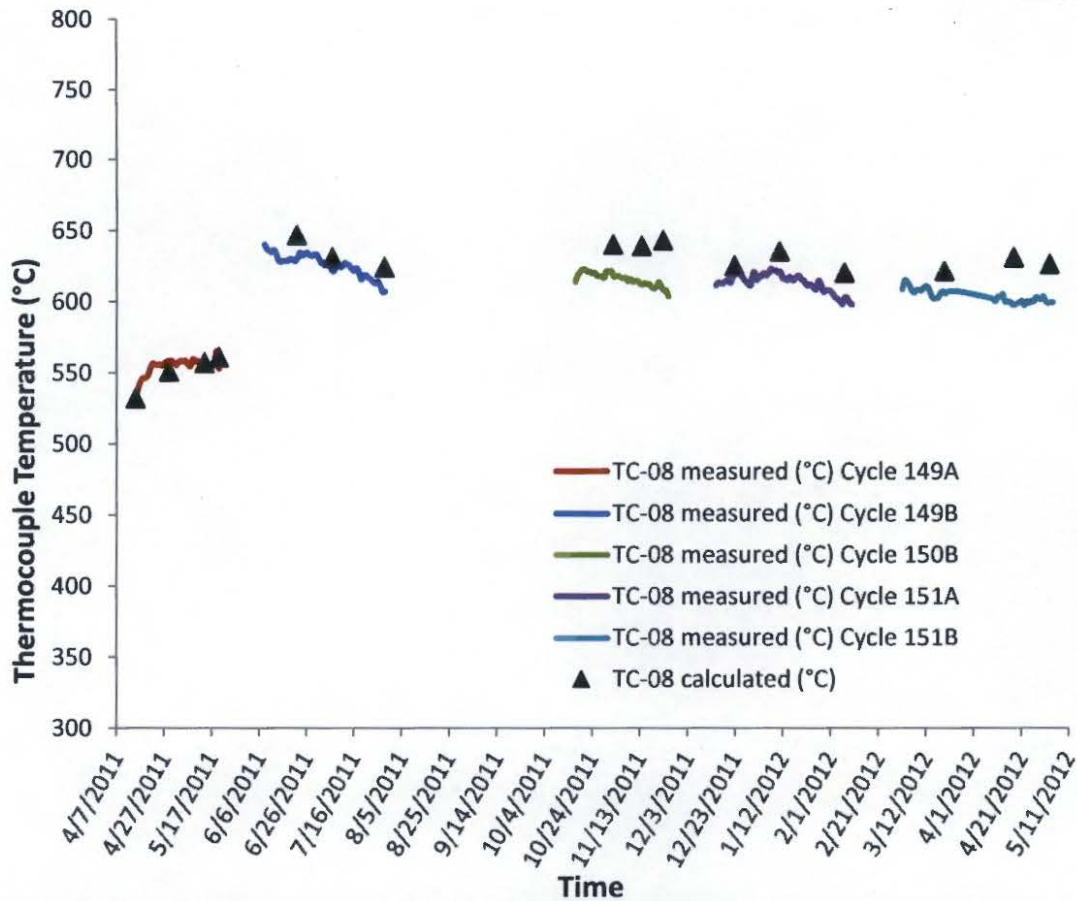


Figure 19. Measured and calculated temperature (°C) of TC-08 (6 inches below core mid-plane) during all irradiation cycles.

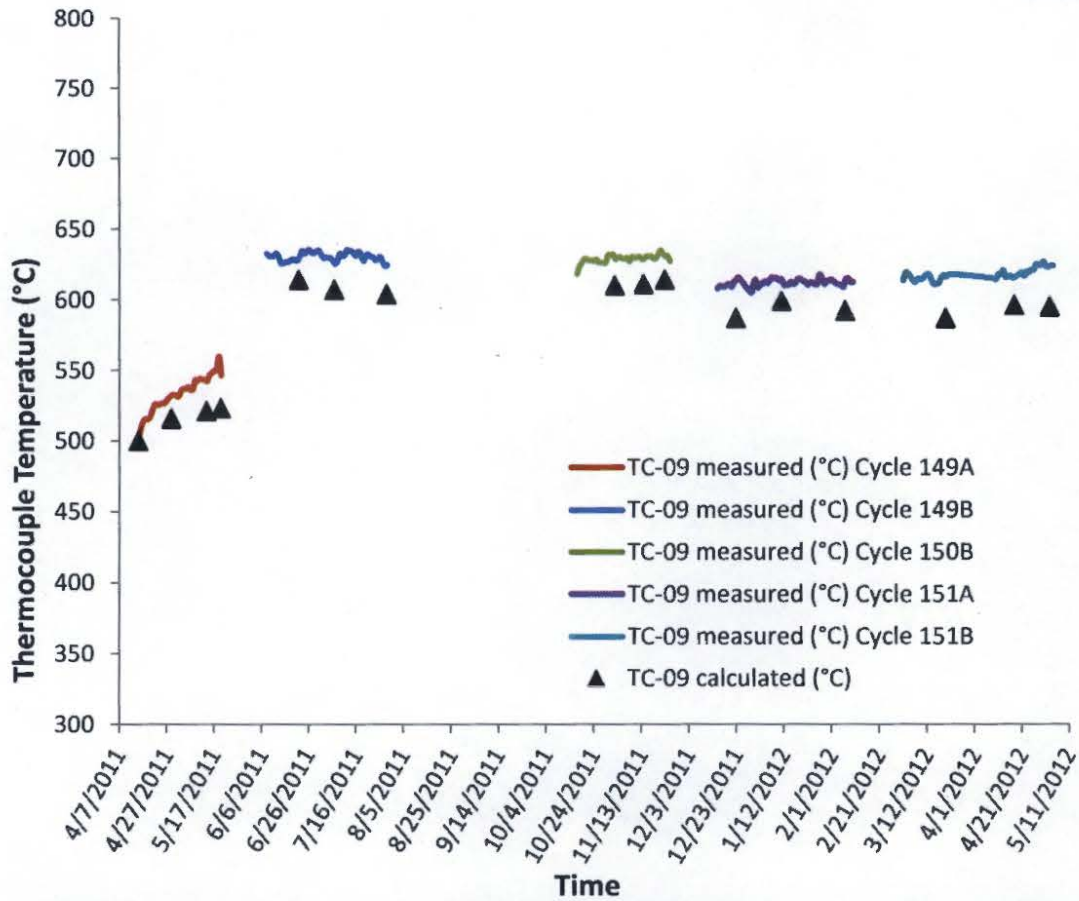


Figure 20. Measured and calculated temperature (°C) of TC-09 (11.25 inches below core mid-plane) during all irradiation cycles.

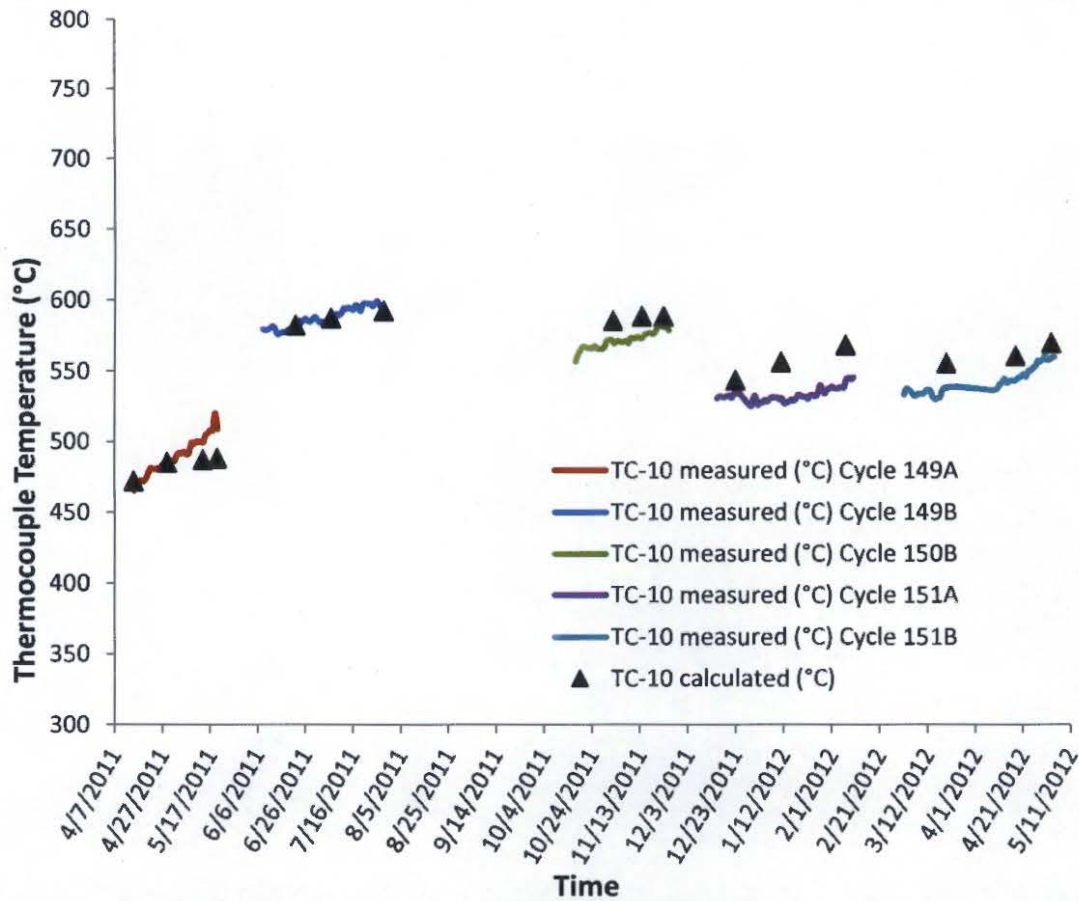


Figure 21. Measured and calculated temperature (°C) of TC-10 (18 inches below core mid-plane) during all irradiation cycles.

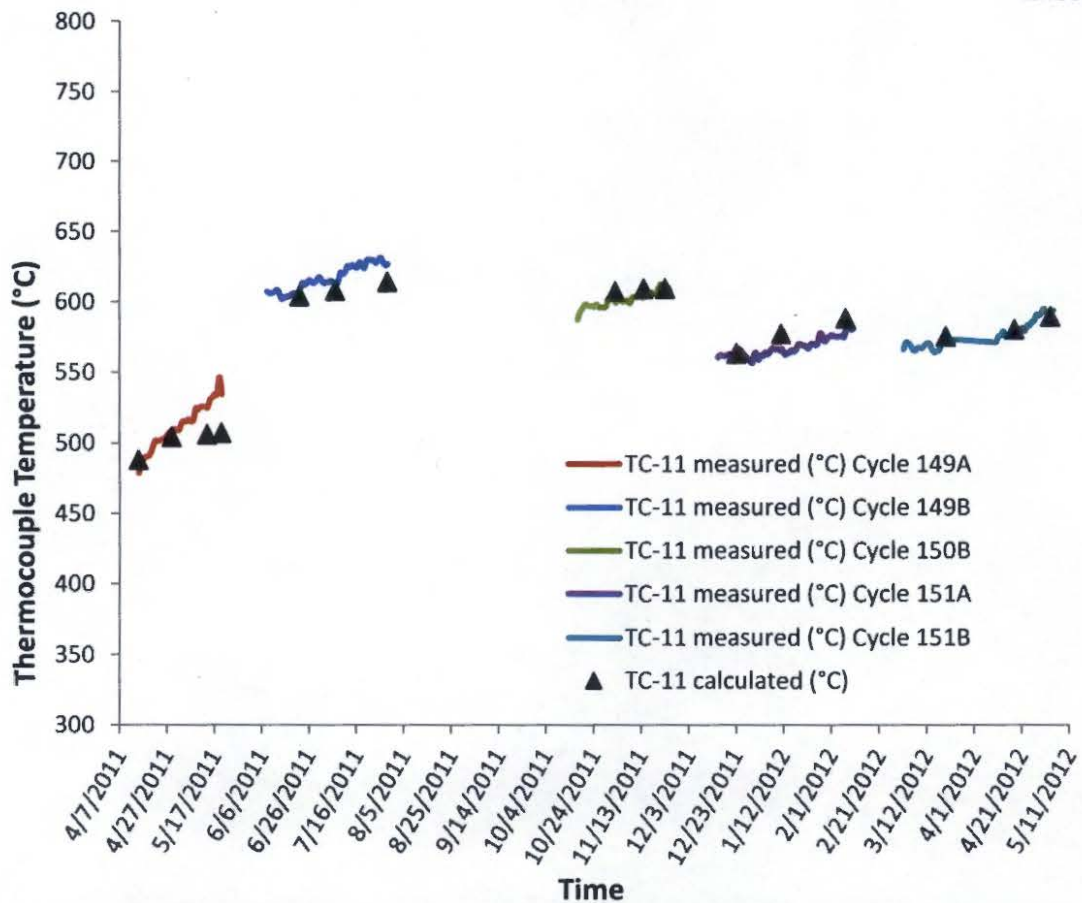


Figure 22. Measured and calculated temperature (°C) of TC-11 (18 inches below core mid-plane) during all irradiation cycles.

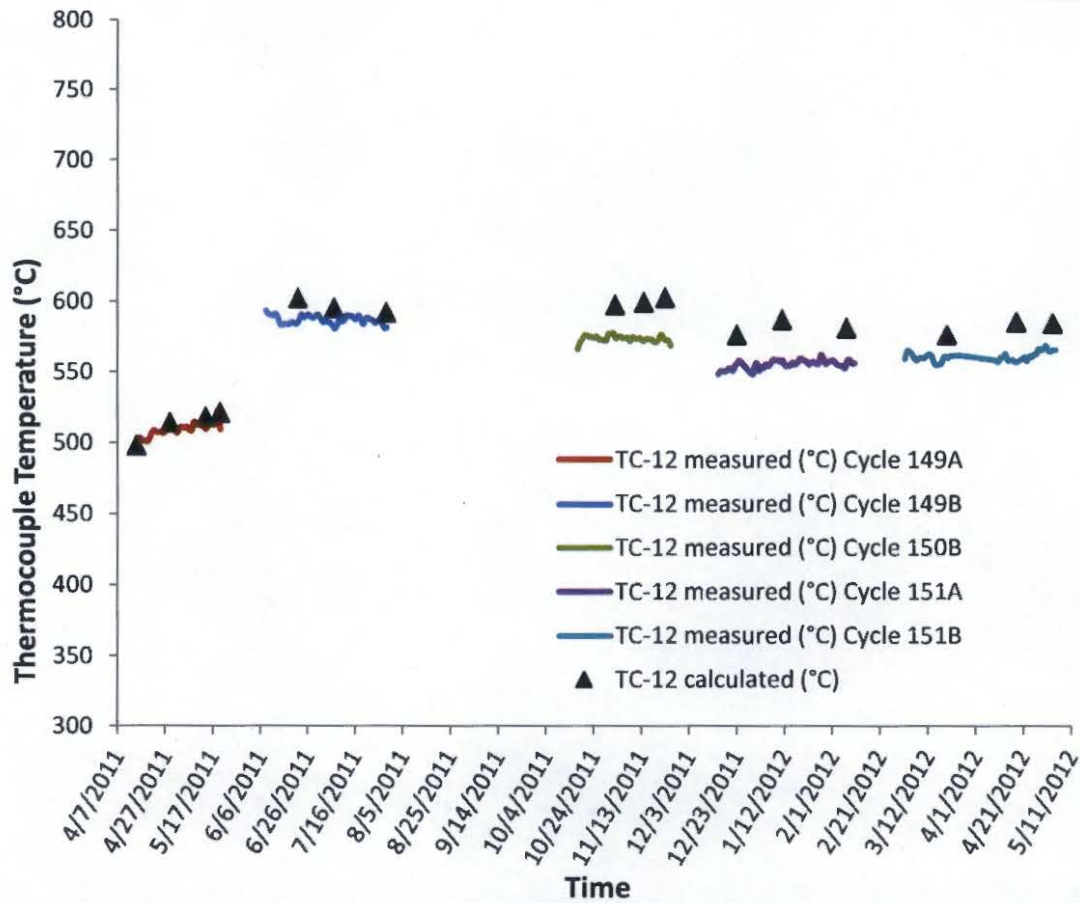


Figure 23. Measured and calculated temperature (°C) of TC-12 (11.25 inches below core mid-plane) during all irradiation cycles.

Plots of the axial distribution of volume-average temperature ($^{\circ}\text{C}$) of each specimen stack, during a selected day in each irradiation cycle, are shown in Figs. 24 – 28. For each creep specimen, the volume-average and time-average temperatures shall be maintained at $600^{\circ}\text{C} \pm 50^{\circ}\text{C}$ (TFR-645, Section 3.3.3). However, the results of this analysis show that temperature of the specimen stacks is outside the desired range at the bottom of the test train where temperature is less than the desired temperature and at core mid-plane where temperature is greater than the desired temperature. In most cases, temperature of the specimen stacks at core mid-plane is approximately 100°C greater than the desired temperature. Moreover, specimen temperature varies significantly with elevation because of the difficulty in attaining temperature uniformity using a single temperature control gas zone. The upturn in the axial temperature profile of the center stack is due to the presence of tungsten at the top of the center stack.

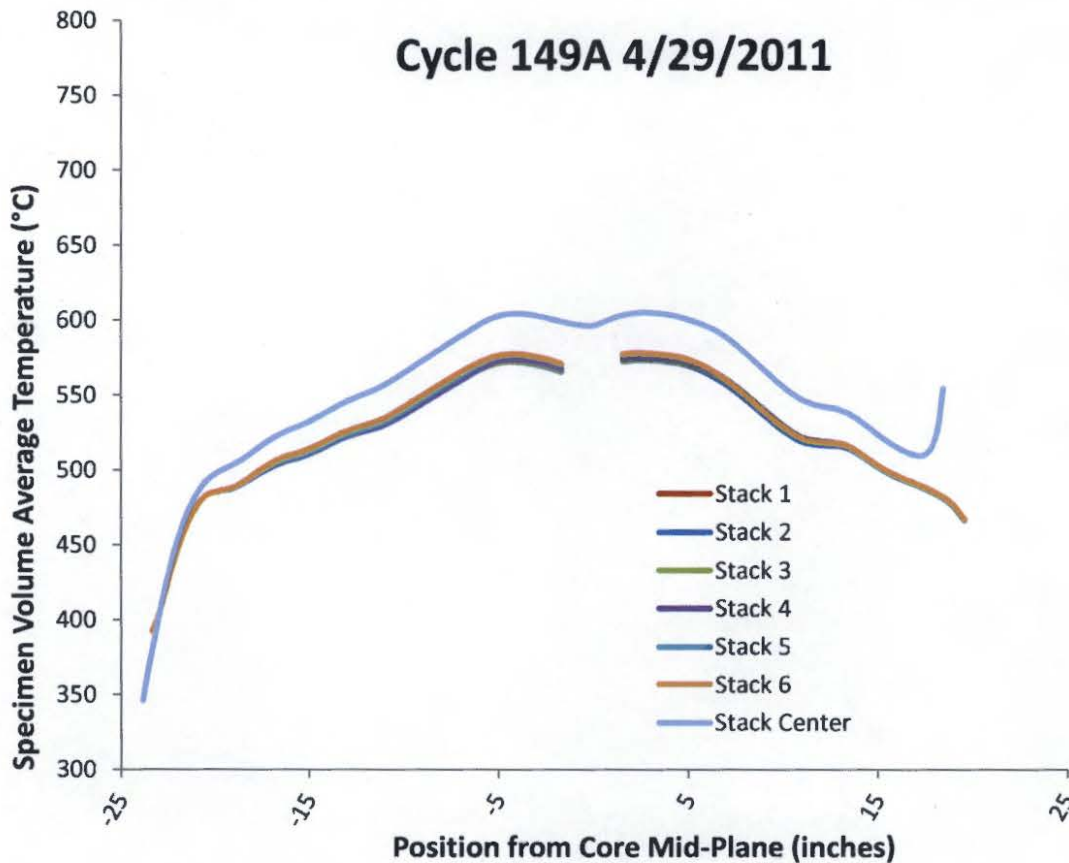


Figure 24. Distribution of specimen temperature ($^{\circ}\text{C}$) during a selected day in cycle 149A.

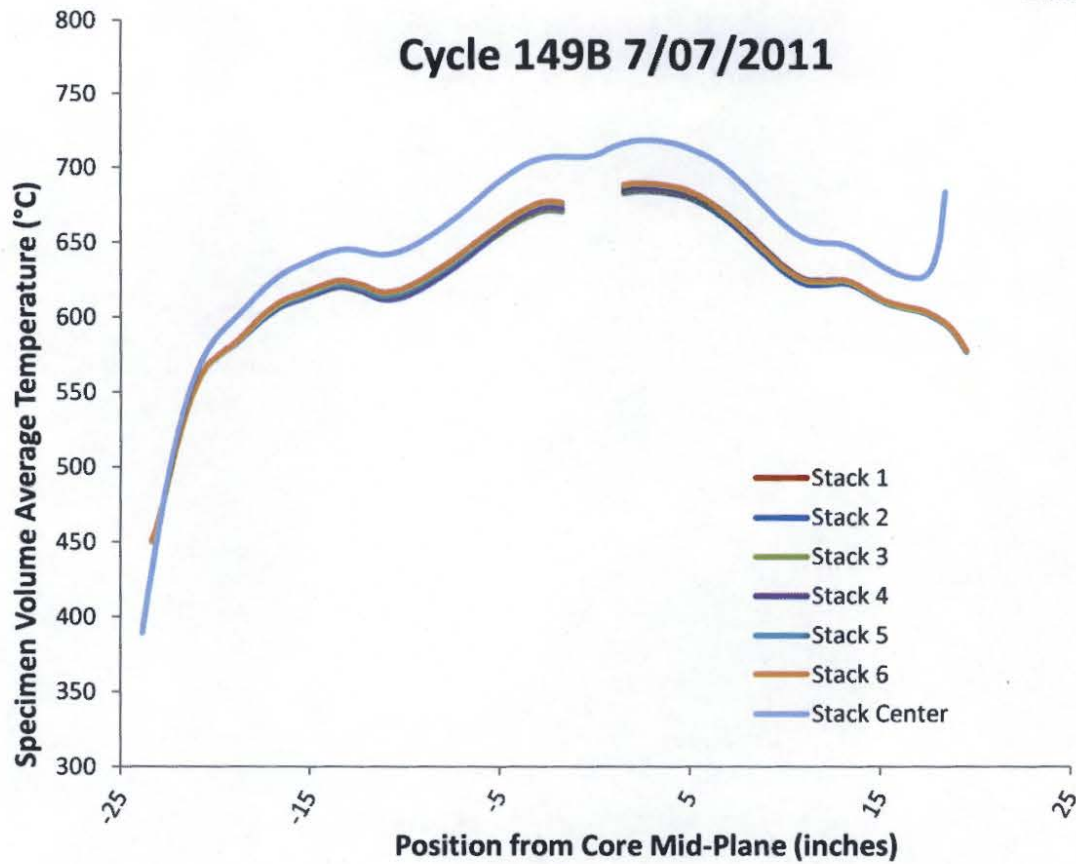


Figure 25. Distribution of specimen temperature (°C) during a selected day in cycle 149B.

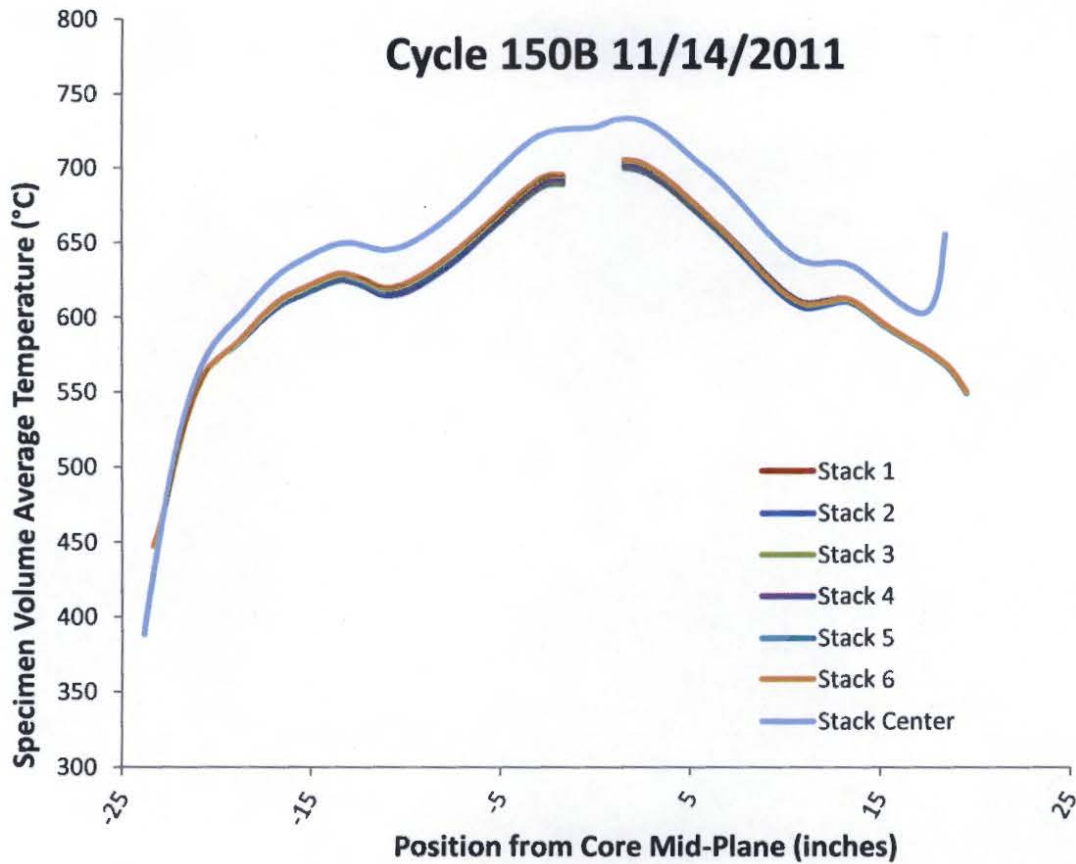


Figure 26. Distribution of specimen temperature (°C) during a selected day in cycle 150B.

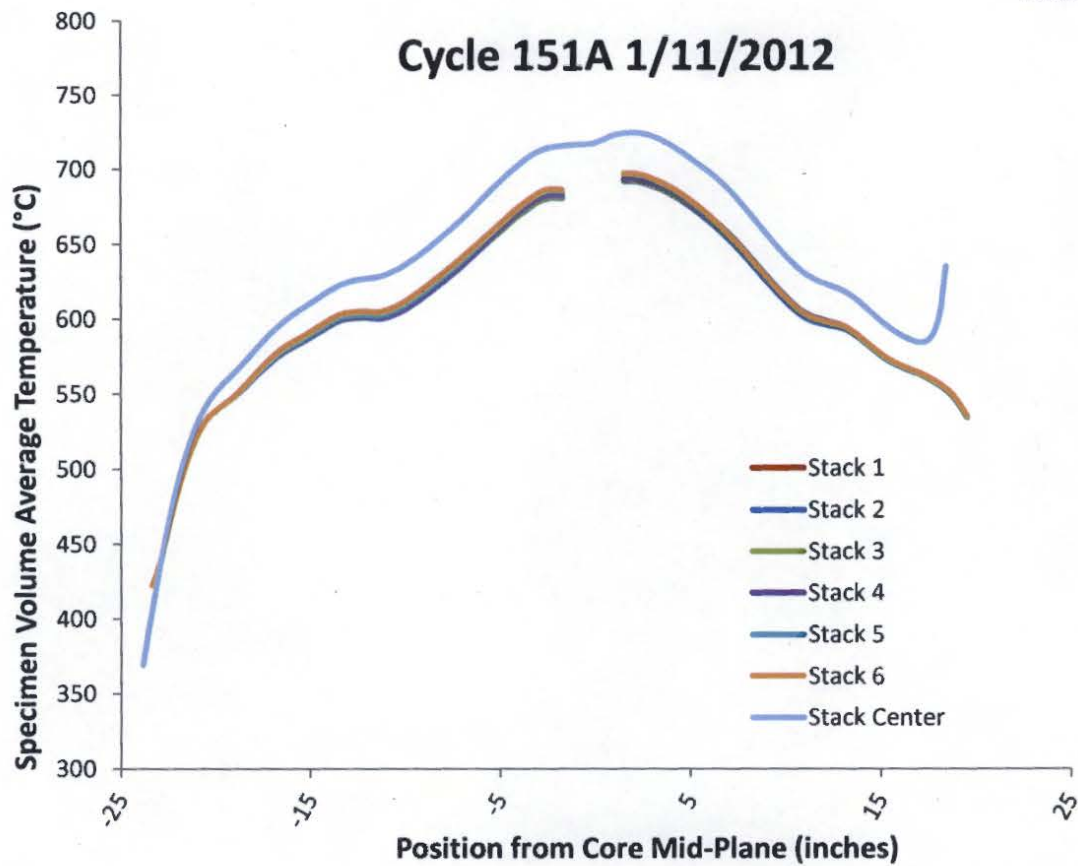


Figure 27. Distribution of specimen temperature (°C) during a selected day in cycle 151A.

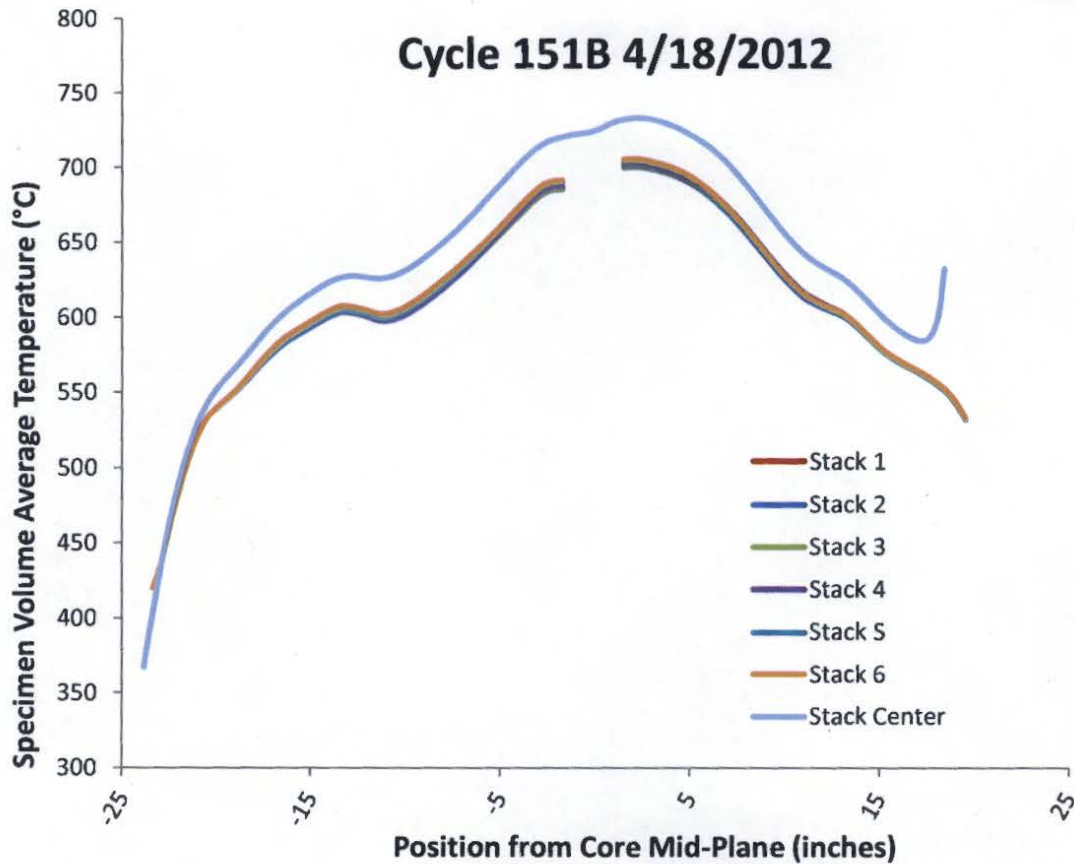


Figure 28. Distribution of specimen temperature (°C) during a selected day in cycle 151B.

CONCLUSIONS AND RECOMMENDATIONS

A finite element, steady-state heat transfer analysis of the entire AGC-2 test train was performed using ABAQUS. The analysis was performed at three selected days during each cycle, using the measured south source power, measured gas flows, as-run heating rates, and as-run graphite DPA, to obtain best-estimate temperatures of the specimens and thermocouples. In order to compensate for uncertainty in the gas gaps between heat shield and capsule, the model was adjusted in order to bring into agreement the measured and calculated thermocouple temperatures. The maximum difference between the measured and calculated temperature of each thermocouple in the test train is 35°C, while in all cases except one the difference is within $\pm 30^\circ\text{C}$.

The experiment requirements on temperature control are that the volume-average and time-average temperatures of each creep specimen shall be maintained at $600^\circ\text{C} \pm 50^\circ\text{C}$ (TFR-645, Section 3.3.3). However, the results of this analysis show that temperature of the specimen stacks is outside the desired range at the bottom of the test train where temperature is less than the desired temperature and at core mid-plane where temperature is greater than the desired temperature. In most cases, temperature of the specimen stacks at core mid-plane is approximately 100°C greater than the desired temperature. Moreover, specimen temperature varies significantly with elevation. This result is to be expected since the experiment includes only a single gas zone and relies on an axially varying temperature control gas gap to compensate for the axial variation in heating. Because of the high sensitivity of temperature to gas gap size, attainment of temperature uniformity is problematical in this case.

DATA FILES

The ABAQUS files containing the models created for this analysis are stored on the HPC file server in directory “/projects/atr_exp/AGC-2.” The files created for each analysis case are listed in Table 1.

Table 1. ABAQUS/CAE model files and ABAQUS input and output files.

File name	Description
AGC-2.cae, AGC-2.jnl	Model files for all cycles
AGC-2-149A-1.inp, AGC-2-149A-1.f, AGC-2-149A-1.odb	Analysis files for cycle 149A step 1
AGC-2-149A-2.inp, AGC-2-149A-2.f, AGC-2-149A-2.odb	Analysis files for cycle 149A step 2
AGC-2-149A-3.inp, AGC-2-149A-3.f, AGC-2-149A-3.odb	Analysis files for cycle 149A step 3
AGC-2-149A-4.inp, AGC-2-149A-4.f, AGC-2-149A-4.odb	Analysis files for cycle 149A step 4
AGC-2-149B-1.inp, AGC-2-149B-1.f, AGC-2-149B-1.odb	Analysis files for cycle 149B step 1
AGC-2-149B-2.inp, AGC-2-149B-2.f, AGC-2-149B-2.odb	Analysis files for cycle 149B step 2
AGC-2-149B-3.inp, AGC-2-149B-3.f, AGC-2-149B-3.odb	Analysis files for cycle 149B step 3
AGC-2-150B-1.inp, AGC-2-150B-1.f, AGC-2-150B-1.odb	Analysis files for cycle 150B step 1
AGC-2-150B-2.inp, AGC-2-150B-2.f, AGC-2-150B-2.odb	Analysis files for cycle 150B step 2
AGC-2-150B-3.inp, AGC-2-150B-3.f, AGC-2-150B-3.odb	Analysis files for cycle 150B step 3
AGC-2-151A-1.inp, AGC-2-151A-1.f, AGC-2-151A-1.odb	Analysis files for cycle 151A step 1
AGC-2-151A-2.inp, AGC-2-151A-2.f, AGC-2-151A-2.odb	Analysis files for cycle 151A step 2
AGC-2-151A-3.inp, AGC-2-151A-3.f, AGC-2-151A-3.odb	Analysis files for cycle 151A step 3
AGC-2-151B-1.inp, AGC-2-151B-1.f, AGC-2-151B-1.odb	Analysis files for cycle 151B step 1
AGC-2-151B-2.inp, AGC-2-151B-2.f, AGC-2-151B-2.odb	Analysis files for cycle 151B step 2
AGC-2-151B-3.inp, AGC-2-151B-3.f, AGC-2-151B-3.odb	Analysis files for cycle 151B step 3

REFERENCES

- ABAQUS Standard, Version 6.12-2, SIMULIA, Inc., Providence, RI, 2012.
- ASM Handbook Vol. 1: Properties and Selection: Irons, Steels, and High-Performance Alloys*, 10th Edition, American Society of Metals, 1990.
- ASM Handbook Vol. 2: Properties and Selection: Nonferrous Alloys and Special-Purpose Materials*, 10th Edition, American Society of Metals, 1990.
- ASM Engineered Materials Handbook Desk Edition*, 1st Edition, American Society of Metals, 1995.
- Biasetto, L., Manzolaro, M., and Andrighetto, A., "Emissivity measurements of opaque gray bodies up to 2000°C by a dual-frequency pyrometer," *The European Physics J. A* 38, p. 167-171, 2008.
- Davenport, M. E., "Advanced Graphite Capsule AGC-2 Experiment Test Train," TFR-645, Rev. 0, 2010.
- Dawson, H. F. and di Marzo, M., "Multi-Droplet Evaporative Cooling: Experimental Results," *AIChE Symposium Series Heat Transfer* 89(295), p. 122-131, 1993.
- Hawkes, G. L., "AGR-1 Daily As-run Thermal Analysis," ECAR-968, Rev. 3, 2012.
- Incropera, F. P. and DeWitt, D. P., *Fundamentals of Heat and Mass Transfer*, 5th ed., John Wiley & Sons, New York, 2002.
- Kaufman, N. C., Durney, J. L., Tappendorf, J. C., and Willis, J. B., "Reactor Physics Results From Low-Power Measurements in the Advanced Test Reactor," U. S. Atomic Energy Commission Report No. IN-1260, February, 1969.
- Marchenkov, E. I. and Shashkov, A. G., "Study of Thermal Conductivity of an He – Ar Mixture in the Temperature Range of 400 – 1500°K on an Installation With a Molybdenum Measuring Cell," *Journal of Engineering Physics and Thermophysics* 28(6), p. 725-731, 1975.
- Maruyama, T. and Harayama, M., "Neutron irradiation effect on the thermal conductivity and dimensional change of graphite materials," *J. Nuclear Materials* 195, p. 44-50, 1992.
- Mason, E. A. and von Ubisch, H., "Thermal Conductivities of Rare Gas Mixture," *Physics of Fluids* 3(3), p. 355-361, 1960.
- Maynard, R. K., "Total Hemispherical Emissivity of Very High Temperature Reactor (VHTR) Candidate Materials: Hastelloy X, Haynes 230, and Alloy 617," Ph.D. Dissertation, University of Missouri, 2011.
- Murray, P. E., "Validation of ABAQUS Standard 6.7-3 Heat Transfer," ECAR-131, Rev. 0, 2008.
- Murray, P. E., "Thermal Analysis of the AGC Thermocouple Experiment," ECAR-2429, Rev. 0, 2014.
- Oberg, E., Jones, F. D., Horton, H. L., Ryffell, H. H., *Machinery's Handbook*, 28th Edition, Industrial Press, 2008.
- Parry, J. R., "As-Run Physics Analysis for the AGC-2 Experiment Irradiated in the ATR," ECAR-2291, Rev. 0, 2013.
- Perry, R. H., and Green, D. W., *Perry's Chemical Engineers' Handbook*, 7th Edition, McGraw-Hill, 1997.
- Price, R. J., "Thermal Conductivity of Neutron-Irradiated Reactor Graphites," *Carbon* 13, p. 201-204, 1975.

Sully, A. H., Brandes, E. A., and Waterhouse, B. A., "Some measurements of the total emissivity of metals and pure refractory oxides and the variation of emissivity with temperature," British J. Applied Physics 3, p. 97-101, 1952.

Vreeling, J. A., Wouters, O., and van der Lann, J. G., "Graphite irradiation testing for HTR technology at the High Flux Reactor in Petten," J. Nuclear Materials 381, p. 68-75, 2008.

Windes, W., "Data Report on Post-Irradiation Dimensional Change in AGC-1 Samples," INL/EXT-12-26255, 2012.

DRAWINGS

601266, "ATR Advanced Graphite Capsule Number 2 (AGC-2) – Capsule Facility Assemblies," Rev. 2.

601258, "ATR Advanced Graphite Capsule Number 2 (AGC-2) – Capsule Specimen Holder Assemblies and Details," Rev. 1.

601256, "ATR Advanced Graphite Capsule Number 2 (AGC-2) – Specimen Stack-Up Arrangements," Rev. 1.

600786, "ATR Advanced Graphite Capsule (AGC-2) – Graphite Specimen Machining Details," Rev. 2.

630427, "ATR Advanced Graphite Capsule (AGC) – Specimen Holder and Insulator Details and Assemblies," Rev. 3.

601260, "ATR Advanced Graphite Capsule (AGC-2) – Heat Shield Detail," Rev. 1.

630434, "ATR Advanced Graphite Capsule (AGC) – Capsule Facility In-Core Pressure Boundary Tube," Rev. 1.

600862, "ATR Advanced Graphite Capsule (AGC) Gas Control System – Test Train Top Head Gas Line Interconnection Diagram," Rev. 2.

Appendix A - Hydrodynamics, heat transfer, and nuclear heating**A.1 Thermophysical properties**

Thermophysical properties of 304 and 304L austenitic stainless steel (Perry's Handbook, 7th edition, Table 2-375; Machinery's Handbook, 28th edition, p. 378):

$$T_S := \left(\frac{212}{932} \right) ^\circ\text{F}$$

$$\rho_{\text{SST}} := 0.29 \cdot \frac{\text{lb}}{\text{in}^3}$$

$$c_{p_SST} := 0.12 \cdot \frac{\text{BTU}}{\text{lb} \cdot \text{R}}$$

$$k_{304_SST} := \left(\frac{9.4}{12.4} \right) \cdot \frac{\text{BTU}}{\text{hr} \cdot \text{ft} \cdot \text{R}} \quad k_{304_SST} = \left(\frac{0.783}{1.033} \right) \cdot \frac{\text{BTU}}{\text{hr} \cdot \text{in} \cdot \text{R}}$$

Thermophysical properties of aluminum 6061 (Machinery's Handbook, p. 377):

$$\rho_{\text{AL}} := 0.098 \cdot \frac{\text{lb}}{\text{in}^3}$$

$$c_{p_AL} := 0.23 \cdot \frac{\text{BTU}}{\text{lb} \cdot \text{R}}$$

$$k_{\text{AL}} := 104 \cdot \frac{\text{BTU}}{\text{hr} \cdot \text{ft} \cdot \text{R}} \quad k_{\text{AL}} = 8.667 \cdot \frac{\text{BTU}}{\text{hr} \cdot \text{in} \cdot \text{R}}$$

Thermophysical properties of tungsten (ASM Metals Handbook Vol. 2,
Properties of Pure Metals - Tungsten):

$$\rho_W := 17.0 \cdot \frac{\text{gm}}{\text{cm}^3}$$

$$\rho_W = 0.614 \cdot \frac{\text{lb}}{\text{in}^3}$$

$$c_{p_W} := 0.131 \cdot \frac{\text{J}}{\text{gm} \cdot \text{K}}$$

$$c_{p_W} = 0.031 \cdot \frac{\text{BTU}}{\text{lb} \cdot \text{R}}$$

$$T_S := \begin{pmatrix} 500 \\ 1000 \\ 1500 \end{pmatrix} \cdot \text{K}$$

$$T_S = \begin{pmatrix} 440 \\ 1340 \\ 2240 \end{pmatrix} \cdot ^\circ\text{F}$$

$$k_W := \begin{pmatrix} 150 \\ 125 \\ 110 \end{pmatrix} \cdot \frac{\text{W}}{\text{m} \cdot \text{K}}$$

$$k_W = \begin{pmatrix} 7.22 \\ 6.02 \\ 5.3 \end{pmatrix} \cdot \frac{\text{BTU}}{\text{hr} \cdot \text{in} \cdot \text{R}}$$

Thermophysical properties of glass ceramic (Macor Machinable Glass Ceramic
Technical Data, Corning Inc., Corning, NY):

$$\rho_{\text{Macor}} := 2.52 \cdot \frac{\text{gm}}{\text{cm}^3}$$

$$\rho_{\text{Macor}} = 0.091 \cdot \frac{\text{lb}}{\text{in}^3}$$

$$c_{p_Macor} := 0.790 \cdot \frac{\text{J}}{\text{gm} \cdot \text{K}}$$

$$c_{p_Macor} = 0.189 \cdot \frac{\text{BTU}}{\text{lb} \cdot \text{R}}$$

$$k_{\text{Macor}} := 1.46 \cdot \frac{\text{W}}{\text{m} \cdot \text{K}}$$

$$k_{\text{Macor}} = 0.0703 \cdot \frac{\text{BTU}}{\text{hr} \cdot \text{in} \cdot \text{R}}$$

Thermophysical properties of zirconia (ASM Engineered Materials Handbook
Desk Edition, Engineering Tables - Ceramics and Glasses):

$$\rho_{\text{ZrO}_2} := 5.65 \cdot \frac{\text{gm}}{\text{cm}^3}$$

$$\rho_{\text{ZrO}_2} = 0.204 \cdot \frac{\text{lb}}{\text{in}^3}$$

$$c_{p_ZrO_2} := 0.590 \cdot \frac{\text{J}}{\text{gm} \cdot \text{K}}$$

$$c_{p_ZrO_2} = 0.141 \cdot \frac{\text{BTU}}{\text{lb} \cdot \text{R}}$$

$$k_{\text{ZrO}_2} := 2.1 \cdot \frac{\text{W}}{\text{m} \cdot \text{K}}$$

$$k_{\text{ZrO}_2} = 0.101 \cdot \frac{\text{BTU}}{\text{hr} \cdot \text{in} \cdot \text{R}}$$

Thermophysical properties of nuclear-grade graphite:

$$\rho_g := 1.822 \frac{\text{gm}}{\text{cm}^3}$$

$$\rho_g = 0.0658 \frac{\text{lb}}{\text{in}^3}$$

Density (Product Certification,
NBG-25 graphite, SGL Group)

$$c_{pg} := 3.92 \frac{\text{cal}}{\text{mole} \cdot \text{K}}$$

$$\frac{c_{pg}}{12 \frac{\text{gm}}{\text{mole}}} = 0.327 \frac{\text{BTU}}{\text{lb} \cdot \text{R}}$$

Specific heat at 600 C (Perry's
Handbook, 7th edition, Table 2-194)

Thermal conductivity of unirradiated fine-grained isotropic graphite
(J. Nuclear Materials 381, p. 68-75, 2008):

$$T := \begin{pmatrix} 300 \\ 400 \\ 600 \\ 800 \\ 1000 \end{pmatrix} ^\circ\text{C}$$

$$T = \begin{pmatrix} 572 \\ 752 \\ 1112 \\ 1472 \\ 1832 \end{pmatrix} ^\circ\text{F}$$

$$k_g := \begin{pmatrix} 95 \\ 85 \\ 72 \\ 65 \\ 60 \end{pmatrix} \frac{\text{W}}{\text{m} \cdot \text{K}}$$

$$k_g = \begin{pmatrix} 4.574 \\ 4.093 \\ 3.467 \\ 3.13 \\ 2.889 \end{pmatrix} \frac{\text{BTU}}{\text{in} \cdot \text{hr} \cdot \text{R}}$$

Experimental data on effect of neutron fluence on thermal conductivity of fine-grained isotropic graphite (J. Nuclear Materials 381, p. 68-75, 2008; J. Nuclear Materials 195, p. 44-50, 1992; Carbon 13, p. 201-204, 1975); data is given at various values of temperature and dpa (displacements per atom computed as a function of fast neutron fluence with energy > 0.1 MeV):

$$\text{dpa} := 0.13 \quad T_{\text{irr}} := 300 ^\circ\text{C} \quad k_{g_irr} := 27.2 \frac{\text{W}}{\text{m} \cdot \text{K}}$$

$$\text{dpa} := 0.82 \quad T_{\text{irr}} := 400 ^\circ\text{C} \quad k_{g_irr} := 26.9 \frac{\text{W}}{\text{m} \cdot \text{K}}$$

$$\text{dpa} := 1.6 \quad T_{\text{irr}} := 600 ^\circ\text{C} \quad k_{g_irr} := 33 \frac{\text{W}}{\text{m} \cdot \text{K}}$$

$$\text{dpa} := 2.2 \quad T_{\text{irr}} := 1000 ^\circ\text{C} \quad k_{g_irr} := 39 \frac{\text{W}}{\text{m} \cdot \text{K}}$$

$$\text{dpa} := 9.0 \quad T_{\text{irr}} := 800 ^\circ\text{C} \quad k_{g_irr} := 37 \frac{\text{W}}{\text{m} \cdot \text{K}}$$

$$\text{dpa} := \begin{pmatrix} 0.1 \\ 1.0 \\ 10 \end{pmatrix} \quad \text{Displacements per atom}$$

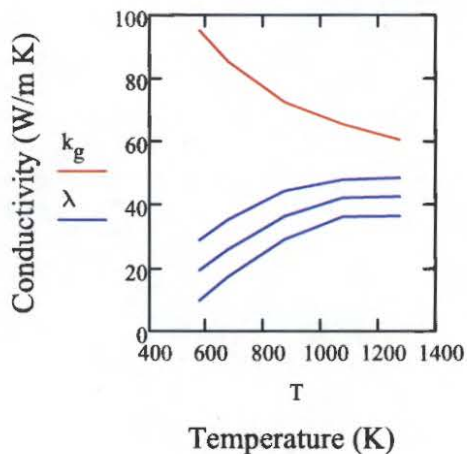
$$T = \begin{pmatrix} 300 \\ 400 \\ 600 \\ 800 \\ 1000 \end{pmatrix} \cdot ^\circ\text{C} \quad \text{Temperature in degrees C}$$

$$\varphi := \begin{pmatrix} 0.30 & 0.20 & 0.10 \\ 0.41 & 0.30 & 0.20 \\ 0.61 & 0.50 & 0.40 \\ 0.73 & 0.64 & 0.55 \\ 0.80 & 0.70 & 0.60 \end{pmatrix} \quad \begin{array}{l} \text{Ratio of irradiated to unirradiated thermal conductivity} \\ \text{as a function of temperature (rows) and dpa (columns),} \\ \text{evaluated using the experimental data given above} \end{array}$$

Thermal conductivity of irradiated graphite at various values of temperature and dpa:

$$i := 0..4 \quad j := 0..2$$

$$\lambda_{i,j} := \varphi_{i,j} \cdot k_{g_i} \quad \lambda = \begin{pmatrix} 1.372 & 0.915 & 0.457 \\ 1.678 & 1.228 & 0.819 \\ 2.115 & 1.733 & 1.387 \\ 2.285 & 2.003 & 1.721 \\ 2.311 & 2.022 & 1.733 \end{pmatrix} \cdot \frac{\text{BTU}}{\text{in} \cdot \text{hr} \cdot \text{R}}$$



Thermophysical properties of compressed water (Perry's Handbook, Tables 2-355 and 2-356):

$$P_L := 20 \cdot \text{bar} = 290 \cdot \text{psi}$$

$$T_L := \begin{pmatrix} 300 \\ 350 \\ 400 \end{pmatrix} \cdot \text{K}$$

$$T_L = \begin{pmatrix} 80 \\ 170 \\ 260 \end{pmatrix} \cdot ^\circ\text{F}$$

$$\rho_{\text{H}_2\text{O}} := \begin{pmatrix} 994.1 \\ 968.2 \\ 929.7 \end{pmatrix} \cdot \frac{\text{kg}}{\text{m}^3}$$

$$\rho_{\text{H}_2\text{O}} = \begin{pmatrix} 0.0359 \\ 0.035 \\ 0.0336 \end{pmatrix} \cdot \frac{\text{lb}}{\text{in}^3}$$

$$c_{p_H_2O} := \begin{pmatrix} 4.17 \\ 4.19 \\ 4.25 \end{pmatrix} \cdot \frac{\text{J}}{\text{gm} \cdot \text{K}}$$

$$c_{p_H_2O} = \begin{pmatrix} 0.996 \\ 1.001 \\ 1.015 \end{pmatrix} \cdot \frac{\text{BTU}}{\text{lb} \cdot \text{R}}$$

$$k_{\text{H}_2\text{O}} := \begin{pmatrix} 0.616 \\ 0.669 \\ 0.689 \end{pmatrix} \cdot \frac{\text{W}}{\text{m} \cdot \text{K}}$$

$$k_{\text{H}_2\text{O}} = \begin{pmatrix} 0.03 \\ 0.032 \\ 0.033 \end{pmatrix} \cdot \frac{\text{BTU}}{\text{hr} \cdot \text{in} \cdot \text{R}}$$

$$\mu_{\text{H}_2\text{O}} := \begin{pmatrix} 0.000856 \\ 0.000371 \\ 0.000218 \end{pmatrix} \cdot \frac{\text{N} \cdot \text{s}}{\text{m}^2}$$

$$\mu_{\text{H}_2\text{O}} = \begin{pmatrix} 0.173 \\ 0.075 \\ 0.044 \end{pmatrix} \cdot \frac{\text{lb}}{\text{hr} \cdot \text{in}}$$

$$\text{Pr}_{\text{H}_2\text{O}} := \begin{pmatrix} 5.80 \\ 2.32 \\ 1.34 \end{pmatrix}$$

$$\rho_w := 0.5 \cdot (\rho_{\text{H}_2\text{O}_0} + \rho_{\text{H}_2\text{O}_1})$$

$$\rho_w = 0.0354 \cdot \frac{\text{lb}}{\text{in}^3}$$

Density of compressed water at
reactor primary coolant inlet
temperature (125 deg F)

Thermal conductivity of helium-argon gas mixtures (Physics of Fluids 3(3), p. 355-361, 1960; Journal of Engineering Physics and Thermophysics 28(6), p. 725-731, 1975):

$$T_{\text{gas}} := \begin{pmatrix} 302 \\ 793 \\ 1173 \end{pmatrix} \cdot \text{K}$$

$$T_{\text{gas}} = \begin{pmatrix} 84 \\ 968 \\ 1652 \end{pmatrix} \cdot ^\circ\text{F}$$

$$k_{100\text{Ar}} := \begin{pmatrix} 0.0182 \\ 0.0383 \\ 0.0480 \end{pmatrix} \cdot \frac{\text{W}}{\text{m} \cdot \text{K}}$$

$$k_{100\text{Ar}} = \begin{pmatrix} 0.00088 \\ 0.00184 \\ 0.00231 \end{pmatrix} \cdot \frac{\text{BTU}}{\text{hr} \cdot \text{in} \cdot \text{R}}$$

$$k_{10\text{He}90\text{Ar}} := \begin{pmatrix} 0.0234 \\ 0.0494 \\ 0.0590 \end{pmatrix} \cdot \frac{\text{W}}{\text{m} \cdot \text{K}}$$

$$k_{10\text{He}90\text{Ar}} = \begin{pmatrix} 0.00113 \\ 0.00238 \\ 0.00284 \end{pmatrix} \cdot \frac{\text{BTU}}{\text{hr} \cdot \text{in} \cdot \text{R}}$$

$$k_{20\text{He}80\text{Ar}} := \begin{pmatrix} 0.0294 \\ 0.0622 \\ 0.0700 \end{pmatrix} \cdot \frac{\text{W}}{\text{m} \cdot \text{K}}$$

$$k_{20\text{He}80\text{Ar}} = \begin{pmatrix} 0.00142 \\ 0.00299 \\ 0.00337 \end{pmatrix} \cdot \frac{\text{BTU}}{\text{hr} \cdot \text{in} \cdot \text{R}}$$

$$k_{30\text{He}70\text{Ar}} := \begin{pmatrix} 0.0364 \\ 0.0772 \\ 0.0880 \end{pmatrix} \cdot \frac{\text{W}}{\text{m} \cdot \text{K}}$$

$$k_{30\text{He}70\text{Ar}} = \begin{pmatrix} 0.00175 \\ 0.00372 \\ 0.00424 \end{pmatrix} \cdot \frac{\text{BTU}}{\text{hr} \cdot \text{in} \cdot \text{R}}$$

$$k_{40\text{He}60\text{Ar}} := \begin{pmatrix} 0.0451 \\ 0.0957 \\ 0.106 \end{pmatrix} \cdot \frac{\text{W}}{\text{m} \cdot \text{K}}$$

$$k_{40\text{He}60\text{Ar}} = \begin{pmatrix} 0.00217 \\ 0.00461 \\ 0.0051 \end{pmatrix} \cdot \frac{\text{BTU}}{\text{hr} \cdot \text{in} \cdot \text{R}}$$

$$k_{50\text{He}50\text{Ar}} := \begin{pmatrix} 0.0551 \\ 0.116 \\ 0.137 \end{pmatrix} \cdot \frac{\text{W}}{\text{m} \cdot \text{K}}$$

$$k_{50\text{He}50\text{Ar}} = \begin{pmatrix} 0.00265 \\ 0.00559 \\ 0.0066 \end{pmatrix} \cdot \frac{\text{BTU}}{\text{hr} \cdot \text{in} \cdot \text{R}}$$

$$k_{60\text{He}40\text{Ar}} := \begin{pmatrix} 0.0667 \\ 0.140 \\ 0.167 \end{pmatrix} \cdot \frac{\text{W}}{\text{m} \cdot \text{K}}$$

$$k_{60\text{He}40\text{Ar}} = \begin{pmatrix} 0.00321 \\ 0.00674 \\ 0.00804 \end{pmatrix} \cdot \frac{\text{BTU}}{\text{hr} \cdot \text{in} \cdot \text{R}}$$

$$k_{70\text{He}30\text{Ar}} := \begin{pmatrix} 0.0809 \\ 0.169 \\ 0.223 \end{pmatrix} \cdot \frac{\text{W}}{\text{m} \cdot \text{K}}$$

$$k_{70\text{He}30\text{Ar}} = \begin{pmatrix} 0.0039 \\ 0.00814 \\ 0.01074 \end{pmatrix} \cdot \frac{\text{BTU}}{\text{hr} \cdot \text{in} \cdot \text{R}}$$

$$k_{80\text{He}20\text{Ar}} := \begin{pmatrix} 0.0993 \\ 0.195 \\ 0.279 \end{pmatrix} \cdot \frac{\text{W}}{\text{m} \cdot \text{K}}$$

$$k_{80\text{He}20\text{Ar}} = \begin{pmatrix} 0.00478 \\ 0.00939 \\ 0.01343 \end{pmatrix} \cdot \frac{\text{BTU}}{\text{hr} \cdot \text{in} \cdot \text{R}}$$

$$k_{90\text{He}10\text{Ar}} := \begin{pmatrix} 0.124 \\ 0.250 \\ 0.338 \end{pmatrix} \cdot \frac{\text{W}}{\text{m} \cdot \text{K}}$$

$$k_{90\text{He}10\text{Ar}} = \begin{pmatrix} 0.00597 \\ 0.01204 \\ 0.01627 \end{pmatrix} \cdot \frac{\text{BTU}}{\text{hr} \cdot \text{in} \cdot \text{R}}$$

$$k_{100\text{He}} := \begin{pmatrix} 0.154 \\ 0.308 \\ 0.397 \end{pmatrix} \cdot \frac{\text{W}}{\text{m} \cdot \text{K}}$$

$$k_{100\text{He}} = \begin{pmatrix} 0.00741 \\ 0.01483 \\ 0.01912 \end{pmatrix} \cdot \frac{\text{BTU}}{\text{hr} \cdot \text{in} \cdot \text{R}}$$

Thermal radiation properties of materials (for stainless steel and tungsten, Table A.11, "Fundamentals of Heat and Mass Transfer," 5th ed., F. Incropera and D. DeWitt, 2002; for graphite, European Physical J. A 38, p. 167-171, 2008; for zirconia, British J. Applied Physics 3, p. 97-101, 1952; for macor, AIChE Symposium Series Heat Transfer 89 (295), p. 122-131, 1993; for stainless steel coated with graphite powder, "Total Hemispherical Emissivity of VHTR Candidate Materials," PhD Dissertation, 2011):

$\epsilon_{\text{SST}_{\text{lo}}} := 0.2$ Emissivity of stainless steel (capsule, outside surface of heat shield)

$\epsilon_{\text{SST}_{\text{hi}}} := 0.4$ Emissivity of stainless steel coated with graphite powder (inside surface of heat shield, TC sheath, gas tubing)

$\epsilon_{\text{W}} := 0.10$ Emissivity of tungsten

$\epsilon_{\text{ZrO}_2} := 0.30$ Emissivity of zirconia

$\epsilon_{\text{C}} := 0.90$ Emissivity of graphite

$\epsilon_{\text{Macor}} := 0.84$ Emissivity of macor

$$\sigma := 5.670 \cdot 10^{-8} \cdot \frac{\text{W}}{\text{m}^2 \cdot \text{K}^4}$$

$$\sigma = 1.189 \times 10^{-11} \cdot \frac{\text{BTU}}{\text{hr} \cdot \text{in}^2 \cdot \text{R}^4}$$

Stefan-Boltzmann constant

A.2 Thermal expansion of capsule components

$$\alpha_g := 4.5 \cdot 10^{-6} \cdot \frac{1}{K}$$

Coefficient of thermal expansion of
graphite (Perry's Handbook, Table 28-29)

$$T_h := 500^\circ C$$

Irradiation temperature of graphite holder

$$T_o := 25^\circ C$$

Reference temperature

$$\Delta T_h := T_h - T_o = 475 \cdot \Delta^\circ C$$

Temperature change of holder

$$r_{o_h} := 0.5 \cdot 2.095 \cdot \text{in}$$

Outside radius of holder
(Drawing 601258)

$$u_{o_h} := \alpha_g \cdot \Delta T_h \cdot r_{o_h} = 0.0022 \cdot \text{in}$$

Radial thermal expansion at
outside surface of holder

$$r_{i_h} := 0.5 \cdot 0.510 \cdot \text{in}$$

Inside radius of channels in holder
(Drawing 601258)

$$u_{i_h} := \alpha_g \cdot \Delta T_h \cdot r_{i_h} = 0.0005 \cdot \text{in}$$

Radial thermal expansion at inside
surface of channels in holder

$$T_s := 600^\circ C$$

Irradiation temperature of specimens

$$\Delta T_s := T_s - T_o = 575 \cdot \Delta^\circ C$$

Temperature change of specimens

$$r_{o_s} := 0.5 \cdot 0.500 \cdot \text{in}$$

Outside radius of specimens
(Drawing 600786)

$$u_{o_s} := \alpha_g \cdot \Delta T_s \cdot r_{o_s} = 0.0006 \cdot \text{in}$$

Radial thermal expansion at
outside surface of specimens

$$u_{i_h} - u_{o_s} = -0.0001 \cdot \text{in}$$

Differential expansion between holder
and specimens is negligible

$$\alpha_s := 17.3 \cdot 10^{-6} \cdot \frac{1}{K}$$

Coefficient of thermal expansion of stainless steel (Perry's Handbook, Table 28-4)

$$T_c := 150^\circ C$$

Irradiation temperature of capsule

$$\Delta T_c := T_c - T_o = 125 \cdot \Delta^\circ C$$

Temperature change of capsule

$$d_i := 2.13 \cdot \text{in}$$

Inside diameter of capsule (drawing 630434)

$$u_{i_c} := \alpha_s \cdot \Delta T_c \cdot 0.5 \cdot d_i = 0.0023 \cdot \text{in}$$

Radial thermal expansion at inside surface of capsule

Calculate gas gap between capsule and heat shield assuming dimples on heat shield contact the inside surface of capsule:

$$h_{\text{dim}} := 0.005 \cdot \text{in}$$

Height of dimple at all sections of heat shield except ends (drawing 601260)

$$r_{o_{\text{hs}}} := 0.5 \cdot d_i + u_{i_c} - h_{\text{dim}} = 1.0623 \cdot \text{in}$$

Outside radius of heat shield after expansion of capsule

$$t_{\text{hs}} := 0.002 \cdot \text{in}$$

Thickness of heat shield (drawing 601260)

$$r_{i_{\text{hs}}} := r_{o_{\text{hs}}} - t_{\text{hs}} = 1.0603 \cdot \text{in}$$

Inside radius of heat shield

$$d_c := 0.5 \cdot d_i + u_{i_c} - r_{o_{\text{hs}}} = 0.005 \cdot \text{in}$$

Gas gap between capsule and heat shield

Calculate gas gap between heat shield and rings at top and bottom of holder:

$$h_{\text{dim}_e} := 0.010 \cdot \text{in}$$

Height of dimple at ends of heat shield (drawing 601260)

$$r_{i_{\text{hs}_e}} := 0.5 \cdot d_i + u_{i_c} - h_{\text{dim}_e} - t_{\text{hs}} = 1.055 \cdot \text{in}$$

Inside radius at end of heat shield

$$d_{o_r} := 2.103 \cdot \text{in}$$

Outside diameter of ring on bottom graphite insulator and top ceramic insulator (drawing 630427)

$$d_r := r_{i_{\text{hs}_e}} - 0.5 \cdot d_{o_r} - u_{o_h} = 0.0016 \cdot \text{in}$$

Gas gap between heat shield and rings at top and bottom of holder

Calculate gas gaps accounting for thermal expansion of heat shield, holder, and capsule:

$$d_h := \begin{pmatrix} 2.095 \\ 2.093 \\ 2.083 \\ 2.073 \\ 2.013 \\ 1.993 \\ 1.982 \end{pmatrix} \cdot \text{in}$$

Outside diameter of holder
sections (drawing 601258)

$$d_g := r_{i_hs} - 0.5 \cdot d_h - u_{o_h} = \begin{pmatrix} 0.011 \\ 0.012 \\ 0.017 \\ 0.022 \\ 0.052 \\ 0.062 \\ 0.067 \end{pmatrix} \cdot \text{in}$$

Gas gaps between holder and heat shield
after expansion

$$d_s := \begin{pmatrix} 0.0035 \\ 0.0050 \\ 0.0075 \\ 0.0090 \end{pmatrix} \cdot \text{in}$$

Gas gaps between lower specimens and
holder, upper specimens and holder,
spacer rod and holder, and push rod and
holder (drawings 601258, 600786, 630427)

$$d_m := 0.030 \text{ in}$$

Gas gap between capsule and
ceramic insulator at top of holder
(drawings 630434, 630427)

$$d_b := 0.0035 \text{ in}$$

Gas gap between capsule and
graphite insulator at bottom of holder
(drawings 630434, 630427)

$$d_t := 0.0095 \text{ in}$$

Gas gap between holder and thermocouple
(drawings 601258, 630427)

$$d_e := 0.008 \text{ in}$$

Gas gap between holder and end caps
at bottom of specimen stack (drawings
601256, 601258)

Gas gap between thermocouples and holder is not known precisely due to the loose fit between these components; the minimum gap is assumed to be equal to 5% of the nominal gap corresponding to the case where the thermocouple is centered (ECAR-2429).

$$d_t := \begin{pmatrix} 0.05 \\ 1.95 \end{pmatrix} \cdot 0.0095 \text{ in} = \begin{pmatrix} 0.0005 \\ 0.0185 \end{pmatrix} \cdot \text{in}$$

Minimum and maximum gas gap between thermocouples and holder

Vary the thermal contact between heat shield and capsule to account for increased heat conductance due to the dimples on the heat shield contacting the capsule and uncertainty in the location of the heat shield; this gas gap is used to adjust the model in order to bring into agreement the measured and calculated temperatures.

$$d_c = 0.005 \cdot \text{in}$$

Nominal gas gap between capsule and heat shield

$$d_v := \begin{pmatrix} 0.0001 \\ 0.0005 \\ 0.001 \\ 0.002 \\ 0.003 \\ 0.004 \\ 0.005 \\ 0.007 \\ 0.010 \\ 0.015 \end{pmatrix} \cdot \text{in}$$

Variable gas gaps between capsule and heat shield to account for variable thermal contact

The following table shows the gas gaps between capsule and heat shield, in each of six axial zones and in each irradiation cycle; zone elevations are given relative to core mid-plane.

Zone Elevation (inches)		Gas Gap (inches)			
Bottom	Top	Cycle 149A All Steps	Cycle 149B Step 1	Cycle 149B Step 2	Cycle 149B Step 3
-24.375	-12	0.005	0.001	0.003	0.005
-12	-4	0.007	0.002	0.002	0.002
-4	4	0.007	0.004	0.004	0.004
4	12	0.007	0.004	0.004	0.004
12	16	0.003	0.0001	0.001	0.003
16	25.88	0.010	0.005	0.010	0.015
Zone Elevation (inches)		Gas Gap (inches)			
Bottom	Top	Cycle 150B Step 1	Cycle 150B Step 2	Cycle 150B Step 3	
-24.375	-12	0.001	0.003	0.003	
-12	-4	0.0001	0.001	0.001	
-4	4	0.003	0.004	0.004	
4	12	0.001	0.002	0.002	
12	16	0.0001	0.0005	0.0005	
16	25.88	0.005	0.007	0.007	
Zone Elevation (inches)		Gas Gap (inches)			
Bottom	Top	Cycle 151A Step 1	Cycle 151A Step 2	Cycle 151A Step 3	
-24.375	-12	0.002	0.003	0.005	
-12	-4	0.002	0.002	0.001	
-4	4	0.005	0.005	0.004	
4	12	0.004	0.004	0.004	
12	16	0.001	0.001	0.001	
16	25.88	0.007	0.010	0.015	
Zone Elevation (inches)		Gas Gap (inches)			
Bottom	Top	Cycle 151B Step 1	Cycle 151B Step 2	Cycle 151B Step 3	
-24.375	-12	0.003	0.003	0.005	
-12	-4	0.0001	0.0001	0.0001	
-4	4	0.004	0.004	0.004	
4	12	0.004	0.004	0.004	
12	16	0.001	0.001	0.001	
16	25.88	0.010	0.010	0.015	

Include effect of change in diameter of graphite due to irradiation-induced shrinkage.

Effect of neutron fluence on graphite dimensions (INL/EXT-12-26255, Appendix A, 2012):

$$\text{dpa} = f(\Phi)$$

Displacements per atom as
a function of neutron fluence

$$\frac{\Delta D}{D} = \beta \cdot \text{dpa}$$

$$\beta := 0.00191$$

Diameter reduction, obtained from linear
regression of data on NBG-25 specimens

Evaluate gas gaps at 1, 2, 3, 4, and 5 dpa:

$$d_h = \begin{pmatrix} 2.095 \\ 2.093 \\ 2.083 \\ 2.073 \\ 2.013 \\ 1.993 \\ 1.982 \end{pmatrix} \cdot \text{in}$$

Diameter of holder sections

$$d_g = \begin{pmatrix} 0.011 \\ 0.012 \\ 0.017 \\ 0.022 \\ 0.052 \\ 0.062 \\ 0.067 \end{pmatrix} \cdot \text{in}$$

Gas gaps (unirradiated)

$$\text{dpa}_1 := 1$$

$$d_{g1} := d_g + 0.5 \cdot \beta \cdot \text{dpa}_1 \cdot d_h = \begin{pmatrix} 0.013 \\ 0.014 \\ 0.019 \\ 0.024 \\ 0.053 \\ 0.063 \\ 0.069 \end{pmatrix} \cdot \text{in}$$

$$\text{dpa}_2 := 2$$

$$d_{g2} := d_g + 0.5 \cdot \beta \cdot \text{dpa}_2 \cdot d_h = \begin{pmatrix} 0.015 \\ 0.016 \\ 0.021 \\ 0.026 \\ 0.055 \\ 0.065 \\ 0.071 \end{pmatrix} \cdot \text{in}$$

$$\text{dpa}_3 := 3$$

$$d_{g3} := d_g + 0.5 \cdot \beta \cdot \text{dpa}_3 \cdot d_h = \begin{pmatrix} 0.017 \\ 0.018 \\ 0.023 \\ 0.028 \\ 0.057 \\ 0.067 \\ 0.073 \end{pmatrix} \cdot \text{in}$$

$$\text{dpa}_4 := 4$$

$$d_{g4} := d_g + 0.5 \cdot \beta \cdot \text{dpa}_4 \cdot d_h = \begin{pmatrix} 0.019 \\ 0.02 \\ 0.025 \\ 0.029 \\ 0.059 \\ 0.069 \\ 0.075 \end{pmatrix} \cdot \text{in}$$

$$\text{dpa}_5 := 5$$

$$d_{g5} := d_g + 0.5 \cdot \beta \cdot \text{dpa}_5 \cdot d_h = \begin{pmatrix} 0.021 \\ 0.022 \\ 0.027 \\ 0.031 \\ 0.061 \\ 0.071 \\ 0.077 \end{pmatrix} \cdot \text{in}$$

A.3 Heat transfer coefficients for conduction across gas gaps

Gas gaps (from Appendix A.2):

$$d_g = \begin{pmatrix} 0.011 \\ 0.012 \\ 0.017 \\ 0.022 \\ 0.052 \\ 0.062 \\ 0.067 \end{pmatrix} \cdot \text{in}$$

Gas gaps between holder and heat shield at various segments of variable diameter holder

$$d_s = \begin{pmatrix} 0.0035 \\ 0.005 \\ 0.0075 \\ 0.009 \end{pmatrix} \cdot \text{in}$$

Gas gaps between lower specimens and holder, upper specimens and holder, spacer rod and holder, and push rod and holder

$$d_v = \begin{pmatrix} 0.0001 \\ 0.0005 \\ 0.001 \\ 0.002 \\ 0.003 \\ 0.004 \\ 0.005 \\ 0.007 \\ 0.01 \\ 0.015 \end{pmatrix} \cdot \text{in}$$

Gas gaps between capsule and heat shield

$$d_t = \begin{pmatrix} 0.0005 \\ 0.0185 \end{pmatrix} \cdot \text{in}$$

Gas gap between holder and thermocouple

$$d_m = 0.03 \cdot \text{in}$$

Gas gap between capsule and ceramic insulator

$$d_r = 0.0016 \cdot \text{in}$$

Gas gap between heat shield and rings at top and bottom of holder

$$d_b = 0.0035 \cdot \text{in}$$

Gas gap between capsule and graphite insulator

$$d_e = 0.008 \cdot \text{in}$$

Gas gap between holder and specimen end caps

Evaluate gas gap conductance using 100% helium:

$$i := 0..2 \quad j := 0..6 \quad k := 0..3 \quad m := 0..1 \quad n := 0..9 \quad T_{\text{gas}} = \begin{pmatrix} 84 \\ 968 \\ 1652 \end{pmatrix} \cdot ^\circ\text{F}$$

$$h_{g,i,j} := \frac{k_{100\text{He}_i}}{d_{g_j}} \quad h_g = \begin{pmatrix} 0.702 & 0.641 & 0.448 & 0.344 & 0.144 & 0.12 & 0.111 \\ 1.404 & 1.282 & 0.895 & 0.688 & 0.288 & 0.241 & 0.221 \\ 1.809 & 1.653 & 1.154 & 0.886 & 0.371 & 0.31 & 0.285 \end{pmatrix} \cdot \frac{\text{BTU}}{\text{in}^2 \cdot \text{hr} \cdot \text{R}}$$

$$h_{s,i,k} := \frac{k_{100\text{He}_i}}{d_{s_k}} \quad h_s = \begin{pmatrix} 2.119 & 1.483 & 0.989 & 0.824 \\ 4.237 & 2.966 & 1.977 & 1.648 \\ 5.461 & 3.823 & 2.549 & 2.124 \end{pmatrix} \cdot \frac{\text{BTU}}{\text{in}^2 \cdot \text{hr} \cdot \text{R}}$$

$$h_{t,i,m} := \frac{k_{100\text{He}_i}}{d_{t_m}} \quad h_t = \begin{pmatrix} 15.61 & 0.4 \\ 31.221 & 0.801 \\ 40.243 & 1.032 \end{pmatrix} \cdot \frac{\text{BTU}}{\text{in}^2 \cdot \text{hr} \cdot \text{R}}$$

$$h_{r,i} := \frac{k_{100\text{He}_i}}{d_r} \quad h_r = \begin{pmatrix} 4.741 \\ 9.482 \\ 12.222 \end{pmatrix} \cdot \frac{\text{BTU}}{\text{in}^2 \cdot \text{hr} \cdot \text{R}}$$

$$h_{v,i,n} := \frac{k_{100\text{He}_i}}{d_{v_n}} \quad h_v = \begin{pmatrix} 74.15 & 14.83 & 7.41 & 3.71 & 2.47 & 1.85 & 1.48 & 1.06 & 0.74 & 0.49 \\ 148.3 & 29.66 & 14.83 & 7.41 & 4.94 & 3.71 & 2.97 & 2.12 & 1.48 & 0.99 \\ 191.15 & 38.23 & 19.12 & 9.56 & 6.37 & 4.78 & 3.82 & 2.73 & 1.91 & 1.27 \end{pmatrix} \cdot \frac{\text{BTU}}{\text{in}^2 \cdot \text{hr} \cdot \text{R}}$$

$$h_{m,i} := \frac{k_{100\text{He}_i}}{d_m} \quad h_m = \begin{pmatrix} 0.247 \\ 0.494 \\ 0.637 \end{pmatrix} \cdot \frac{\text{BTU}}{\text{in}^2 \cdot \text{hr} \cdot \text{R}}$$

$$h_{b,i} := \frac{k_{100\text{He}_i}}{d_b} \quad h_b = \begin{pmatrix} 2.119 \\ 4.237 \\ 5.461 \end{pmatrix} \cdot \frac{\text{BTU}}{\text{in}^2 \cdot \text{hr} \cdot \text{R}}$$

$$h_{e,i} := \frac{k_{100\text{He}_i}}{d_e} \quad h_e = \begin{pmatrix} 0.927 \\ 1.854 \\ 2.389 \end{pmatrix} \cdot \frac{\text{BTU}}{\text{in}^2 \cdot \text{hr} \cdot \text{R}}$$

Evaluate gas gap conductance using 90% helium 10% argon:

$$h_{g,i,j} := \frac{k_{90\text{He}10\text{Ar}_i}}{d_{g_j}} \quad h_g = \begin{pmatrix} 0.565 & 0.516 & 0.36 & 0.277 & 0.116 & 0.097 & 0.089 \\ 1.139 & 1.041 & 0.727 & 0.558 & 0.233 & 0.196 & 0.179 \\ 1.541 & 1.407 & 0.983 & 0.755 & 0.316 & 0.264 & 0.243 \end{pmatrix} \cdot \frac{\text{BTU}}{\text{in}^2 \cdot \text{hr} \cdot \text{R}}$$

$$h_{s,i,k} := \frac{k_{90\text{He}10\text{Ar}_i}}{d_{s_k}} \quad h_s = \begin{pmatrix} 1.706 & 1.194 & 0.796 & 0.663 \\ 3.439 & 2.407 & 1.605 & 1.337 \\ 4.65 & 3.255 & 2.17 & 1.808 \end{pmatrix} \cdot \frac{\text{BTU}}{\text{in}^2 \cdot \text{hr} \cdot \text{R}}$$

$$h_{t,i,m} := \frac{k_{90\text{He}10\text{Ar}_i}}{d_{t_m}} \quad h_t = \begin{pmatrix} 12.569 & 0.322 \\ 25.342 & 0.65 \\ 34.262 & 0.879 \end{pmatrix} \cdot \frac{\text{BTU}}{\text{in}^2 \cdot \text{hr} \cdot \text{R}}$$

$$h_{r,i} := \frac{k_{90\text{He}10\text{Ar}_i}}{d_r} \quad h_r = \begin{pmatrix} 3.817 \\ 7.696 \\ 10.405 \end{pmatrix} \cdot \frac{\text{BTU}}{\text{in}^2 \cdot \text{hr} \cdot \text{R}}$$

$$h_{v,i,n} := \frac{k_{90\text{He}10\text{Ar}_i}}{d_{v_n}} \quad h_v = \begin{pmatrix} 59.7 & 11.94 & 5.97 & 2.99 & 1.99 & 1.49 & 1.19 & 0.85 & 0.6 & 0.4 \\ 120.37 & 24.07 & 12.04 & 6.02 & 4.01 & 3.01 & 2.41 & 1.72 & 1.2 & 0.8 \\ 162.74 & 32.55 & 16.27 & 8.14 & 5.42 & 4.07 & 3.25 & 2.32 & 1.63 & 1.08 \end{pmatrix} \cdot \frac{\text{BTU}}{\text{in}^2 \cdot \text{hr} \cdot \text{R}}$$

$$h_{m,i} := \frac{k_{90\text{He}10\text{Ar}_i}}{d_m} \quad h_m = \begin{pmatrix} 0.199 \\ 0.401 \\ 0.542 \end{pmatrix} \cdot \frac{\text{BTU}}{\text{in}^2 \cdot \text{hr} \cdot \text{R}}$$

$$h_{b,i} := \frac{k_{90\text{He}10\text{Ar}_i}}{d_b} \quad h_b = \begin{pmatrix} 1.706 \\ 3.439 \\ 4.65 \end{pmatrix} \cdot \frac{\text{BTU}}{\text{in}^2 \cdot \text{hr} \cdot \text{R}}$$

$$h_{e,i} := \frac{k_{90\text{He}10\text{Ar}_i}}{d_e} \quad h_e = \begin{pmatrix} 0.746 \\ 1.505 \\ 2.034 \end{pmatrix} \cdot \frac{\text{BTU}}{\text{in}^2 \cdot \text{hr} \cdot \text{R}}$$

Evaluate gas gap conductance using 80% helium 20% argon:

$$h_{g,i,j} := \frac{k_{80\text{He}20\text{Ar}_i}}{d_{g_j}} \quad h_g = \begin{pmatrix} 0.453 & 0.413 & 0.289 & 0.222 & 0.093 & 0.078 & 0.071 \\ 0.889 & 0.812 & 0.567 & 0.435 & 0.182 & 0.153 & 0.14 \\ 1.272 & 1.162 & 0.811 & 0.623 & 0.261 & 0.218 & 0.2 \end{pmatrix} \cdot \frac{\text{BTU}}{\text{in}^2 \cdot \text{hr} \cdot \text{R}}$$

$$h_{s,i,k} := \frac{k_{80\text{He}20\text{Ar}_i}}{d_{s_k}} \quad h_s = \begin{pmatrix} 1.366 & 0.956 & 0.637 & 0.531 \\ 2.683 & 1.878 & 1.252 & 1.043 \\ 3.838 & 2.687 & 1.791 & 1.493 \end{pmatrix} \cdot \frac{\text{BTU}}{\text{in}^2 \cdot \text{hr} \cdot \text{R}}$$

$$h_{t,i,m} := \frac{k_{80\text{He}20\text{Ar}_i}}{d_{t_m}} \quad h_t = \begin{pmatrix} 10.066 & 0.258 \\ 19.766 & 0.507 \\ 28.281 & 0.725 \end{pmatrix} \cdot \frac{\text{BTU}}{\text{in}^2 \cdot \text{hr} \cdot \text{R}}$$

$$h_{r,i} := \frac{k_{80\text{He}20\text{Ar}_i}}{d_r} \quad h_r = \begin{pmatrix} 3.057 \\ 6.003 \\ 8.589 \end{pmatrix} \cdot \frac{\text{BTU}}{\text{in}^2 \cdot \text{hr} \cdot \text{R}}$$

$$h_{v,i,n} := \frac{k_{80\text{He}20\text{Ar}_i}}{d_{v_n}} \quad h_v = \begin{pmatrix} 47.81 & 9.56 & 4.78 & 2.39 & 1.59 & 1.2 & 0.96 & 0.68 & 0.48 & 0.32 \\ 93.89 & 18.78 & 9.39 & 4.69 & 3.13 & 2.35 & 1.88 & 1.34 & 0.94 & 0.63 \\ 134.34 & 26.87 & 13.43 & 6.72 & 4.48 & 3.36 & 2.69 & 1.92 & 1.34 & 0.9 \end{pmatrix} \cdot \frac{\text{BTU}}{\text{in}^2 \cdot \text{hr} \cdot \text{R}}$$

$$h_{m,i} := \frac{k_{80\text{He}20\text{Ar}_i}}{d_m} \quad h_m = \begin{pmatrix} 0.159 \\ 0.313 \\ 0.448 \end{pmatrix} \cdot \frac{\text{BTU}}{\text{in}^2 \cdot \text{hr} \cdot \text{R}}$$

$$h_{b,i} := \frac{k_{80\text{He}20\text{Ar}_i}}{d_b} \quad h_b = \begin{pmatrix} 1.366 \\ 2.683 \\ 3.838 \end{pmatrix} \cdot \frac{\text{BTU}}{\text{in}^2 \cdot \text{hr} \cdot \text{R}}$$

$$h_{e,i} := \frac{k_{80\text{He}20\text{Ar}_i}}{d_e} \quad h_e = \begin{pmatrix} 0.598 \\ 1.174 \\ 1.679 \end{pmatrix} \cdot \frac{\text{BTU}}{\text{in}^2 \cdot \text{hr} \cdot \text{R}}$$

Evaluate gas gap conductance using 70% helium 30% argon:

$$h_{g,i,j} := \frac{k_{70\text{He}30\text{Ar}_i}}{d_{g_j}} \quad h_g = \begin{pmatrix} 0.369 & 0.337 & 0.235 & 0.181 & 0.076 & 0.063 & 0.058 \\ 0.77 & 0.704 & 0.491 & 0.377 & 0.158 & 0.132 & 0.121 \\ 1.016 & 0.929 & 0.648 & 0.498 & 0.208 & 0.174 & 0.16 \end{pmatrix} \cdot \frac{\text{BTU}}{\text{in}^2 \cdot \text{hr} \cdot \text{R}}$$

$$h_{s,i,k} := \frac{k_{70\text{He}30\text{Ar}_i}}{d_{s_k}} \quad h_s = \begin{pmatrix} 1.113 & 0.779 & 0.519 & 0.433 \\ 2.325 & 1.627 & 1.085 & 0.904 \\ 3.068 & 2.147 & 1.432 & 1.193 \end{pmatrix} \cdot \frac{\text{BTU}}{\text{in}^2 \cdot \text{hr} \cdot \text{R}}$$

$$h_{t,i,m} := \frac{k_{70\text{He}30\text{Ar}_i}}{d_{t_m}} \quad h_t = \begin{pmatrix} 8.201 & 0.21 \\ 17.131 & 0.439 \\ 22.605 & 0.58 \end{pmatrix} \cdot \frac{\text{BTU}}{\text{in}^2 \cdot \text{hr} \cdot \text{R}}$$

$$h_{r_i} := \frac{k_{70\text{He}30\text{Ar}_i}}{d_r} \quad h_r = \begin{pmatrix} 2.491 \\ 5.203 \\ 6.865 \end{pmatrix} \cdot \frac{\text{BTU}}{\text{in}^2 \cdot \text{hr} \cdot \text{R}}$$

$$h_{v,i,n} := \frac{k_{70\text{He}30\text{Ar}_i}}{d_{v_n}} \quad h_v = \begin{pmatrix} 38.95 & 7.79 & 3.9 & 1.95 & 1.3 & 0.97 & 0.78 & 0.56 & 0.39 & 0.26 \\ 81.37 & 16.27 & 8.14 & 4.07 & 2.71 & 2.03 & 1.63 & 1.16 & 0.81 & 0.54 \\ 107.37 & 21.47 & 10.74 & 5.37 & 3.58 & 2.68 & 2.15 & 1.53 & 1.07 & 0.72 \end{pmatrix} \cdot \frac{\text{BTU}}{\text{in}^2 \cdot \text{hr} \cdot \text{R}}$$

$$h_{m_i} := \frac{k_{70\text{He}30\text{Ar}_i}}{d_m} \quad h_m = \begin{pmatrix} 0.13 \\ 0.271 \\ 0.358 \end{pmatrix} \cdot \frac{\text{BTU}}{\text{in}^2 \cdot \text{hr} \cdot \text{R}}$$

$$h_{b_i} := \frac{k_{70\text{He}30\text{Ar}_i}}{d_b} \quad h_b = \begin{pmatrix} 1.113 \\ 2.325 \\ 3.068 \end{pmatrix} \cdot \frac{\text{BTU}}{\text{in}^2 \cdot \text{hr} \cdot \text{R}}$$

$$h_{e_i} := \frac{k_{70\text{He}30\text{Ar}_i}}{d_e} \quad h_e = \begin{pmatrix} 0.487 \\ 1.017 \\ 1.342 \end{pmatrix} \cdot \frac{\text{BTU}}{\text{in}^2 \cdot \text{hr} \cdot \text{R}}$$

Evaluate temperature control gas gap conductance including
the effect of irradiation-induced shrinkage of graphite at 1 dpa:

Evaluate gas gap conductance using 100% helium:

$$i := 0..2 \quad j := 0..6 \quad T_{\text{gas}} = \begin{pmatrix} 84 \\ 968 \\ 1652 \end{pmatrix} \cdot ^\circ\text{F}$$

$$h_{g_{i,j}} := \frac{k_{100\text{He}_i}}{d_{g1_j}} \quad h_g = \begin{pmatrix} 0.59 & 0.547 & 0.4 & 0.315 & 0.139 & 0.117 & 0.108 \\ 1.18 & 1.093 & 0.799 & 0.63 & 0.277 & 0.234 & 0.215 \\ 1.521 & 1.409 & 1.03 & 0.812 & 0.357 & 0.301 & 0.277 \end{pmatrix} \cdot \frac{\text{BTU}}{\text{in}^2 \cdot \text{hr} \cdot \text{R}}$$

Evaluate gas gap conductance using 90% helium 10% argon:

$$h_{g_{i,j}} := \frac{k_{90\text{He}10\text{Ar}_i}}{d_{g1_j}} \quad h_g = \begin{pmatrix} 0.475 & 0.44 & 0.322 & 0.254 & 0.112 & 0.094 & 0.087 \\ 0.958 & 0.888 & 0.649 & 0.511 & 0.225 & 0.19 & 0.175 \\ 1.295 & 1.2 & 0.877 & 0.691 & 0.304 & 0.256 & 0.236 \end{pmatrix} \cdot \frac{\text{BTU}}{\text{in}^2 \cdot \text{hr} \cdot \text{R}}$$

Evaluate gas gap conductance using 80% helium 20% argon:

$$h_{g_{i,j}} := \frac{k_{80\text{He}20\text{Ar}_i}}{d_{g1_j}} \quad h_g = \begin{pmatrix} 0.381 & 0.353 & 0.258 & 0.203 & 0.089 & 0.075 & 0.069 \\ 0.747 & 0.692 & 0.506 & 0.399 & 0.176 & 0.148 & 0.136 \\ 1.069 & 0.99 & 0.724 & 0.571 & 0.251 & 0.212 & 0.195 \end{pmatrix} \cdot \frac{\text{BTU}}{\text{in}^2 \cdot \text{hr} \cdot \text{R}}$$

Evaluate gas gap conductance using 70% helium 30% argon:

$$h_{g_{i,j}} := \frac{k_{70\text{He}30\text{Ar}_i}}{d_{g1_j}} \quad h_g = \begin{pmatrix} 0.31 & 0.287 & 0.21 & 0.165 & 0.073 & 0.061 & 0.056 \\ 0.648 & 0.6 & 0.439 & 0.346 & 0.152 & 0.128 & 0.118 \\ 0.855 & 0.792 & 0.579 & 0.456 & 0.201 & 0.169 & 0.156 \end{pmatrix} \cdot \frac{\text{BTU}}{\text{in}^2 \cdot \text{hr} \cdot \text{R}}$$

Evaluate temperature control gas gap conductance including
the effect of irradiation-induced shrinkage of graphite at 2 dpa:

Evaluate gas gap conductance using 100% helium:

$$i := 0..2 \quad j := 0..6 \quad T_{\text{gas}} = \begin{pmatrix} 84 \\ 968 \\ 1652 \end{pmatrix} \cdot ^\circ\text{F}$$

$$h_{g,i,j} := \frac{k_{100\text{He}_i}}{d_{g2_j}} \quad h_g = \begin{pmatrix} 0.509 & 0.476 & 0.361 & 0.291 & 0.134 & 0.113 & 0.105 \\ 1.018 & 0.953 & 0.722 & 0.581 & 0.268 & 0.227 & 0.209 \\ 1.312 & 1.228 & 0.931 & 0.749 & 0.345 & 0.292 & 0.27 \end{pmatrix} \cdot \frac{\text{BTU}}{\text{in}^2 \cdot \text{hr} \cdot \text{R}}$$

Evaluate gas gap conductance using 90% helium 10% argon:

$$h_{g,i,j} := \frac{k_{90\text{He}10\text{Ar}_i}}{d_{g2_j}} \quad h_g = \begin{pmatrix} 0.41 & 0.384 & 0.291 & 0.234 & 0.108 & 0.091 & 0.084 \\ 0.826 & 0.774 & 0.586 & 0.472 & 0.217 & 0.184 & 0.17 \\ 1.117 & 1.046 & 0.792 & 0.638 & 0.294 & 0.249 & 0.23 \end{pmatrix} \cdot \frac{\text{BTU}}{\text{in}^2 \cdot \text{hr} \cdot \text{R}}$$

Evaluate gas gap conductance using 80% helium 20% argon:

$$h_{g,i,j} := \frac{k_{80\text{He}20\text{Ar}_i}}{d_{g2_j}} \quad h_g = \begin{pmatrix} 0.328 & 0.307 & 0.233 & 0.187 & 0.086 & 0.073 & 0.067 \\ 0.645 & 0.603 & 0.457 & 0.368 & 0.169 & 0.144 & 0.133 \\ 0.922 & 0.863 & 0.654 & 0.526 & 0.242 & 0.205 & 0.19 \end{pmatrix} \cdot \frac{\text{BTU}}{\text{in}^2 \cdot \text{hr} \cdot \text{R}}$$

Evaluate gas gap conductance using 70% helium 30% argon:

$$h_{g,i,j} := \frac{k_{70\text{He}30\text{Ar}_i}}{d_{g2_j}} \quad h_g = \begin{pmatrix} 0.267 & 0.25 & 0.19 & 0.153 & 0.07 & 0.06 & 0.055 \\ 0.559 & 0.523 & 0.396 & 0.319 & 0.147 & 0.124 & 0.115 \\ 0.737 & 0.69 & 0.523 & 0.421 & 0.194 & 0.164 & 0.152 \end{pmatrix} \cdot \frac{\text{BTU}}{\text{in}^2 \cdot \text{hr} \cdot \text{R}}$$

Evaluate temperature control gas gap conductance including
the effect of irradiation-induced shrinkage of graphite at 3 dpa:

Evaluate gas gap conductance using 100% helium:

$$i := 0..2 \quad j := 0..6 \quad T_{\text{gas}} = \begin{pmatrix} 84 \\ 968 \\ 1652 \end{pmatrix} \cdot ^\circ\text{F}$$

$$h_{g_{i,j}} := \frac{k_{100\text{He}_i}}{d_{g3_j}} \quad h_g = \begin{pmatrix} 0.448 & 0.422 & 0.329 & 0.27 & 0.129 & 0.11 & 0.102 \\ 0.895 & 0.845 & 0.658 & 0.539 & 0.259 & 0.22 & 0.204 \\ 1.154 & 1.089 & 0.848 & 0.695 & 0.333 & 0.284 & 0.263 \end{pmatrix} \cdot \frac{\text{BTU}}{\text{in}^2 \cdot \text{hr} \cdot \text{R}}$$

Evaluate gas gap conductance using 90% helium 10% argon:

$$h_{g_{i,j}} := \frac{k_{90\text{He}10\text{Ar}_i}}{d_{g3_j}} \quad h_g = \begin{pmatrix} 0.36 & 0.34 & 0.265 & 0.217 & 0.104 & 0.089 & 0.082 \\ 0.727 & 0.685 & 0.534 & 0.438 & 0.21 & 0.179 & 0.165 \\ 0.982 & 0.927 & 0.722 & 0.592 & 0.284 & 0.242 & 0.224 \end{pmatrix} \cdot \frac{\text{BTU}}{\text{in}^2 \cdot \text{hr} \cdot \text{R}}$$

Evaluate gas gap conductance using 80% helium 20% argon:

$$h_{g_{i,j}} := \frac{k_{80\text{He}20\text{Ar}_i}}{d_{g3_j}} \quad h_g = \begin{pmatrix} 0.289 & 0.272 & 0.212 & 0.174 & 0.083 & 0.071 & 0.066 \\ 0.567 & 0.535 & 0.417 & 0.341 & 0.164 & 0.14 & 0.129 \\ 0.811 & 0.765 & 0.596 & 0.488 & 0.234 & 0.2 & 0.185 \end{pmatrix} \cdot \frac{\text{BTU}}{\text{in}^2 \cdot \text{hr} \cdot \text{R}}$$

Evaluate gas gap conductance using 70% helium 30% argon:

$$h_{g_{i,j}} := \frac{k_{70\text{He}30\text{Ar}_i}}{d_{g3_j}} \quad h_g = \begin{pmatrix} 0.235 & 0.222 & 0.173 & 0.142 & 0.068 & 0.058 & 0.054 \\ 0.491 & 0.463 & 0.361 & 0.296 & 0.142 & 0.121 & 0.112 \\ 0.648 & 0.611 & 0.477 & 0.39 & 0.187 & 0.16 & 0.148 \end{pmatrix} \cdot \frac{\text{BTU}}{\text{in}^2 \cdot \text{hr} \cdot \text{R}}$$

Evaluate temperature control gas gap conductance including
the effect of irradiation-induced shrinkage of graphite at 4 dpa:

Evaluate gas gap conductance using 100% helium:

$$i := 0..2 \quad j := 0..6 \quad T_{\text{gas}} = \begin{pmatrix} 84 \\ 968 \\ 1652 \end{pmatrix} \cdot ^\circ\text{F}$$

$$h_{g,i,j} := \frac{k_{100\text{He}_i}}{d_{g4,j}} \quad h_g = \begin{pmatrix} 0.399 & 0.379 & 0.302 & 0.252 & 0.125 & 0.107 & 0.099 \\ 0.799 & 0.758 & 0.605 & 0.503 & 0.25 & 0.214 & 0.199 \\ 1.03 & 0.977 & 0.78 & 0.648 & 0.323 & 0.276 & 0.256 \end{pmatrix} \cdot \frac{\text{BTU}}{\text{in}^2 \cdot \text{hr} \cdot \text{R}}$$

Evaluate gas gap conductance using 90% helium 10% argon:

$$h_{g,i,j} := \frac{k_{90\text{He}10\text{Ar}_i}}{d_{g4,j}} \quad h_g = \begin{pmatrix} 0.322 & 0.305 & 0.243 & 0.203 & 0.101 & 0.086 & 0.08 \\ 0.648 & 0.615 & 0.491 & 0.408 & 0.203 & 0.174 & 0.161 \\ 0.877 & 0.832 & 0.664 & 0.552 & 0.275 & 0.235 & 0.218 \end{pmatrix} \cdot \frac{\text{BTU}}{\text{in}^2 \cdot \text{hr} \cdot \text{R}}$$

Evaluate gas gap conductance using 80% helium 20% argon:

$$h_{g,i,j} := \frac{k_{80\text{He}20\text{Ar}_i}}{d_{g4,j}} \quad h_g = \begin{pmatrix} 0.258 & 0.244 & 0.195 & 0.162 & 0.081 & 0.069 & 0.064 \\ 0.506 & 0.48 & 0.383 & 0.318 & 0.158 & 0.136 & 0.126 \\ 0.724 & 0.687 & 0.548 & 0.456 & 0.227 & 0.194 & 0.18 \end{pmatrix} \cdot \frac{\text{BTU}}{\text{in}^2 \cdot \text{hr} \cdot \text{R}}$$

Evaluate gas gap conductance using 70% helium 30% argon:

$$h_{g,i,j} := \frac{k_{70\text{He}30\text{Ar}_i}}{d_{g4,j}} \quad h_g = \begin{pmatrix} 0.21 & 0.199 & 0.159 & 0.132 & 0.066 & 0.056 & 0.052 \\ 0.438 & 0.416 & 0.332 & 0.276 & 0.137 & 0.118 & 0.109 \\ 0.578 & 0.549 & 0.438 & 0.364 & 0.181 & 0.155 & 0.144 \end{pmatrix} \cdot \frac{\text{BTU}}{\text{in}^2 \cdot \text{hr} \cdot \text{R}}$$

Evaluate temperature control gas gap conductance including
the effect of irradiation-induced shrinkage of graphite at 5 dpa:

Evaluate gas gap conductance using 100% helium:

$$i := 0..2 \quad j := 0..6 \quad T_{\text{gas}} = \begin{pmatrix} 84 \\ 968 \\ 1652 \end{pmatrix} \cdot ^\circ\text{F}$$

$$h_{g,i,j} := \frac{k_{100\text{He}_i}}{d_{g5_j}} \quad h_g = \begin{pmatrix} 0.361 & 0.344 & 0.28 & 0.236 & 0.121 & 0.104 & 0.097 \\ 0.721 & 0.688 & 0.559 & 0.471 & 0.242 & 0.209 & 0.194 \\ 0.929 & 0.887 & 0.721 & 0.608 & 0.312 & 0.269 & 0.25 \end{pmatrix} \cdot \frac{\text{BTU}}{\text{in}^2 \cdot \text{hr} \cdot \text{R}}$$

Evaluate gas gap conductance using 90% helium 10% argon:

$$h_{g,i,j} := \frac{k_{90\text{He}10\text{Ar}_i}}{d_{g5_j}} \quad h_g = \begin{pmatrix} 0.29 & 0.277 & 0.225 & 0.19 & 0.098 & 0.084 & 0.078 \\ 0.585 & 0.558 & 0.454 & 0.383 & 0.197 & 0.169 & 0.157 \\ 0.791 & 0.755 & 0.614 & 0.517 & 0.266 & 0.229 & 0.213 \end{pmatrix} \cdot \frac{\text{BTU}}{\text{in}^2 \cdot \text{hr} \cdot \text{R}}$$

Evaluate gas gap conductance using 80% helium 20% argon:

$$h_{g,i,j} := \frac{k_{80\text{He}20\text{Ar}_i}}{d_{g5_j}} \quad h_g = \begin{pmatrix} 0.232 & 0.222 & 0.18 & 0.152 & 0.078 & 0.067 & 0.062 \\ 0.456 & 0.436 & 0.354 & 0.298 & 0.153 & 0.132 & 0.123 \\ 0.653 & 0.623 & 0.507 & 0.427 & 0.22 & 0.189 & 0.176 \end{pmatrix} \cdot \frac{\text{BTU}}{\text{in}^2 \cdot \text{hr} \cdot \text{R}}$$

Evaluate gas gap conductance using 70% helium 30% argon:

$$h_{g,i,j} := \frac{k_{70\text{He}30\text{Ar}_i}}{d_{g5_j}} \quad h_g = \begin{pmatrix} 0.189 & 0.181 & 0.147 & 0.124 & 0.064 & 0.055 & 0.051 \\ 0.396 & 0.377 & 0.307 & 0.259 & 0.133 & 0.114 & 0.106 \\ 0.522 & 0.498 & 0.405 & 0.341 & 0.176 & 0.151 & 0.14 \end{pmatrix} \cdot \frac{\text{BTU}}{\text{in}^2 \cdot \text{hr} \cdot \text{R}}$$

**A.4 Turbulent forced convection in the annulus between capsule
and chopped dummy in-pile tube**

$T_{\text{inlet}} := 125^\circ\text{F}$ $P_{\text{inlet}} := 360\cdot\text{psi}$ Primary coolant inlet temperature and pressure

$\Delta p := 77\cdot\text{psi}$ Core pressure drop for 2-pump operation

$T_{\text{film}} := \begin{pmatrix} 125 \\ 170 \\ 260 \end{pmatrix}^\circ\text{F}$ Assumed range of film temperature

Interpolated thermophysical property values at film temperature:

$$\rho := \begin{bmatrix} 0.5 \cdot (\rho_{\text{H}_2\text{O}_0} + \rho_{\text{H}_2\text{O}_1}) \\ \rho_{\text{H}_2\text{O}_1} \\ \rho_{\text{H}_2\text{O}_2} \end{bmatrix} \quad \rho = \begin{pmatrix} 0.0354 \\ 0.035 \\ 0.0336 \end{pmatrix} \cdot \frac{\text{lb}}{\text{in}^3}$$

$$c_p := \begin{bmatrix} 0.5 \cdot (c_{p_H_2O_0} + c_{p_H_2O_1}) \\ c_{p_H_2O_1} \\ c_{p_H_2O_2} \end{bmatrix} \quad c_p = \begin{pmatrix} 0.998 \\ 1.001 \\ 1.015 \end{pmatrix} \cdot \frac{\text{BTU}}{\text{lb} \cdot \text{R}}$$

$$k := \begin{bmatrix} 0.5 \cdot (k_{\text{H}_2\text{O}_0} + k_{\text{H}_2\text{O}_1}) \\ k_{\text{H}_2\text{O}_1} \\ k_{\text{H}_2\text{O}_2} \end{bmatrix} \quad k = \begin{pmatrix} 0.031 \\ 0.032 \\ 0.033 \end{pmatrix} \cdot \frac{\text{BTU}}{\text{hr} \cdot \text{in} \cdot \text{R}}$$

$$\mu := \begin{bmatrix} 0.5 \cdot (\mu_{\text{H}_2\text{O}_0} + \mu_{\text{H}_2\text{O}_1}) \\ \mu_{\text{H}_2\text{O}_1} \\ \mu_{\text{H}_2\text{O}_2} \end{bmatrix} \quad \mu = \begin{pmatrix} 0.124 \\ 0.075 \\ 0.044 \end{pmatrix} \cdot \frac{\text{lb}}{\text{hr} \cdot \text{in}}$$

$$\text{Pr} := \begin{bmatrix} 0.5 \cdot (\text{Pr}_{\text{H}_2\text{O}_0} + \text{Pr}_{\text{H}_2\text{O}_1}) \\ \text{Pr}_{\text{H}_2\text{O}_1} \\ \text{Pr}_{\text{H}_2\text{O}_2} \end{bmatrix} \quad \text{Pr} = \begin{pmatrix} 4.06 \\ 2.32 \\ 1.34 \end{pmatrix}$$

Hydrodynamics in the annulus between capsule and chopped dummy in-pile tube:

$D_i := 2.50 \cdot \text{in}$		Outside diameter of capsule (drawing 630434)
$D_o := 2.624 \cdot \text{in}$		Inside diameter of chopped dummy in-pile tube (drawing 443027)
$D_{hy} := D_o - D_i$	$D_{hy} = 0.124 \cdot \text{in}$	Hydraulic diameter of annulus
$A_f := \frac{\pi}{4} \cdot (D_o + D_i) \cdot D_{hy}$	$A_f = 0.499 \cdot \text{in}^2$	Flow area of annulus
$L_f := 145 \cdot \text{in}$		Length of annulus (Drawings 601266 and 443027)
$V_f := 218.7 \cdot \frac{\text{in}}{\text{s}}$		Flow velocity (initially assumed due to nonlinear f-Re dependence)
$Re := \frac{\rho_0 \cdot D_{hy} \cdot V_f}{\mu_0}$	$Re = 27981$	
$\epsilon := 250 \times 10^{-6} \text{ in}$		Wall roughness (Perry's Handbook, Table 6-1)
$f := \left[-4 \cdot \log \left[\frac{0.27 \cdot \epsilon}{D_{hy}} + \left(\frac{7}{Re} \right)^{0.9} \right] \right]^{-2}$		Turbulent Fanning friction factor for rough tubes (Perry's Handbook, Eq. 6-39)
$f = 0.00717$		
$K_c := 0.5$		Maximum loss coefficient for sudden contraction (Perry's Handbook, Eq. 6-91)
$K_e := 1.0$		Maximum loss coefficient for sudden enlargement (Perry's Handbook, Eq. 6-95)
$K_f := \frac{4 \cdot f \cdot L_f}{D_{hy}}$	$K_f = 33.554$	Loss coefficient for pipe friction (Perry's Handbook, Eq. 6-32)

Bemoulli equation (Perry's Handbook, Eq. 6-90):

$$V_f := \sqrt{\frac{2 \cdot \Delta p}{\rho_0 \cdot (K_c + K_e + K_f)}} \quad V_f = 218.7 \cdot \frac{\text{in}}{\text{s}} \quad \text{Checks (equal to velocity assumed in Re)}$$

$$Q_f := V_f \cdot A_f \quad Q_f = 28.4 \cdot \frac{\text{gal}}{\text{min}}$$

$$m_f := \rho_0 \cdot V_f \quad m_f = 27914 \cdot \frac{\text{lb}}{\text{in}^2 \cdot \text{hr}}$$

Heat transfer coefficient for turbulent forced convection in an annulus:

Colburn correlation (Perry's Handbook, Eq. 5-50c, using film temperature method to account for fluid property variation):

$$i := 0..1$$

$$Re_{i_i} := \frac{\rho_i \cdot D_{hy} \cdot V_f}{\mu_i} \quad Re_i = \left(\frac{27987}{45670} \right) \quad \text{Reynolds number}$$

Nusselt number (applies to both surfaces of annulus):

$$Nu_i := 0.023 \cdot (Re_{i_i})^{0.8} \cdot (Pr_i)^{0.33} \quad Nu = \left(\frac{131.858}{162.196} \right)$$

$$h_i := \frac{Nu_i \cdot k_i}{D_{hy}} \quad h = \left(\frac{32.9}{42.13} \right) \cdot \frac{\text{BTU}}{\text{hr} \cdot \text{in}^2 \cdot \text{R}}$$

A.5 Nuclear heating rates

Heating rates at 23.2 MW south power (ECAR-2291):

For the following materials, a cosine function is used to represent the axial heating profile (IN-1260, "Reactor Physics Results for Low-Power Measurements in the Advanced Test Reactor," p.45). For each axial position, heating rate is an average over azimuthal segments.

Heating rates of stainless steel capsule (ECAR-2291, Table 3):

-24.12	2.13
-23.125	2.58
-21.125	3.41
-19.125	4.22
-17.125	5.03
-15.125	5.76
-13.125	6.42
-11.125	7.01
-9.125	7.49
-7.125	7.86
-5.125	8.19
-3.125	8.34
-1.125	8.39
1.125	8.38
3.125	8.24
5.125	8.02
7.125	7.62
9.125	7.16
11.125	6.6
13.125	5.9
15.125	5.17
17.125	4.35
19.125	3.39
21.125	2.43
23.125	1.48
24.125	1.17

x :=

in

q_{capsule} := $\frac{W}{gm}$

$$f(x, a, b, c) := a \cdot \cos[b \cdot (x + c)]$$

Axial heating profile

$$g_s := \begin{pmatrix} 10 \\ 0.05 \\ 1 \end{pmatrix}$$

Initial guess of regression coefficients

$$s_f := \text{genfit}\left(\frac{x}{\text{in}}, \frac{q_{\text{capsule}}}{\frac{W}{\text{gm}}}, g_s, f\right)$$

Calculate regression coefficients
for heating profile

$$s_f = \begin{pmatrix} 8.447 \\ 0.057 \\ 0.935 \end{pmatrix}$$

$$F_f(x) := f\left(x, s_{f_0}, s_{f_1}, s_{f_2}\right)$$

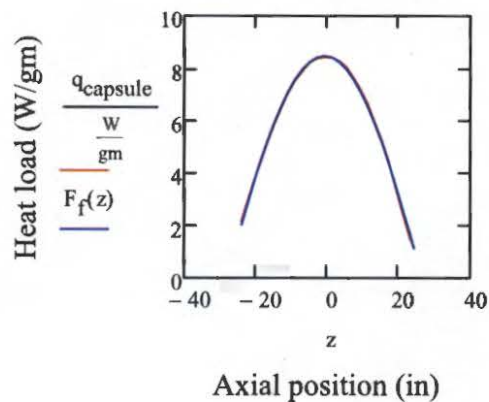
Axial heating profile

$$\rho_{\text{SST}} \cdot s_{f_0} \cdot \frac{W}{\text{gm}} = 3791 \cdot \frac{\text{BTU}}{\text{hr} \cdot \text{in}^3}$$

Peak heating

Plot comparing calculated heating data to heating data fitted to a cosine function:

$$z := \frac{x}{\text{in}}$$



Heating rates of stainless steel heat shield (ECAR-2291, Table 4):

$x :=$	(-24.12	$q_{\text{shield}} :=$	(2.07
	-23.125		2.57
	-21.125		3.42
	-19.125		4.22
	-17.125		5.02
	-15.125		5.8
	-13.125		6.33
	-11.125		6.97
	-9.125		7.5
	-7.125		7.81
	-5.125		8.13
	-3.125		8.31
	-1.125		8.33
	1.125		8.25
	3.125		8.13
	5.125		7.9
	7.125		7.55
	9.125		7.06
	11.125		6.52
	13.125		5.86
	15.125		5.1
	17.125		4.27
	19.125		3.3
	21.125		2.42
	23.125		1.52
	24.125)		1.17)

·in

 $\frac{\text{W}}{\text{gm}}$

$$f(x, a, b, c) := a \cdot \cos[b \cdot (x + c)]$$

Axial heating profile

$$g_s := \begin{pmatrix} 10 \\ 0.05 \\ 1 \end{pmatrix}$$

Initial guess of regression coefficients

$$s_f := \text{genfit}\left(\frac{x}{\text{in}}, \frac{q_{\text{shield}}}{\frac{W}{\text{gm}}}, g_s, f\right)$$

Calculate regression coefficients
for heating profile

$$s_f = \begin{pmatrix} 8.371 \\ 0.057 \\ 0.983 \end{pmatrix}$$

$$F_f(x) := f\left(x, s_{f_0}, s_{f_1}, s_{f_2}\right)$$

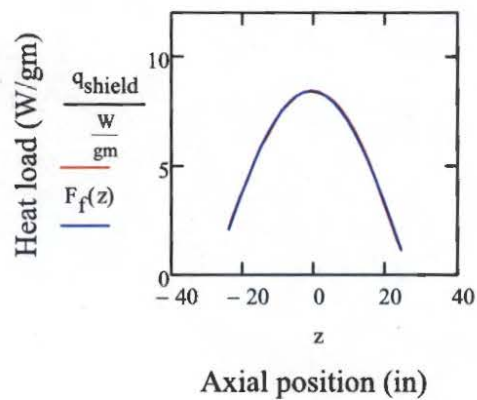
Axial heating profile

$$\rho_{\text{SST}} \cdot s_{f_0} \cdot \frac{W}{\text{gm}} = 3757 \cdot \frac{\text{BTU}}{\text{hr} \cdot \text{in}^3}$$

Peak heating

Plot comparing calculated heating data to heating data fitted to a cosine function:

$$z := \frac{x}{\text{in}}$$



Heating rates of graphite holder (ECAR-2291, Table 5):

$x :=$	(-24.12	$q_{\text{holder}} :=$	(1.81
	-23.125		2.2
	-21.125		2.89
	-19.125		3.56
	-17.125		4.24
	-15.125		4.85
	-13.125		5.39
	-11.125		5.88
	-9.125		6.33
	-7.125		6.64
	-5.125		6.9
	-3.125		7.04
	-1.125		7.13
	1.125		7.09
	3.125		6.98
	5.125		6.76
	7.125		6.48
	9.125		6.06
	11.125		5.59
	13.125		5.04
	15.125		4.41
	17.125		3.73
	19.125		2.94
	21.125		2.25
	23.125		1.52
	24.125		1.2

·in

$\frac{W}{gm}$

$$f(x, a, b, c) := a \cdot \cos[b \cdot (x + c)]$$

Axial heating profile

$$g_s := \begin{pmatrix} 10 \\ 0.05 \\ 1 \end{pmatrix}$$

Initial guess of regression coefficients

$$s_f := \text{genfit}\left(\frac{x}{\text{in}}, \frac{q_{\text{holder}}}{\frac{W}{\text{gm}}}, g_s, f\right)$$

Calculate regression coefficients
for heating profile

$$s_f = \begin{pmatrix} 7.118 \\ 0.057 \\ 0.771 \end{pmatrix}$$

$$F_f(x) := f\left(x, s_{f_0}, s_{f_1}, s_{f_2}\right)$$

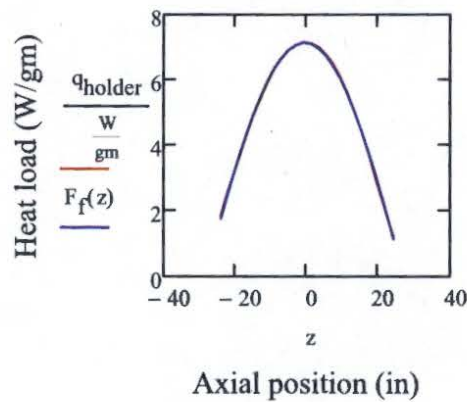
Axial heating profile

$$\rho_g \cdot s_{f_0} \cdot \frac{W}{\text{gm}} = 725 \cdot \frac{\text{BTU}}{\text{hr} \cdot \text{in}^3}$$

Peak heating

Plot comparing calculated heating data to heating data fitted to a cosine function:

$$z := \frac{x}{\text{in}}$$



Heating rates of graphite specimens (ECAR-2291, Table 6):

$x :=$	(-24.12	$q_{\text{specimen}} :=$	(1.72
	-23.125		2.16
	-21.125		2.86
	-19.125		3.5
	-17.125		4.18
	-15.125		4.78
	-13.125		5.33
	-11.125		5.79
	-9.125		6.25
	-7.125		6.56
	-5.125		6.79
	-3.125		6.94
	-1.125		7
$\cdot \text{in}$	1.125		6.96
	3.125		6.89
	5.125		6.65
	7.125		6.38
	9.125		6.01
	11.125		5.5
	13.125		4.94
	15.125		4.36
	17.125		3.67
	19.125		3.08
	21.125		2.22
	23.125		1.51
	24.125		1.19

$\frac{W}{gm}$

$$f(x, a, b, c) := a \cdot \cos[b \cdot (x + c)]$$

Axial heating profile

$$g_s := \begin{pmatrix} 10 \\ 0.05 \\ 1 \end{pmatrix}$$

Initial guess of regression coefficients

$$s_f := \text{genfit}\left(\frac{x}{\text{in}}, \frac{q_{\text{specimen}}}{\frac{W}{\text{gm}}}, g_s, f\right)$$

Calculate regression coefficients
for heating profile

$$s_f = \begin{pmatrix} 7.014 \\ 0.057 \\ 0.727 \end{pmatrix}$$

$$F_f(x) := f\left(x, s_{f_0}, s_{f_1}, s_{f_2}\right)$$

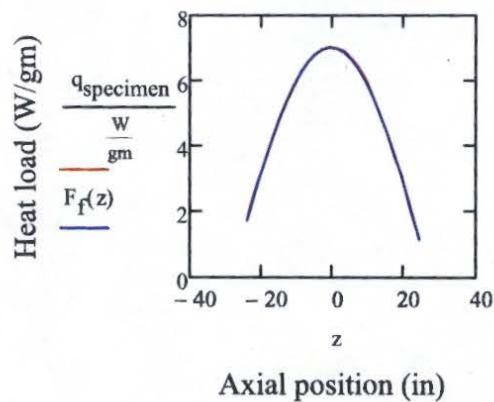
Axial heating profile

$$\rho_g \cdot s_{f_0} \cdot \frac{W}{\text{gm}} = 715 \cdot \frac{\text{BTU}}{\text{hr} \cdot \text{in}^3}$$

Peak heating

Plot comparing calculated heating data to heating data fitted to a cosine function:

$$z := \frac{x}{\text{in}}$$



Heating rates of coolant (ECAR-2291, Table 9):

$x :=$	$\left(\begin{array}{c} -24.12 \\ -23.125 \\ -21.125 \\ -19.125 \\ -17.125 \\ -15.125 \\ -13.125 \\ -11.125 \\ -9.125 \\ -7.125 \\ -5.125 \\ -3.125 \\ -1.125 \\ 1.125 \\ 3.125 \\ 5.125 \\ 7.125 \\ 9.125 \\ 11.125 \\ 13.125 \\ 15.125 \\ 17.125 \\ 19.125 \\ 21.125 \\ 23.125 \\ 24.125 \end{array} \right)$	$\cdot \text{in}$	$q_{\text{coolant}} :=$	$\left(\begin{array}{c} 3.56 \\ 4.45 \\ 6.01 \\ 7.49 \\ 8.97 \\ 10.27 \\ 11.43 \\ 12.51 \\ 13.37 \\ 14.04 \\ 14.56 \\ 14.92 \\ 15.05 \\ 14.99 \\ 14.82 \\ 14.33 \\ 13.67 \\ 12.89 \\ 11.85 \\ 10.58 \\ 9.31 \\ 7.87 \\ 6.23 \\ 4.7 \\ 3.14 \\ 2.44 \end{array} \right)$	$\frac{\text{W}}{\text{gm}}$
--------	--	-------------------	-------------------------	--	------------------------------

$$f(x, a, b, c) := a \cdot \cos[b \cdot (x + c)]$$

Axial heating profile

$$g_s := \begin{pmatrix} 10 \\ 0.05 \\ 1 \end{pmatrix}$$

Initial guess of regression coefficients

$$s_f := \text{genfit}\left(\frac{x}{\text{in}}, \frac{q_{\text{coolant}}}{\frac{W}{\text{gm}}}, g_s, f\right)$$

Calculate regression coefficients
for heating profile

$$s_f = \begin{pmatrix} 15.091 \\ 0.057 \\ 0.735 \end{pmatrix}$$

$$F_f(x) := f(x, s_{f_0}, s_{f_1}, s_{f_2})$$

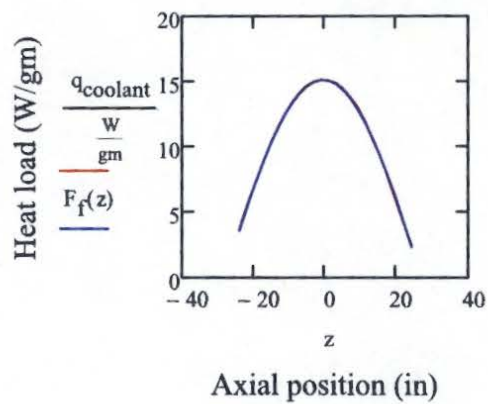
Axial heating profile

$$\rho_0 \cdot s_{f_0} \cdot \frac{W}{\text{gm}} = 828 \cdot \frac{\text{BTU}}{\text{hr} \cdot \text{in}^3}$$

Peak heating

Plot comparing calculated heating data to heating data fitted to a cosine function:

$$z := \frac{x}{\text{in}}$$



Heating rates of thermocouples (ECAR-2291, Tables 7 and 8):

$x :=$	$\begin{pmatrix} -17.125 \\ -15.125 \\ -13.125 \\ -11.125 \\ -9.125 \\ -7.125 \\ -5.125 \\ -3.125 \\ -1.125 \\ 1.125 \\ 3.125 \\ 5.125 \\ 7.125 \\ 9.125 \\ 11.125 \\ 13.125 \\ 15.125 \\ 17.125 \\ 19.125 \\ 21.125 \\ 23.125 \\ 24.125 \end{pmatrix}$	$\cdot \text{in}$	$q_{tc} :=$	$\begin{pmatrix} 6.22 \\ 7.17 \\ 7.98 \\ 8.55 \\ 9.18 \\ 9.68 \\ 10.11 \\ 10.27 \\ 10.48 \\ 10.26 \\ 10.15 \\ 9.78 \\ 9.33 \\ 8.71 \\ 8.07 \\ 7.25 \\ 6.41 \\ 5.3 \\ 3.99 \\ 2.86 \\ 1.85 \\ 1.37 \end{pmatrix}$	$\frac{\text{W}}{\text{gm}}$
--------	---	-------------------	-------------	--	------------------------------

Calculate average density of thermocouple (composite material consisting of inconel sheath, MgO insulation, and wires); technical specifications for mineral insulated cable (item 83 on drawing 601266), Idaho Labs Corp., Idaho Falls, ID:

$$D_{o_tc} := 0.125 \cdot \text{in} \quad \text{Outside diameter of thermocouple sheath}$$

$$t_{\text{sheath}} := 0.016 \cdot \text{in} \quad \text{Thickness of thermocouple sheath}$$

$$D_{i_tc} := D_{o_tc} - 2 \cdot t_{\text{sheath}} = 0.093 \cdot \text{in} \quad \text{Inside diameter of thermocouple sheath}$$

$$D_{\text{wire}} := 0.025 \cdot \text{in} \quad \text{Diameter of thermocouple wire}$$

$$A_{\text{wire}} := 2 \cdot \frac{\pi}{4} \cdot D_{\text{wire}}^2 \quad \text{Cross sectional area of 2 wires}$$

$$D_{i_ins} := \sqrt{\frac{4}{\pi} \cdot A_{\text{wire}}} = 0.0354 \cdot \text{in} \quad \text{Inside diameter of insulation}$$

$$A_{\text{sheath}} := \frac{\pi}{4} \cdot (D_{o_tc}^2 - D_{i_tc}^2) = 0.0055 \cdot \text{in}^2 \quad \text{Cross sectional area of sheath}$$

$$A_{\text{ins}} := \frac{\pi}{4} \cdot (D_{i_tc}^2 - D_{i_ins}^2) = 0.0375 \cdot \text{cm}^2 \quad \text{Cross sectional area of insulation}$$

$$\rho_{\text{metal}} := 8.41 \frac{\text{gm}}{\text{cm}^3} \quad \text{Density of Inconel 600 sheath and type N TC wires (ASM Metals Handbook Vol. 1, Wrought Nickel Alloys)}$$

$$\rho_{\text{MgO}} := 3.64 \frac{\text{gm}}{\text{cm}^3} \quad \text{Density of MgO insulation (Perry's Handbook, 7th edition, Table 2-382)}$$

$$\rho_{tc} := \frac{\rho_{\text{metal}} \cdot (A_{\text{sheath}} + A_{\text{wire}}) + \rho_{\text{MgO}} \cdot A_{\text{ins}}}{A_{\text{sheath}} + A_{\text{wire}} + A_{\text{ins}}} = 6.15 \cdot \frac{\text{gm}}{\text{cm}^3} \quad \text{Density of thermocouple}$$

$$f(x, a, b, c) := a \cdot \cos[b \cdot (x + c)]$$

Axial heating profile

$$g_s := \begin{pmatrix} 10 \\ 0.05 \\ 1 \end{pmatrix}$$

Initial guess of regression coefficients

$$s_f := \text{genfit}\left(\frac{x}{\text{in}}, \frac{q_{tc}}{W}, g_s, f\right)$$

Calculate regression coefficients
for heating profile

$$s_f = \begin{pmatrix} 10.414 \\ 0.058 \\ 0.912 \end{pmatrix}$$

$$F_f(x) := f(x, s_{f_0}, s_{f_1}, s_{f_2})$$

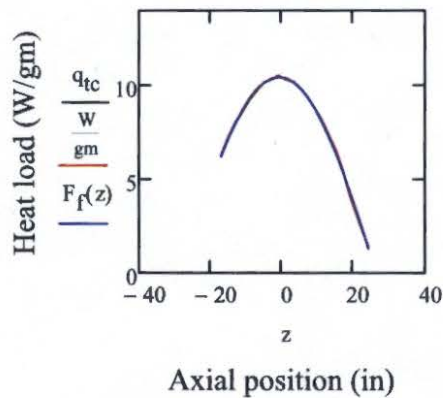
Axial heating profile

$$\rho_{tc} \cdot s_{f_0} \cdot \frac{W}{\text{gm}} = 3582 \cdot \frac{\text{BTU}}{\text{hr} \cdot \text{in}^3}$$

Peak heating

Plot comparing calculated heating data to heating data fitted to a cosine function:

$$z := \frac{x}{\text{in}}$$



Heating rates of other components with uniform heating rather than an axial heating profile (ECAR-2291, Tables 10 and 11):

Tungsten:

$$q_W := 4.12 \cdot \frac{W}{gm}$$

$$\rho_W \cdot q_W = 3916 \cdot \frac{BTU}{hr \cdot in^3}$$

Zirconia:

$$q_{ZrO_2} := 2.50 \cdot \frac{W}{gm}$$

$$\rho_{ZrO_2} \cdot q_{ZrO_2} = 790 \cdot \frac{BTU}{hr \cdot in^3}$$

Macor:

$$q_{Macor} := 0.71 \cdot \frac{W}{gm}$$

$$\rho_{Macor} \cdot q_{Macor} = 100 \cdot \frac{BTU}{hr \cdot in^3}$$

Normalized heating profile obtained by fitting heating data to a cosine function:

$$P_{\text{norm}}(x) := \cos[0.057 \cdot (x + 0.9)]$$

Integrate normalized heating profile to obtain total heating in core:

$$I := \int_{-27.5}^{27.5} P_{\text{norm}}(x) \, dx \cdot \text{in} = 35 \cdot \text{in}$$

Split into separate profiles below and above core mid-plane:

$$P_{\text{norm_below}}(x) := \cos[0.053 \cdot (x + 0.9)]$$

$$I_{\text{below}} := \int_{-27.5}^0 P_{\text{norm_below}}(x) \, dx \cdot \text{in} = 19.5 \cdot \text{in}$$

$$P_{\text{norm_above}}(x) := \cos[0.060 \cdot (x + 0.9)]$$

$$I_{\text{above}} := \int_0^{27.5} P_{\text{norm_above}}(x) \, dx \cdot \text{in} = 15.6 \cdot \text{in}$$

Integrate normalized heating profiles to check that total core heating is unchanged:

$$I_{\text{below}} + I_{\text{above}} = 35.1 \cdot \text{in}$$

Define array of coordinates:

$$i := 0..24$$

$$\zeta_i := -24 + 2 \cdot i$$

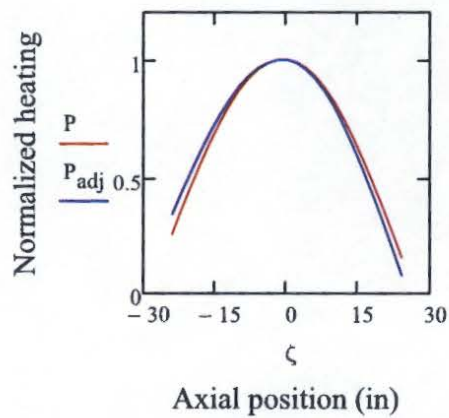
Define arrays of normalized heating values:

$$i := 0..24 \quad P := P_{\text{norm}}(\zeta)$$

$$j := 0..12 \quad P_{\text{adj}_j} := P_{\text{norm_below}}(\zeta_j)$$

$$k := 13..24 \quad P_{\text{adj}_k} := P_{\text{norm_above}}(\zeta_k)$$

Plot symmetric and unsymmetric heating profiles:



Note: The unsymmetric heating profile (blue trace) was shown to improve temperature calculations in the AGC-2 test as compared to using the symmetric heating profile (red trace).

A.6 Cycle power, gas flows, and peak DPA

South source power and gas flows are obtained from RDAS system; spreadsheets containing data recorded at 5 minute intervals are stored in folder \\fsisc1\PROJECTS\; values given here are for selected days during the cycle and are computed by averaging the data over the entire day:

Peak DPA in graphite at selected days during irradiation (ECAR-2291, Table 23); peak DPA occurs at core mid-plane and is the average over azimuthal segments:

Note: After adjusting the gas gaps between heat shield and capsule (see Assumptions section in this document), the measured and calculated thermocouple temperatures matched well except during the beginning of cycle 151A. Since the gas flows and temperatures during the beginning of cycle 151A are inconsistent with those during the remainder of the cycle, this discrepancy was assumed to be due to a faulty flow controller recording inaccurate values of gas flows. Therefore, the gas flow at the beginning of cycle 151A was changed from 81% He to 87% He in order to bring into agreement the measured and calculated thermocouple temperatures.

Cycle: 149A

Date: 4/15/2011, Power: 23.41 MW, Temperature control gas: 99% He	DPA := 0.0
Date: 4/29/2011, Power: 23.85 MW, Temperature control gas: 99% He	DPA := 0.303
Date: 5/14/2011, Power: 23.70 MW, Temperature control gas: 99% He	DPA := 0.590
Date: 5/21/2011, Power: 23.67 MW, Temperature control gas: 99% He	DPA := 0.728

Cycle: 149B

Date: 6/22/2011, Power: 23.11 MW, Temperature control gas: 75.4% He	DPA := 1.028
Date: 7/07/2011, Power: 23.26 MW, Temperature control gas: 80.8% He	DPA := 1.333
Date: 7/29/2011, Power: 23.58 MW, Temperature control gas: 84.4% He	DPA := 1.780

Cycle: 150B

Date: 11/02/2011, Power: 23.43 MW, Temperature control gas: 79.7% He DPA := 2.132

Date: 11/14/2011, Power: 23.61 MW, Temperature control gas: 83.4% He DPA := 2.380

Date: 11/23/2011, Power: 23.53 MW, Temperature control gas: 83.6% He DPA := 2.588

Cycle: 151A

Date: 12/23/2011, Power: 22.51 MW, Temperature control gas: 87.0% He DPA := 2.878

Date: 1/11/2012, Power: 22.86 MW, Temperature control gas: 88.0% He DPA := 3.238

Date: 2/07/2012, Power: 23.20 MW, Temperature control gas: 90.6% He DPA := 3.643

Cycle: 151B

Date: 3/20/2012, Power: 22.43 MW, Temperature control gas: 88.6% He DPA := 4.072

Date: 4/18/2012, Power: 22.82 MW, Temperature control gas: 89.4% He DPA := 4.370

Date: 5/03/2012, Power: 22.97 MW, Temperature control gas: 91.4% He DPA := 4.592

ECAR-2322	As-Run Thermal Analysis of the AGC-2 Experiment	Page B1 of B4
-----------	--	---------------

Appendix B – Report file containing results of ABAQUS validation

ABQ EXE: abq6122.exe
 COMPUTER: quark_inel_gov
 OS: Linux
 OS TYPE: 2.6.37.6-0.20-default
 t1

```
=====
ODB: Test-1
dictTest[Test-1].Keys:  ['Grp1']
#####
      NT11-n325
Max error: 1.20% <-----
      Max1:  37.3320      Min1:  10.5200 Range:  26.8120
Abq Max2:  37.7813 Abq Min2:  10.6362 Range:  27.1451
      NT11-n281
Max error: 1.48% <-----
      Max1:  55.1070      Min1:  13.9970 Range:  41.1100
Abq Max2:  54.7760 Abq Min2:  14.2043 Range:  40.5717
=====
```

```
t2
=====
ODB: Test-2
dictTest[Test-2].Keys:  ['Grp2', 'Grp1']
#####
      NT15-n61
Max error: 1.34% <-----
      Max1:  37.3320      Min1:  10.5200 Range:  26.8120
Abq Max2:  37.7366 Abq Min2:  10.6609 Range:  27.0756
#####
      NT11-n61
Max error: 1.54% <-----
      Max1:  55.1070      Min1:  13.9970 Range:  41.1100
Abq Max2:  54.7444 Abq Min2:  14.2131 Range:  40.5313
=====
```

```
t3
=====
ODB: Test-3
dictTest[Test-3].Keys:  ['Grp1']
#####
      NT11-n130
Max error: 1.65% <-----
      Max1:  44.5920      Min1:  12.5210 Range:  32.0710
Abq Max2:  44.7825 Abq Min2:  12.7270 Range:  32.0555
      NT11-n59
Max error: 1.85% <-----
      Max1:  55.3390      Min1:  14.7770 Range:  40.5620
Abq Max2:  55.0396 Abq Min2:  15.0511 Range:  39.9885
=====
```

ECAR-2322	As-Run Thermal Analysis of the AGC-2 Experiment	Page B2 of B4
-----------	--	---------------

t4

```
=====
ODB: Test-4
dictTest[Test-4].Keys:  ['Grp1']
#####
      NT11-n281
Error: 0.00%    <-----
Ans:      13.7600    Abq:      13.7600
      NT11-n303
Error: 0.00%    <-----
Ans:      11.3200    Abq:      11.3200
      NT11-n325
Error: 0.00%    <-----
Ans:       4.0000    Abq:       4.0000
      NT11-n314
Error: 0.00%    <-----
Ans:       8.2700    Abq:       8.2700
      NT11-n292
Error: 0.00%    <-----
Ans:      13.1500    Abq:      13.1500
=====
```

t5

```
=====
ODB: Test-5
dictTest[Test-5].Keys:  ['Grp3', 'Grp2', 'Grp1', 'Grp5', 'Grp4']
#####
      NT13-n62
Error: 0.00%    <-----
Ans:      11.3200    Abq:      11.3200
#####
      NT12-n62
Error: 0.00%    <-----
Ans:      13.1500    Abq:      13.1500
#####
      NT11-n62
Error: 0.00%    <-----
Ans:      13.7600    Abq:      13.7600
#####
      NT15-n62
Error: 0.00%    <-----
Ans:       4.0000    Abq:       4.0000
#####
      NT14-n62
Error: 0.00%    <-----
Ans:       8.2700    Abq:       8.2700
=====
```

t6

```
=====
ODB: Test-6
```

ECAR-2322	As-Run Thermal Analysis of the AGC-2 Experiment	Page B3 of B4
-----------	--	---------------

dictTest[Test-6].Keys: ['Grp1']

#####

NT11-n533

Max error: 0.39% <-----

Max1: 80.7640 Min1: 61.8970 Range: 18.8670

Abq Max2: 80.4914 Abq Min2: 61.7364 Range: 18.7551

NT11-n803

Max error: 0.38% <-----

Max1: 94.5930 Min1: 71.5310 Range: 23.0620

Abq Max2: 94.3007 Abq Min2: 71.2781 Range: 23.0226

t7

ODB: Test-7

dictTest[Test-7].Keys: ['Grp1']

#####

HFL-e56

Error: 0.19% <-----

Ans: -0.1700 Abq: -0.1697

t8

ODB: Test-8

dictTest[Test-8].Keys: ['Grp1']

#####

HFL-e1121

Error: 1.74% <-----

Ans: 0.1710 Abq: 0.1740

HFL-e3678

Error: 2.25% <-----

Ans: -0.1620 Abq: -0.1656

t9

ODB: Test-9

dictTest[Test-9].Keys: ['Grp1']

#####

NT11-n13

Error: 0.01% <-----

Ans: 50.0010 Abq: 50.0036

NT11-n17

Error: 0.00% <-----

Ans: 55.5500 Abq: 55.5500

NT11-n328

Error: 0.20% <-----

Ans: 51.6040 Abq: 51.7074

NT11-n38

Error: 0.05% <-----

Ans: 50.0890 Abq: 50.1148

ECAR-2322	As-Run Thermal Analysis of the AGC-2 Experiment	Page B4 of B4
-----------	--	---------------

```

      NT11-n28
Error: 0.11%  <-----
Ans:      50.7010      Abq:      50.7550
      NT11-n218
Error: 0.01%  <-----
Ans:      50.0110      Abq:      50.0176
      NT11-n32
Error: 0.10%  <-----
Ans:      50.3060      Abq:      50.3555
      NT11-n324
Error: 0.20%  <-----
Ans:      52.4260      Abq:      52.5321
      NT11-n4
Error: 0.08%  <-----
Ans:      51.0600      Abq:      51.1006
      NT11-n320
Error: 0.16%  <-----
Ans:      53.6690      Abq:      53.7552
=====

```

t10

```

=====
ODB: Test-10
dictTest[Test-10].Keys:  ['Grp1']
#####
      NT11-n325
Error: 0.15%  <-----
Ans:      215.7130      Abq:      216.0345
=====

```

t11

```

=====
ODB: Test-11
dictTest[Test-11].Keys:  ['Grp1']
#####
      HFL-e55
Error: 0.02%  <-----
Ans:      -5.5000      Abq:      -5.4989
=====

```

t12

```

=====
ODB: Test-12
dictTest[Test-12].Keys:  ['Grp1']
#####
      NT11-n336
Error: 0.00%  <-----
Ans:      406.6667      Abq:      406.6667
=====

```